PBTK modeled perfluoroalkyl acid kinetics in zebrafish eleutheroembryos suggests impacts on bioconcentrations by chorion porosity dynamics

Pierre-André Billat, Carolina Vogs, Clément Blassiau, Céline Brochot, Emma Wincent, François Brion, Rémy Beaudouin

PBTK modeled perfluoroalkyl acid kinetics in zebrafish eleutheroembryos suggests impacts on bioconcentrations by chorion porosity dynamics

Pierre-André Billat[a], Carolina Vogs[b,c], Clément Blassiau[a], Céline Brochot[a], Emma Wincent[c], François Brion[d,e], Rémy Beaudouin[a,e*].

[a] INERIS, Experimental toxicology and modeling unit (TEAM), Parc ALATA BP2, Verneuil en Halatte, France

[b] Department of Biomedical Science and Veterinary Public Health, Swedish University of Agricultural Science (SLU), Uppsala, Sweden.

[c] Institute of Environmental Medicine, Karolinska Institutet (KI), Stockholm, Sweden

[d] INERIS, Ecotoxicology of substances and environments unit (ESMI), Parc ALATA BP2, Verneuil en Halatte, France

[e] UMR-I 02 SEBIO, Parc ALATA BP2, Verneuil en Halatte, France INERIS

* Phone: +33 3 44 55 82 38; fax: +33 3 44 55 67 67; e-mail: Remy.Beaudouin@ineris.fr

ABSTRACT

The zebrafish eleutheroembryo (zfe) is widely used as a model to characterize the toxicity of chemicals. However, analytical methods are still missing to measure organ concentrations. Therefore, physiologically-based toxicokinetic (PBTK) modeling may overcome current limitations to help understand the relationship between toxic effects and internal exposure in various organs.

A previous PBTK model has been updated to include the chorionic transport barrier and its permeabilization, hatching dynamics within a zfe population over development, and active mediated transport mechanisms. The zfe PBTK model has been calibrated using measured time-dependent internal concentrations of PFBA, PFHxS, PFOA, and PFOS in a zfe population and evaluated using external datasets from the literature.

Calibration was successful with 96% of the predictions falling within a 2-fold range of the observed concentrations. The external dataset was correctly estimated with about 50% of the predictions falling within a factor of 3 of the observed data and 10% of the predictions are out of the 10-fold error. The calibrated model suggested that active mediated transport differs between PFAS with sulfonic and carboxylic acid functional end groups.

This PBTK model predicts well the fate of PFAS in zfe. Therefore, this model may improve the use of zfe as an alternative model in toxicokinetic-toxicodynamic studies and help to refine and reduce zfe-based experiments, while giving insights into chemicals internal kinetics .

KEYWORDS

Physiologically-based toxicokinetic (PBTK) model, Zebrafish embryos (zfe), Danio rerio, Bayesian calibration, perfluoroalkyl acid (PFAS), internal exposure.

1. Introduction

The zebrafish eleutheroembryo (zfe) model offers many attractive advantages for toxicity testing of chemicals as a physiologically relevant and ethically sound alternative vertebrate model. For example, zfe are translucent, allowing one to observe phenotypical effects following chemical exposure, and are legally considered a non-animal model until 120 hours post fertilization (hpf). Moreover, zfe-based assays are cheap and rapid to set up as compared to traditional toxicology *in vivo* models, allowing medium to high throughput testing for chemical safety assessment (Hill et al., 2005). In addition, the zebrafish genome has been completely sequenced, revealing high genetic similarity to humans. At the regulatory level, the two zfe-based embryo assays TG236 and TG250 have been validated and adopted as OECD test guidelines to assess acute toxicity or endocrine activity of chemicals, respectively (OCDE, 2021; OECD, 2013). Several additional endpoints can be measured with the zfe that are relevant to the regulatory assessment of chemicals, as for example, neurotoxicity, behavior changes, immunotoxicity, and genotoxicity (Canedo and Rocha, 2021; Fitzgerald et al., 2021; Garcia et al., 2016; Silva Brito et al., 2022). The usefulness of the zfe model is however currently hampered due to the inaccessibility of organ concentrations of chemicals, as in comparison to traditional animal toxicity testing using rodent models. Although internal concentrations in the whole zfe have been measured for a range of chemicals (Brox et al., 2014a; Brox et al., 2014b; Kühnert et al., 2013), organ concentrations are still difficult to determine analytically due to the small size of this model.

For this purpose, physiologically-based toxicokinetic (PBTK) models may aid to estimate the spatio-temporal distribution of chemicals in the zfe during the rapid morphological and physiological changes occurring in the first 120 hours of development (Siméon et al., 2020). PBTK models mathematically express toxicokinetic (TK) processes of absorption, distribution, metabolization, and excretion (ADME) of a chemical in an organism, resulting in simulated organ concentrations over time. Hence, the combination of zfe assays together with PBTK modeling of chemicals allows a better characterization of the target organ concentrations in zfe linked to the measured effects (Grech et al., 2017; Nagel, 2002; Simeon et al., 2020). PBTK models that were previously developed for zfe to simulate the TK of valproic acid analogs and bisphenols (Billat et al., 2022; Simeon et al., 2020), successfully demonstrated a better understanding of dose-response relationships by predicting internal whole-body concentrations. However, these models need to be further developed to

better consider the influence of the chorion as a transport barrier and the hatching dynamics within a zfe population over development, as these factors may influence the ADME processes and therefore the simulated organ concentrations of chemicals at the early developmental stages, as suggested by Warner et al. (2022).

Three challenges of chorion physiology and hatching dynamics thus have to be considered. First, the change in chorion permeability may influence the absorption of chemical molecules in the zfe during the early development until hatching and, consequently, the chemical toxicity (Brox et al., 2014a; Wiegand et al., 2000). The hatching (*i.e.* the loss of the chorion) occurs through a three-phase event between 50-100 hour-post fertilization (hpf) depending on temperature and photoperiod, as shown by Villamizar et al. (2012). Second, the chorion's external structure is negatively charged and thus favoring the binding of cationic molecules or ions (Böhme et al., 2017; Hart and Donovan, 1983). Due to chemical molecules binding to the chorion, the apparent internal concentration is artificially high until hatching and decreases after the loss of the chorion (Wiegand et al., 2000). Unfortunately, due to the heterogenic hatching dynamic within the zfe population and the experimental difficulty to mechanically dechorionate numerous zfe during sampling, internal concentrations are often measured on a mix of chorionated and hatched zfe. In addition, the hatching time is rarely closely monitored, neither individually nor at the sample level (*e.g.* proportion of hatched zfe). Third, an “average” TK profile from a single-embryo model could not accurately consider stochastic population events such as hatching. Accordingly, the PBTK model must integrate the diurnal dynamic of the hatching process, its variation due to the temperature, the photocycle, and the inter-individual variability to accurately predict the TK process under different experimental conditions.

To implement those important factors to the existing PBTK model for zfe, we used per- and polyfluoroalkyl substances (PFAS) as model chemicals. Internal concentrations in zfe were previously published for the four PFAS perfuorobutanoic acid (PFBA), perfluorooctanoic acid (PFOA), perfluorohexanesulfonic acid (PFHxS) and perfluorooctanesulfonic acid (PFOS) (Vogs et al., 2019). Moreover, several studies have explored the relationship between the external and internal concentration of PFAS in the early life stage zebrafish model (Gaballah et al., 2020; Han et al., 2021; Huang et al., 2010; Menger et al., 2020; Spulber et al., 2014; Tu et al., 2019; Wang et al., 2020), providing a unique opportunity to evaluate the PBTK model developed in our study.

PFAS have been ubiquitously used in industrial applications due to their favorable characteristics of high thermal and chemical stability as well as their amphiphilic character (Glüge et al., 2020). However, some PFAS have also emerged as a global environmental threat to humans and wildlife due to their long persistence in the environment, their high bioaccumulation capability, and their potential to cause toxicity (Kannan et al., 2004). Various adverse effects have been reported in experimental and epidemiological studies (DeWitt, 2015; Fenton et al., 2021), especially immunotoxicity, hepatotoxicity, and endocrine disruption (Blake et al., 2018; EFSA CONTAM Panel et al., 2020; Kahn et al., 2020). Thus, the "legacy PFAS", PFOA and PFOS, were added to the list of persistent organic pollutants in May 2009, subsequently prompting global manufacturers to shift to shorter-chain PFAS such as PFHxS and PFBA. In zfe toxicity studies, PFAS exposure has caused abnormal morphology (PFHxS, PFOS, PFOA), altered heart rate (PFOS), and hyperactivity during light or night periods (PFHxS, PFOS), whilst PFBA appears to be the least toxic of the four studied compounds (Hagenaars et al., 2011; Truong et al., 2022; Ulhaq et al., 2013; Zheng et al., 2012). However, TK differences between PFAS with varying alkyl chain lengths and functional end groups have been shown to explain toxicity differences observed in zfe by orders of magnitude (Tal and Vogs, 2021; Vogs et al., 2019).

Here, we aimed to develop a zfe PBTK model by (i) incorporating the permeability dynamic of the zfe chorion under different photoperiods and temperature scenarios considering stochastic population hatching events, (ii) studying the effect of the sorption capacity of PFAS on the chorion, and (iii) exploring the ADME processes to better understand and compare the TKs of PFAS, differing in the alkyl chain lengths and functional end groups. The newly developed PBTK model has been calibrated using data produced in the same experimental conditions for the PFOA, PFOS, PFHxS, and PFBA (Vogs et al., 2019) and evaluated using external data published for the four PFAS (Gaballah et al., 2020; Han et al., 2021; Huang et al., 2010; Menger et al., 2020; Spulber et al., 2014; Tu et al., 2019; Wang et al., 2020).

2. Materials and Methods

2.1. Zebrafish eleutheroembryo PBTK model

The PBTK model is based on the model developed by Siméon et al. (2020) and Billat et al. (2022), including the ten initial compartments of the previous PBTK model (*i.e.* yolk, liver, skeleton, gut, eye, brain, heart, skin, muscles and a compartment lumping other organs and tissues). Additionally, the chorion is implemented in the model structure to store and release compounds (mainly by nonspecific binding), and to restrict the exchange flows between water (experimental medium) and zfe tissues (Figure 1).

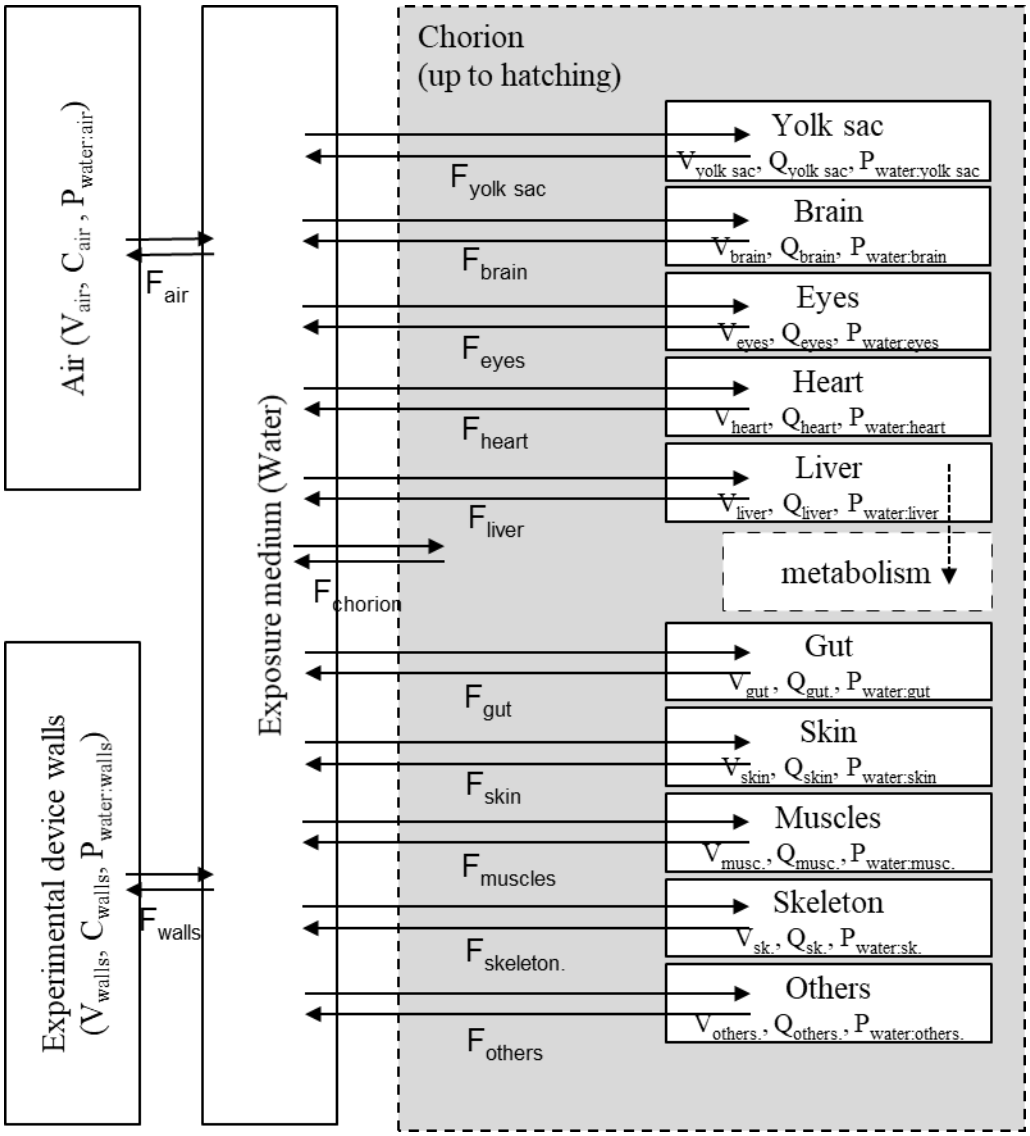

Figure 1. Structure of the updated zebrafish eleutheroembryo PBTK model. F stands for flow (µL/h), V for volume (µL), Q for quantity (nmol), and P for partition coefficient (unitless).

Before hatching, the perivitelline space is not considered since the exchange between the perivitelline space and the zfe is very rapid (less than 5 minutes) once the chorion is crossed (Wiegand et al., 2000). Regarding the physiological development of the zfe, the growth of the zfe and the effect of water temperature on ontogenesis are modeled as previously proposed (Billat et al., 2022; Simeon et al., 2020). All equations, the model structure, and the informatic code of the PBTK model (GNU MCSim, (Bois, 2009)) are provided in the supplemental information (S.I.).

Regarding the experimental device, the nonspecific binding of PFAS to the walls of the device (polymer or borosilicate glass depending on the experiment, C_{wall}, nmol/mm²) and the evaporation of the compound to the air (C_{air}, nmol/mm^3) are modeled with dynamic flows as previously proposed in Billat et al. (2022).

The distribution of PFAS between the water and the different zfe compartments is modeled by dynamic diffusion equations to describe the concentration changes over time in the respective organ:

$$\frac{dQ_i}{dt} = F_i.\left(C_{water} - \frac{C_i}{P_{i:water}}\right) \qquad \textit{Eq. (1)}$$

where Q_i (nmol) is the time-dependent amount of chemicals in the zfe organ *i*, F_i (µL/h) is a time-dependent transfer coefficient of the chemical between the culture medium and the zfe organ *i,* and C_{water} (mM or nmol/µL) is the time-dependent concentration of the chemical in the exposure medium. C_i (mM or nmol/µL) is the time-dependent concentration of the chemical in the zfe organ *i* (*i.e*, Q_i divided by the volume of the organ *i* in µL*, noted* V_i). $P_{i:water}$ (unitless) is the partition coefficient of the compound between the exposure medium and the organ *i*. The partition coefficient of the chemical is predicted with the virtual *in vitro* distribution model, VIVD, a generic quantitative structure-activity relationship approach, described by Fisher et al. (2019).

The total concentration in the whole zfe (C_{embryo}, mM) is computed by the total quantity in the whole zfe, Q_{embryo} (nmol) as the sum of all organ quantities divided by the sum of all organ volumes:

$$C_{embryo} = \sum_{i=1}^{n} Q_i \Big/ \sum_{i=1}^{n} V_i \qquad \textit{Eq. (2)}$$

2.1.1. Chorion permeability

The hatching process, defined as an increased chorion permeability until its complete separation from the zfe, is a time-dependent process related to the levels of free Zn^{2+} in the cells of the hatching gland (Muraina

et al., 2020) and the proteolytic activities at the prehatching stage (Kim et al., 2006; Trikić et al., 2011). To model this physiological process, the dynamics of the chorion permeability are assumed to have a similar dynamic as the easily observable hatching. In a population of zfe, highest probability of hatching occurs 50, 75, and 100 hours post-fertilization (hpf), depending on factors such as temperature and light (Villamizar et al., 2012). Therefore, the hatching process is modeled by using three normal distributions with relative weights (W_1, W_2, W_3), following a normal law (μ_n, σ), with μ_n (hpf) corresponding to the mean hour of the complete separation from chorion within the daily hatching process, and σ represents the daily variability of the chorion separation process (hpf). The temperature effect on the hatching is modeled by modulating the relative weights (W_1, W_2, W_3) using the Arrhenius equation:

$$W_1 = W_{1,ref} \times exp^{\frac{TA}{TR} - \frac{TA}{T}} \quad \textit{Eq. (3)}$$

$$W_3 = W_{3,ref} \times {}^{1}\Big/_{exp^{\frac{TA}{TR} - \frac{TA}{T}}} \quad \textit{Eq. (4)}$$

$$W_2 = 1 - W_3 - W_1 \quad \textit{Eq. (5)}$$

$W_{i,ref}$ is the relative weight *i* at the reference temperature. TA, TR, and T are the Arrhenius temperature, the reference temperature (here 298.15 K, corresponding to 25°C), and the temperature of the assay, expressed in Kelvin, respectively. According to the equation 3 and 4, W_1 increases with temperature, W_3 decreases with temperature and W_2 is deduced from the values of the two other weights as the sum of the weights must be equal to one. . In addition, the hatching process depends on the experimental duration of light as shown by Villamizar et al. (2012). Consequently, three independent parametrizations (μ_1, μ_2, μ_3, σ, W_1, and W_3) of this sub-model were calibrated based on the data of Villamizar et al. (2012) obtained under three light regimes : (i) 0 hours, (ii) 12 hours and (iii) 24 hours of light per day.

The cumulative distribution function (CDF, unitless) of the hatching process has been used to compute the flow from water to the zfe ($F_{e:w}$, µL/h) based on both the simulated frequency of the unhatched zfe with a limited flow in presence of a chorion (1-CDF(time)), and the simulated frequency of the hatched zfe with a complete flow in absence of the chorion (CDF(time)) within the population.

$$F_{e:w} = \big(1 - CDF(time)\big) \times \varphi_{e:chorion:w} + CDF(time) \times \big[\varphi_{e:w} \times S_{embryo}\big] \quad \textit{Eq. (6)}$$

Where $\varphi_{e:\text{chorion}:w}$ (µL/h) is the exchange rate between water and zfe limited by the chorion permeability and $\varphi_{e:w}$ (µL/h/mm²) is the direct exchange rate between water and zfe per zfe body surface area S_{embryo} (mm²).

Using the exchange rate *Fe:w*, equation 1 is reformulated as follows*:*

$$\frac{dQ_i}{dt} = F_{e:w} \times \frac{V_i}{V_{embryo}} \times \left(C_{water} - \frac{C_i}{P_{i:water}}\right) \qquad \textit{Eq. (7)}$$

Where V_i and V_{embryo} are the volumes of the organs and the whole zfe (µL or mm³), respectively, and $P_{i:water}$ the tissue (or yolk):water partition coefficient.

The separation of the chorion is the final step of the hatching process, whilst the exchanges between water and zfe increase with the permeability of the chorion. Thus, a parameter ϕ (hpf) - considered as the shift between the start of the permeabilization and the observed separation of the chorion – has been calibrated on the TK experimental data to realign the sub-model to the beginning of the permeabilization process. This parameter is subtracted from the mean of each of the three hatching events (μ_n) to obtain the estimated time of permeabilization start of the chorion.

2.1.2. PBTK models to study the influence of saturation of flow exchanges

The TKs of PFAS in zfe are speculated to be influenced by active transport-mediated processes resulting in saturated accumulation at higher exposure concentrations (Gaballah et al., 2020; Tal and Vogs, 2021; Vogs et al., 2019). To better apprehend the specific fate of PFAS in zfe, three saturation processes have been evaluated for each compound in addition to model 0 without saturation (Figure 2). These saturation processes lump the limitation of influx processes (passive diffusion, active uptake, pinocytosis, *etc.*) but also the impact of efflux processes on the compound uptake. Model I describes a saturation in the compound uptake to the hatched zfe as follows:

$$F_{e:w} = \left(1 - CDF(time)\right) \times \varphi_{e:chorion:w} + CDF(time) \times \left[\varphi_{e:w} \times S_{embryo}\right] \times \left(\frac{EC_{sat,e}}{EC_{sat,e} + C_{water}}\right) \qquad \textit{Eq. (8)}$$

where $EC_{sat,e}$ (mM) is the half-saturation concentration of the zfe permeability after hatching.

Model II characterizes the saturated influx to both pre- and posthatched zfe during the whole exposure as follows:

$$F_{e:w} = \left(\left(1 - CDF(time)\right) \times \varphi_{e:chorion:w} + CDF(time) \times \left[\varphi_{e:w} \times S_{embryo}\right]\right) \times \left(\frac{EC_{sat,e}}{EC_{sat,e} + C_{water}}\right) \quad \textit{Eq. (9)}$$

where $EC_{sat,e}$ (mM) is the half-saturation concentration of the zfe permeability during the whole exposure. Model III represents a saturated influx resulting from a combination of specific chorion and zfe saturations, *ie* chorion and zfe could limit the uptake with different saturation constants, as follows

$$F_{e:w} = \left(1 - CDF(time)\right) \times \varphi_{e:chorion:w} \times \left(\frac{EC_{sat,c,e}}{EC_{sat,c,e} + C_{water}}\right) + CDF(time) \times \left[\varphi_{e:w} \times S_{embryo}\right] \times \left(\frac{EC_{sat,e}}{EC_{sat,e} + C_{water}}\right) \quad \textit{Eq. (10)}$$

where $EC_{sat,c,e}$ (mM) is the half-saturation concentration of the chorion and zfe permeability. These saturation terms provide information on a reduced uptake of PFAS from water to the internal tissues, depending on the water concentration but independent from the partition coefficient. A pure saturation of the chorion may have been an additional hypothesis to test. However, an estimation of this parameter may be highly uncertain as PFAS concentrations in the chorion have not been measured.

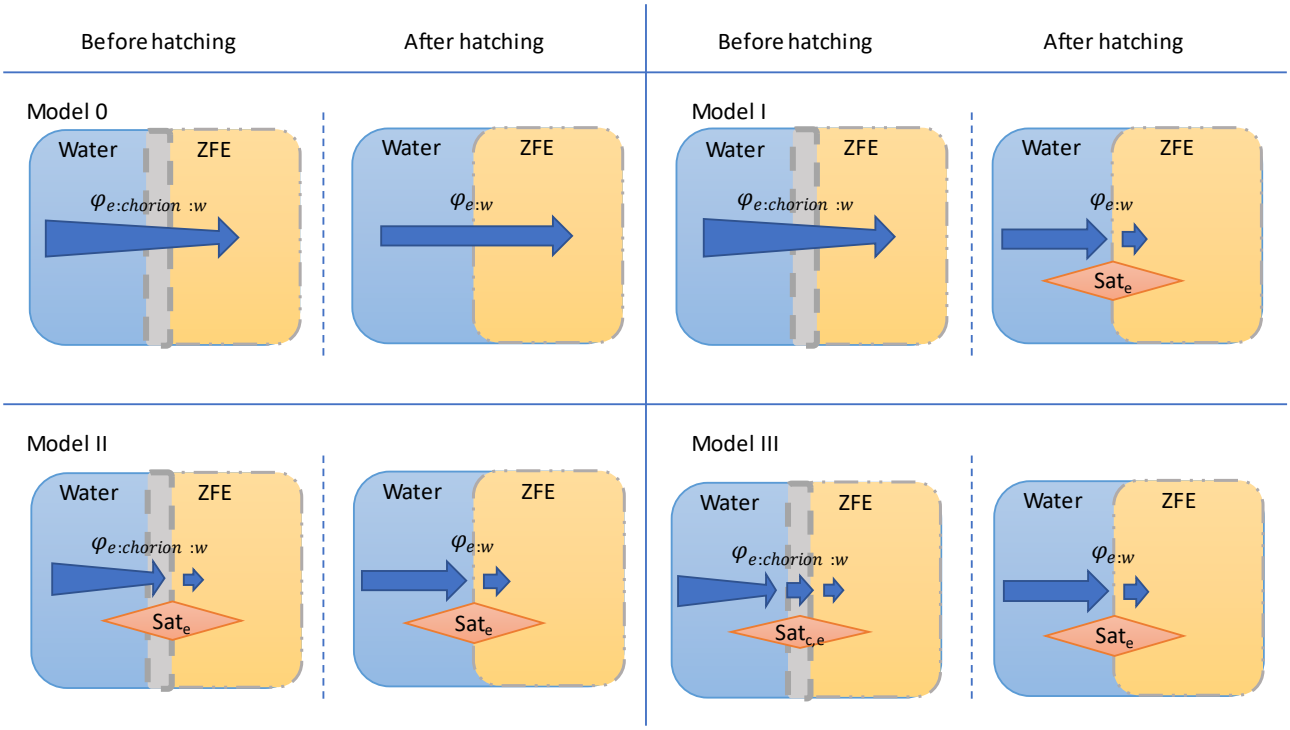

Figure 2. Structure of the four tested models to study the influence of saturation influx ($\varphi_{e:w}$ is the exchange rate between the water and the embryo per zfe body surface area, $\varphi_{e:chorion:w}$ is the exchange rate between the water and the embryo limited by the chorion permeability, Sat_e is the saturation of the embryo permeability, $Sat_{c,e}$ is the saturation of the chorion and embryo permeability).

2.1.3. Model parameters

2.1.3.1 Physiological parameters

The physiological parameters of the model are those of the original model (Billat et al., 2022; Simeon et al., 2020). These are the ontogenesis of the different organs, the growth rate of the organs, the rate of consumption of the yolk sac, and information on the volumes of the different organs.

2.1.3.2 PFAS-specific fixed parameters of the QSAR VIVD model

Partition coefficients ($P_{i:water}$) have been estimated using a QSAR model (VIVD model) (Fisher et al., 2019) except for the chorion:water partition coefficient (obtained by calibration). This QSAR approach has been developed using small acidic or neutral molecules whilst PFAS consist of long fluorinated chains with both acidic and lipophilic properties. Therefore, these parameters have been adjusted by Bayesian calibration using a correcting factor (fpc) (Table S1).

2.1.3.3 PFAS-specific fixed parameters of the PBTK model

Measured PFOA, PFHxS, and PFBA concentrations in the exposure water without zfe do not change over time, suggesting low or no interaction with glass or air (Vogs et al., 2019). Moreover, these compounds are mainly present in ionic form, and their Henry constants are less than $1E^{-7}$ $atm.m^3.mol^{-1}$, implying a very limited evaporation capacity. Therefore, the exposure water/container and exposure water/air transfer coefficient have been set to null values for PFOA, PFHxS, and PFBA.

PFOS evaporation has been also ruled out for the same reasons as the other PFAS (log K_{aw} very low and ionic form predominant). However, PFOS medium concentrations decreased over the first three hours of the experiment with *c.a. 20 %* observed in media with and without zfe present, suggesting adsorption of PFOS to the glass of the exposure vessel. The initial diffusion equations involving the recipient and water have been therefore modified, to introduce this loss due to adsorption (SI, Model code). In the absence of further data, it is not possible to propose an explanation for this phenomenon with enough certainty. An empirical equation leading to a good fit of the model to the kinetic data of PFOS in water with zfe has been chosen (Figure S1):

$$\frac{dQ_{wall}}{dt} = F_{wall} \cdot \left(S_{pw} \cdot C_{water} - \frac{Q_{wall}}{P_{pw}} \right) \qquad \textit{Eq. (11)}$$

S_{pw} (mm^2) is the contact surface between the water and the exposure vessel. This equation admits two parameters F_{wall} and P_{pw} calibrated with the kinetic data in the culture medium without zfe, using the nominal concentrations, $4.0E^{-2}$ µM (C1), $8.0E^{-2}$ µM (C2), and 0.76 µM (C3). The parameter values obtained (Table S1) are used to simulate the water concentration as input to the model for PFOS.

No metabolites have been quantified for PFBA, PFHxS, PFOA, and PFOS in zfe, and PFAS metabolism in zfe is therefore considered low or absent depending on the compound (Han et al., 2021). Together with the high bioconcentration factors reported in Vogs et al. (2019), the metabolic clearance has been therefore set to 0. The *a priori* distribution values of the parameters selected for the input to the PBTK model are given in Table S2.

2.2. Calibration

2.2.1. Experimental design

The zfe TK data for the included PFAS have been generated at the Karolinska Institute (Vogs et al., 2019). Briefly, 30 zfe have been exposed to 30 mL of three different measured exposure concentrations of respective PFAS in a glass petri dish over 120 hours: 240, 550, and 4800 µM for PFBA, $6.0E^{-1}$, $8.0E^{-1}$, and 7.8 µM for PFHxS, 21, 41, and 340 µM for PFOA and $4.0E^{-2}$, $8.0E^{-2}$, and $7.6E^{-1}$ µM for PFOS. Five replicates with 5 pooled zfe in each have been sampled at each time-point: 3, 6, 9, 24, 31, 48, 72, 96, and 120 hpf. Experiments have been conducted twice, thus providing 10 measured concentrations of internal concentrations in the whole zfe per time-point. Detailed descriptions of the protocol and experimental design are provided in Vogs et al. (2019).

2.2.2. Data handling

Raw data of the chromatogram peak areas have been provided by the authors from Vogs et al. (2019). Outliers have been excluded when values are contrasting by, at least, four standard deviations from the rest of the observations. The data expressed in moles have been transformed into millimolar concentrations, using the zfe growth model proposed by Simeon et al. (2020).

2.2.3. Sensitivity analysis

The parameters influencing the zfe PBTK model the most have been identified with a sensitivity analysis (SA) using the variance-based Sobol method (Saltelli et al., 2010; Sobol' et al., 2007). The sensitivity of the exchange rates between water and zfe ($\varphi_{e:chorion:w}$, $\varphi_{e:w}$), partition coefficients, permeability delay (ϕ), and uptake saturations ($EC_{sat,c,e}$, $EC_{sat,c,e}$) have been estimated with uniform distributions ± 10%. In this SA analysis, partition coefficients have been set to the values calculated using the VIVD model corrected by the scaling factor (simulation design detailed in Table S3).

The influence of the parameters has been investigated at the whole zfe level and selected tissues including liver, muscle, and yolk at 12, 24, 48, 72, 96, and 120 hpf. The SA has been carried out using the experimental factors of Vogs et al. (2019) including a temperature of 28 ± 1 °C and exposure under 24 h dark conditions.

2.2.4. Fitting the model to the experimental data by Bayesian inference

Bayesian inference has been used to fit parameter distributions of the four versions of the model (model 0 – model III) to each observed concentration (geometric mean of the 10 experimental values) per PFAS using the prior distributions presented in Tables S1 and S2. Regarding the experimental data distribution, it has been assumed that $C_{embryo\ total}(t)$ follows a lognormal distribution around the PBTK model predictions (taken as geometric mean). The error has been estimated to be 10 %, corresponding to both analytical errors and inter-individual variability. Three independent Monte-Carlo Markov chains of 100,000 iterations have been generated for each fit. Different initial values have been randomly assigned to each chain. The convergence of the chains has been assumed when the Gelman and Rubin convergence criteria is lower than 1.1 (Gelman and Rubin, 1996). After convergence of the chains, the last 1000 parameter vectors of each chain have been kept, forming the *a posteriori* distribution of the parameter values, used for simulations afterward. The 95 % credibility interval has been constructed using the *a posteriori* quantiles (0.025-quantile and 0.975-quantile, respectively). Finally, the values of estimated priors for which the likelihood value is maximized have been selected and referred to as maximum posterior values (MPV).

2.3. Selection of the final model

For each compound, the best model has been selected using the Akaike information criterion (AIC), Bayesian information criteria (BIC) and the normalized root mean square error (NRMSE). In case of discrepancies between the two measures, the AIC has been preferred as it favors the more parsimonious submodel.

2.4. Evaluation dataset

An extensive review of the literature has been performed on February 16th, 2022, to collect literature-reported PFAS concentrations measured in zfe to be used as an external validation dataset. The following keywords have been used on both Pubmed® and ISI Web of knowledge™ databases: “ALL =(((zebrafish*) OR (danio*)) AND ((PFBA)OR(PFHxS)OR(PFOA)OR(PFOS)) AND ((Juvenile) OR (larva*) OR (embryo*) OR (eleuthero*)))” and returned 146 results. The papers have been selected when i) at least one concentration is measured both in the exposure water and the zfe and ii) the zfe age is no older than 120 hpf at the time of

first dosing. Finally, seven unique publications have been identified (Gaballah et al., 2020; Han et al., 2021; Huang et al., 2010; Menger et al., 2020; Spulber et al., 2014; Tu et al., 2019; Wang et al., 2020) (Table 1).

Carboxylesterases are highly expressed and active in the lungs (Morris, 1990; Satoh and Hosokawa, 2010) and even in the mucus (Kang et al., 2021)

Table 1. Toxicokinetic studies of PFAS selected for external validation dataset.

Molecule	Nominal water concentrations (µM)	Exposure medium volume (mL)	Device material	Number of timepoints per dose level	Number of eleutheroembryos pooled per timepoint	Age at the time of dosing (hpf)	Exposure duration (hours)	Temperature (K)	Light exposure (hours)	Reference
PFBA	0.5, 5	3	24-well plate, assumed to be plastic	1	20	2	120	301.65	14	(Han et al., 2021)
PFHxS	0.5, 5	3	24-well plate, assumed to be plastic	1	20	2	120	301.65	14	(Han et al., 2021)
	2.1	10	Plastic Petri dish	1	40	0	144	299.15	12	(Menger et al., 2020)
	14, 25, 45	0.25	Styrene 96-well plate	1	10	4	144	299.15	14	(Gaballah et al., 2020)
PFOA	0.5, 5	3	24-well plate, assumed to be plastic	1	20	2	120	301.65	14	(Han et al., 2021)
	2.4	10	Plastic Petri dish	1	40	0	144	299.15	12	(Menger et al., 2020)
	25, 45, 80	0.25	Styrene 96-well plate	1	10	4	144	299.15	14	(Gaballah et al., 2020)
	96.6	5	6-well plate, assumed to be plastic	1	10	6	120	301.15	14	(Wang et al., 2020)
PFOS	0.186, 1.86	0.75	48-well plate, assumed to be plastic	1	63	2	144	301.15	14	(Spulber et al., 2014)
	0.27	10	Plastic Petri dish	1	40	0	144	299.15	12	(Menger et al., 2020)
	0.5, 5	3	24-well plate, assumed to be plastic	1	20	2	120	301.65	14	(Han et al., 2021)
	1, 1.8, 3.12	0.25	Styrene 96-well plate	1	10	4	144	299.15	14	(Gaballah et al., 2020)
	0.05, 0.5, 5	500	Glass beaker	1	No data (set to 30)	3	96	301.65	12	(Tu et al., 2019)
	1, 4, 8	6	96-well plate, assumed to be plastic	1	30	6	120	301.15	10	(Huang et al., 2010)
	4	6		9	10	1	120	301.15	10	(Huang et al., 2010)

2.5. Software

The implementation of the PBTK model and the Bayesian inference calculations using the MCMC algorithm have been carried out using the GNU MCSim software, version 6.2.0 (Bois, 2009). The analysis of the quality of the inference as well as the graphical representations of the results have been performed on R version 4.0.2. The R packages msm (version 1.6.9), and IDPmisc (version 1.1.20) have been used when processing the output of the MCMC strings provided by GNU MCSim and ggplot2 (version 3.3.5) have been used for the generation of the graphics.

3. Results

3.1. Hatching submodel

The observed and predicted kinetic of hatching for 12h:12h light:dark cycles at different experiment temperatures are represented in Figure 3. A higher proportion of hatched zfe in the first batch (45 to 50 hpf) with higher incubation temperatures are clearly observed and modelled: from less than 5% at 24 °C to approximately 80% at 28 °C. Interestingly, at the highest temperature (28°C), almost all the zfe hatched during two sessions: from 45 to 50 hpf and from 68 to 76 hpf. However, at 24 and 26°C, three hatching sessions are identified: from 45 to 50 hpf, 68 to 74 hpf, and 90 to 96 hpf.

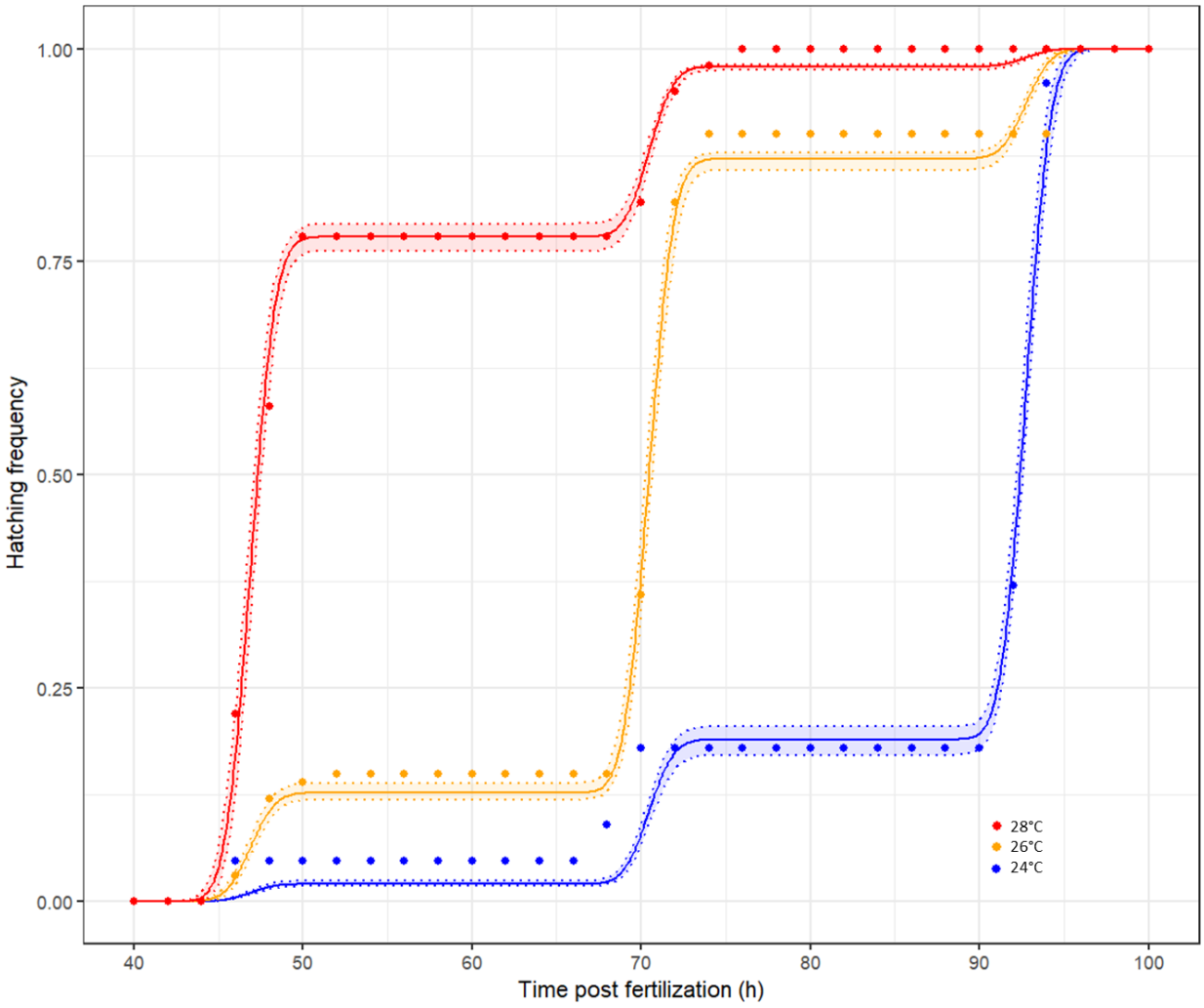

Figure 3. Cumulated frequency of hatched zebrafish embryos at daily exposure to 12:12h light:dark cycles in dependence of three incubation temperatures according to (Villamizar et al., 2012). The blue, orange and red dots are hatching frequencies observed every two hours at 24°C, 26°C, and 28°C, respectively (30 zfe per temperature group) reported by (Villamizar et al., 2012). The corresponding blue, orange, and red solid lines

represent the predicted cumulated frequency at 24°C, 26°C, and 28°C, respectively. The bands between the dotted lines are the 95% credibility intervals.

The hatching sub-model parameters resulting from model fitting are given in Table 2 for the three different photoperiods as reported by Villamizar et al. (2012). Photoperiods seem to have a clear impact on the proportion of hatching zfe in the first and last hatching sessions, whilst having a weak impact on the average time of each session.

Table 2. Maximized posterior values of hatching parameters depending on light exposure and temperature. The parameter values shown below are for the reference temperature(T_R = 25°C).

Daily light exposure (h)	0	12	24
Average time of hatching on first event (hpf)	49.0	46.9	49.1
Average time of hatching on second event (hpf)	66.0	70.4	65.6
Average time of hatching on third event (hpf)	92.5	92.7	89.0
Standard deviation of hatching time (hpf)	1.76	1.16	1.49
$W_{1,ref}$	0.013	0.051	0.093
$W_{3,ref}$	0.49	0.32	0.31
TA (K)	25100	81600	27700

3.2. Model selection

The evaluation criteria (AIC, BIC, RMSE, and NRMSE) of the different sub-model structures for PFBA, PFHxS, PFOS, and PFOA are summarized in Table S4. Based on these results, the most appropriate structure models were the structures including Sat_e (Equation 9, model II) for both carboxylic acids (PFBA and PFOA) and with both saturation (Sat_e and $Sat_{c,e}$, Equation 10, model III) for both sulfonic acids (PFHxS and PFOS), in the range of the tested dose levels.

3.3. Sensitivity analysis

Before the calibration process, a SA has been performed for each PFAS. Considering the whole zfe concentration, the most influential parameter before hatching is the PFAS binding to the chorion (12 hpf,

Figure 4, upper panel). The parameters influence profiles on zfe PFAS concentrations are slightly different between Model II (used for both carboxylic acids) and Model III (sulfonic acids) at 12hpf. For instance,

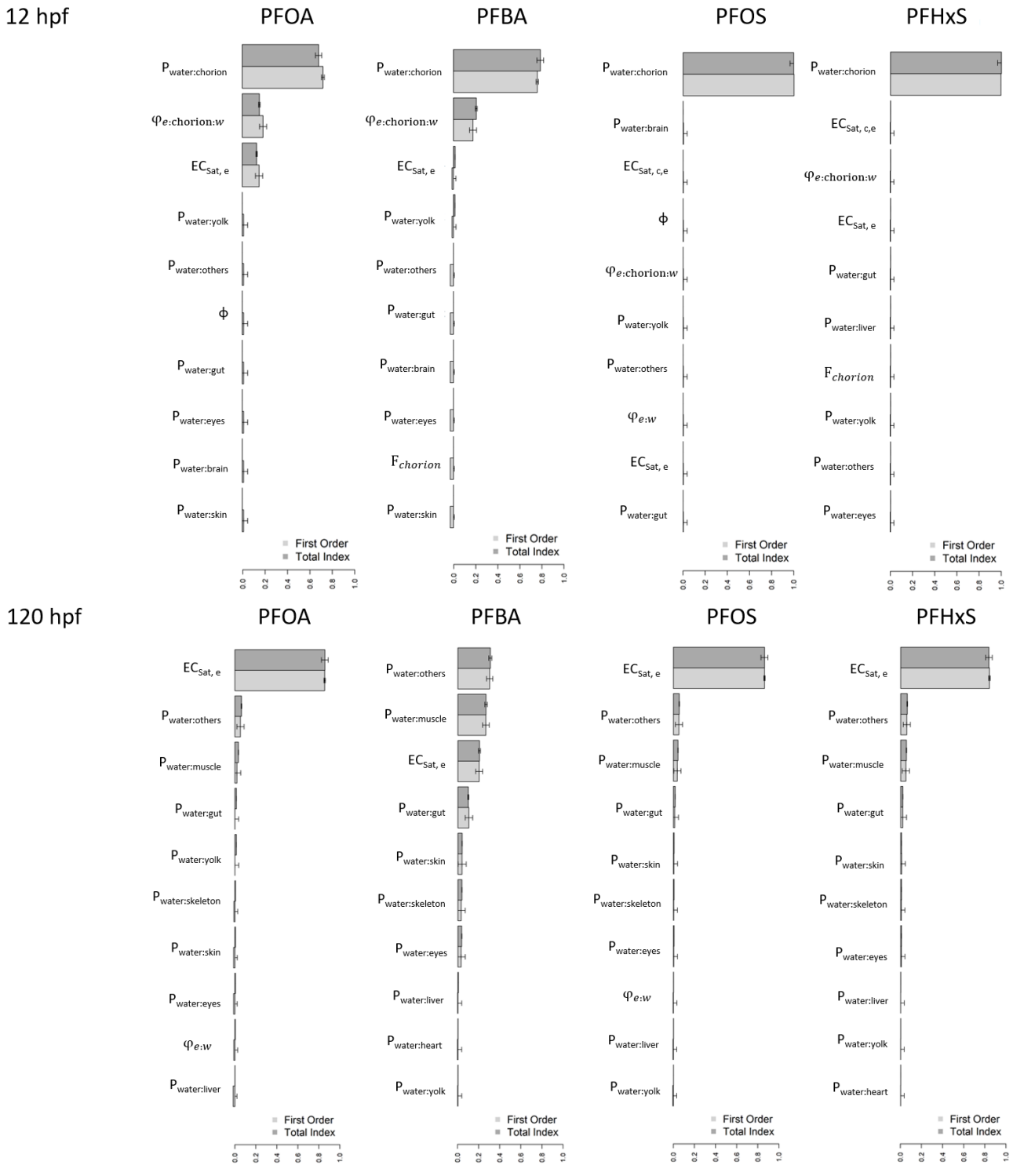

$\varphi_{e:chorion:w}$ and $EC_{sat,e}$ seem to have also a clear impact on the zfe concentration before hatching using Model II (PFOA and PFBA), whilst using Model III (PFOS and PFHxS), the compound binding to the chorion seems to be the only parameter influencing the TK at 12hpf.

Figure 4. Sensitivity analysis on the zfe total concentrations predicted by Model II (PFOA and PFBA) and Model III (PFOS and PFHxS) at 12, and 120 hpf (upper and lower panels, respectively). The 10 most influential parameters are represented. P stands for partition coefficient, F for flow, EC_{Sat} for saturation constant, and ϕ for the delay between the start of permeabilization of the chorion and the hatching.

The order of the most influencing parameters changes during zfe development (Figure S2-S17). Between 12 and 24 hpf, the parameter ϕ (shift time between chorion permeability start time and the overall zfe population hatching dynamics) is the most influencing parameter for PFOA, PFOS, and PFHxS, underlying the central role of chorion permeability and hatching for PFAS exposure in the whole zfe. Post-hatching, however, exposure to PFOA, PFOS, and PFHxS is mostly influenced by the uptake saturation ($EC_{sat,e}$). In contrast, PFBA sensitivity analysis shows a slightly different profile with uptake saturation ($EC_{sat,e}$) as the second or third most influential parameter after partition coefficients (other organs and muscles to water), in line with its TK profile suggesting a rapid initial uptake.

At the tissue level, as expected, the 3 most influential parameters before hatching are the exchange rate between water and zfe limited by the chorion permeability ($\varphi_{water:chorion:embryo}$), the uptake saturation constant ($EC_{sat,c,e}$), and the related tissue:water partition coefficient ($PC_{i:water}$) (Fig S2-17). The influencing parameters pattern at tissue level is similar as those observed for the whole embryo at later timepoints.

3.4. Bayesian calibration of *a posterior* distributions

The maximum posterior values are given in Table 3. Convergence of chains has been successful for all calibrated parameters, with narrow posterior distributions. 96% of the simulations are within a 2-fold error interval and all simulations fall with a 3-fold error interval except for one concentration for PFOS, namely the second concentration (C2) at 6 hpf for which an over-prediction of a 3.14 factor is observed (Figure 5). The simulated TK profiles fit accurately the observations as shown in Figure 6 for the highest concentration (C1). Figures S18, S19, S20, and S21 present the observed and predicted concentrations of PFBA, PFHxS, PFOA, and PFOS, respectively, in the total zfe as a function of time, for the respective retained models.

Table 3. Summary of posterior distributions for the estimated parameters of the PBTK model for PFBA, PFHxS, PFOA, PFOS. The distributions were obtained using a Bayesian calibration approach.

Compound (model structure)	Maximum posterior value (MPV)	Median	CI 95%
PFBA (model II)			
f_{pc}	2.22	2.17	[1.99 ; 2.33]
$\varphi_{water:embryo}$ (µL/h/mm²)	82.7	64.1	[15.1 ; 98.5]
$\varphi_{water:chorion:embryo}$ (µL/h)	4.04E^{-4}	4.28E^{-4}	[2.93E^{-4} ; 6.31E^{-4}]
$\varphi_{water:chorion}$ (µL/h)	48.8	49.8	[2.28 ; 97.4]
$P_{water:chorion}$	0.881	0.867	[0.756 ; 0.973]
ϕ (h)	2.11	1.42	[-0.185 ; 2.49]
$EC_{sat,e}$ (mM)	3.76	4.19	[3.33 ; 5.41]
PFHxS (model III)			
f_{pc}	502	493	[465 ; 522]
$\varphi_{water:embryo}$ (µL/h/mm²)	99.4	88.3	[50.4 ; 99.6]
$\varphi_{water:chorion:embryo}$ (µL/h)	1.17E^{-2}	1.13E^{-2}	[8.48E^{-3} ; 1.44E^{-2}]
$\varphi_{water:chorion}$ (µL/h)	81.4	50.3	[2.95 ; 97.9]
$P_{water:chorion}$	5.38	5.55	[4.49; 6.64]
ϕ (h)	-23.8	-23.9	[-24.5 ; -23.6]
$EC_{sat,e}$ (mM)	5.84E^{-2}	8.84E^{-2}	[4.07E^{-2} ; 3.205E^{-1}]
$EC_{sat,c,e}$ (mM)	5.32E^{-3}	5.51E^{-3}	[3.91E^{-3} ; 7.72E^{-3}]
PFOA (model II)			
f_{pc}	184	186	[166 ; 208]
$\varphi_{water:embryo}$ (µL/h/mm²)	0.801	0.997	[0.642 ; 1.88]
$\varphi_{water:chorion:embryo}$ (µL/h)	7.09E^{-3}	1.00E^{-2}	[5.72E$_{-3}$; 1.19E^{-2}]
$\varphi_{water:chorion}$ (µL/h)	19.0	55.7	[13.0 ; 97.5]
$P_{water:chorion}$	2.68	2.49	[2.14 ; 2.97]
ϕ (h)	-27.4	-22.3	[-28.3 ; -19.6]
$EC_{sat,e}$ (mM)	8.61E^{-2}	8.48E^{-2}	[7.02E^{-2} ; 0.101]
PFOS (model III)			
f_{pc}	10400	10300	[9530 ; 11100]

$\varphi_{water:embryo}$ (µL/h/mm²)	99.9	98.3	[91.2 ; 99.9]
$\varphi_{water:chorion:embryo}$ (µL/h)	0.793	0.848	[0.705 ; 1.10]
$\varphi_{water:chorion}$ (µL/h)	98.6	49.1	[2.77 ; 97.4]
$P_{water:chorion}$	31.7	31.9	[22.9 ; 42.2]
ϕ (h)	-28.7	-29.1	[-30.5 ; -27.9]
$EC_{sat,c,e}$ (mM)	$7.33E^{-5}$	$6.75E^{-5}$	[$4.12E^{-5}$; $9.87E^{-5}$]
$EC_{sat,e}$ (mM)	$1.10E^{-3}$	$1.18E^{-3}$	[$8.13E^{-4}$; $1.90E^{-3}$]

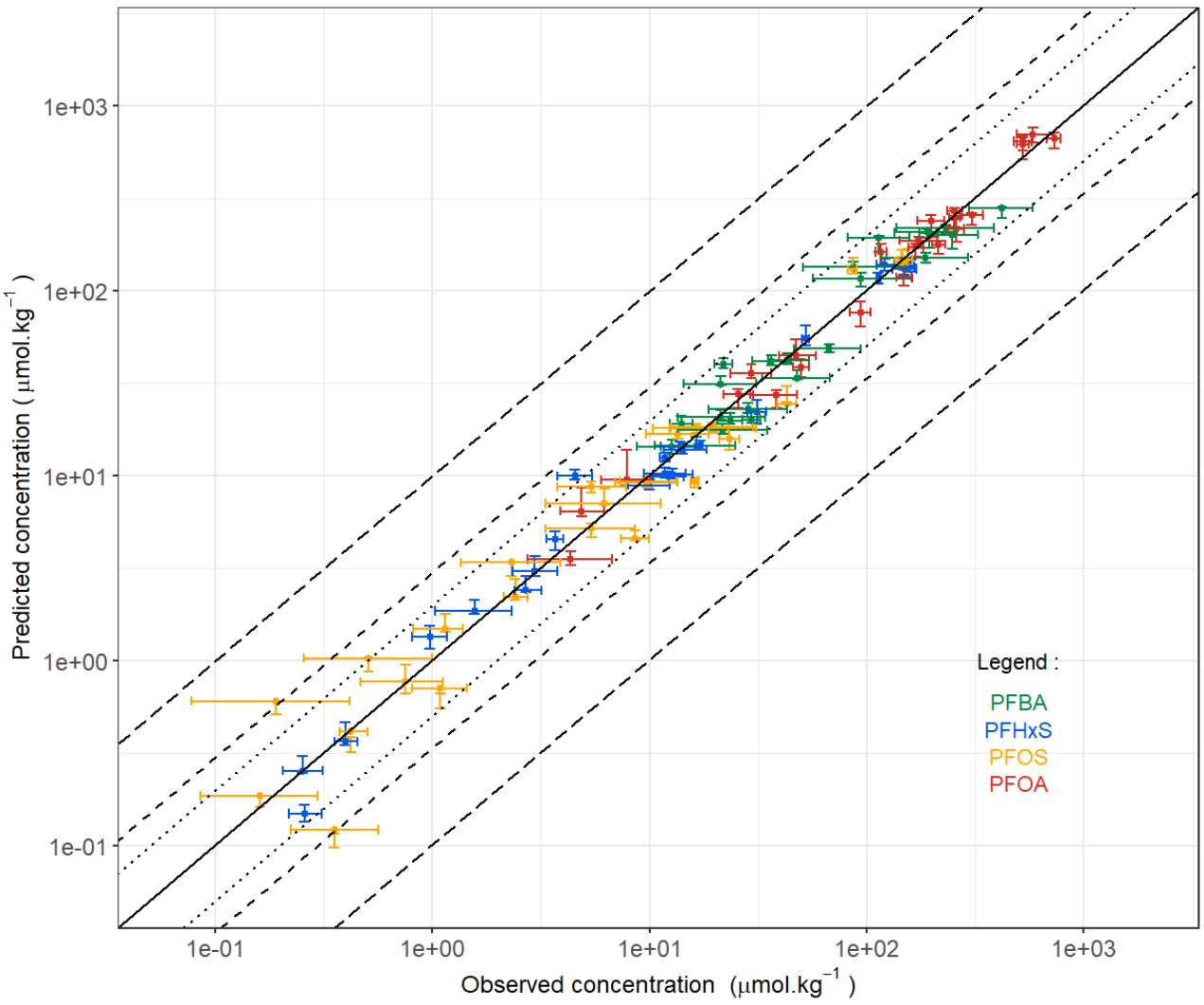

Figure 5. Measured vs. predicted internal whole-body concentrations for PFBA, PFHxS, PFOS, and PFOA. The modeled zfe internal concentrations were predicted based on maximum posterior values of parameters. Each predicted value is given as geometric mean and its 95% credibility interval. Similarly, each measured value is given by its geometric mean and 95% confidence interval (n = 10). The dotted intervals represent the 2-fold, 3-fold and 10-fold error intervals.

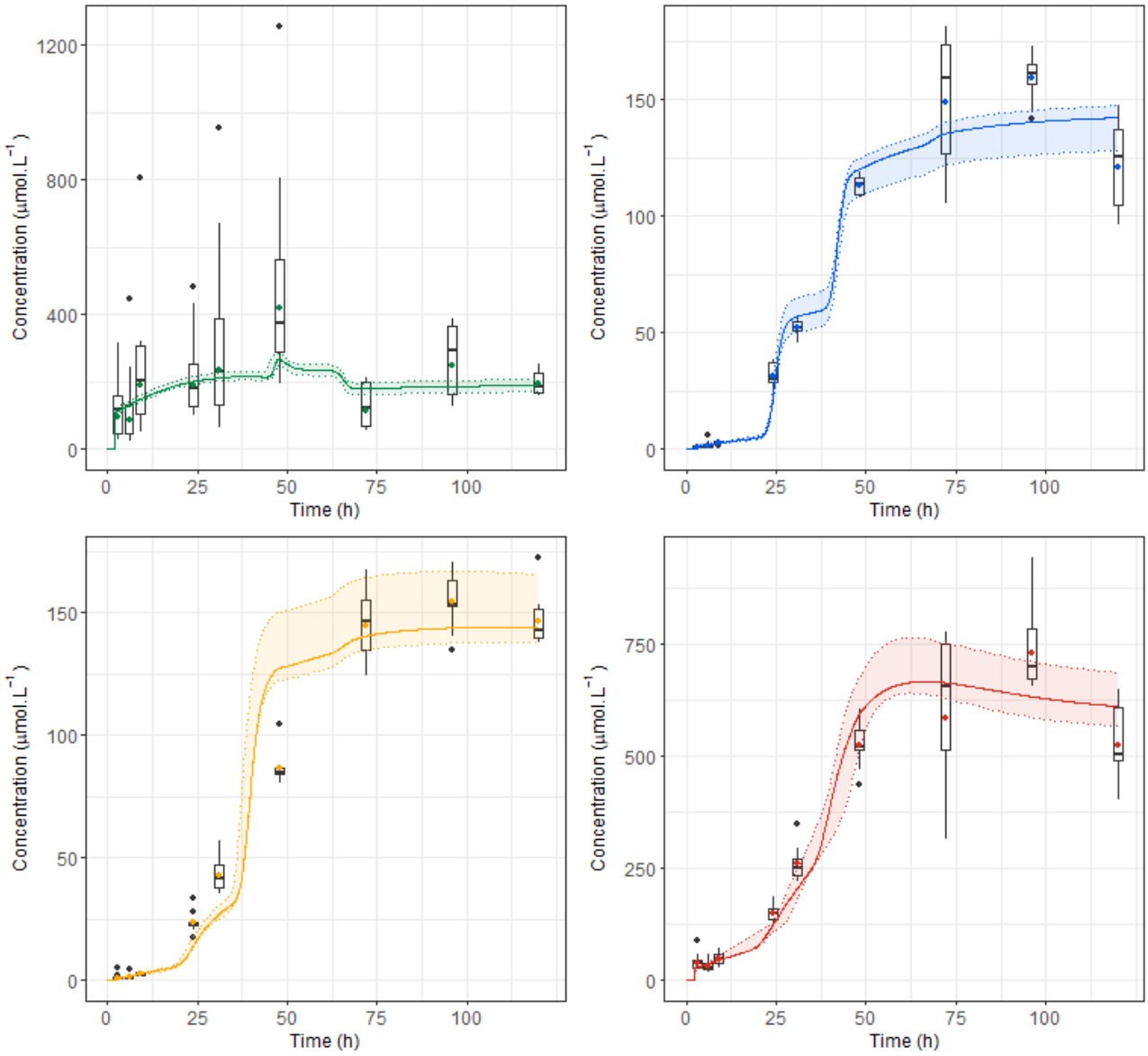

Figure 6. Predicted and observed internal concentrations of PFBA (green), PFHxS (blue), PFOS (yellow), and PFOA (red) in the whole embryo exposed to the highest concentration in the function of time. The colored points are geometric means of the experimental data. Boxplots have been superimposed on the experimental points. The colored trajectories are the internal predicted concentrations at the joint a posteriori mode. The area between the dotted lines corresponds to the 95% credibility interval.

Regarding PFBA, model II (including a saturable zfe uptake) accurately fits the observed decrease in the zfe concentrations between 48 and 72 hpf. The calibrated value of the correction factor of the partition coefficient, fpc, is slightly greater than 1 (Table 2 and Table S5) suggesting that the QSAR VIVD model under-predicted the partition coefficients, for the selected fit. The $EC_{sat,e}$ (3.76 mM) is close to the highest

concentration tested (4.80 mM) suggesting that the zfe uptake is half saturated at this concentration. Finally, the permeabilization of the chorion occurs 2.11 hours after the theoretical hatching time.

Model II is also the most appropriate one to fit PFOA kinetics. The saturation term $EC_{sat,e}$ (86.1 µM) is lower than the highest nominal concentration (340 µM) and close to the intermediary concentration (41 µM) of the three datasets. Finally, fpc is equal to 186, thus VIVD model predictions are strongly revalued upwards by the calibration.

Regarding PFHxS (Model III), there is a constant increase of internal PFHxS concentrations in contrast to PFBA, with uptake accelerating after 24 hpf and then slowing down as the steady-state is approached. Furthermore, the saturation term $EC_{sat,c,e}$ (5.32 µM) is also close to the value of the highest nominal concentration of the three tested concentrations, at 7.8 µM (C1), whilst the uptake saturation occurring after permeabilization of the chorion is higher (58.4 µM) than the C1 concentration (Table 3). The partition coefficient predictions of the QSAR VIVD model are strongly under-predicted and increase by a 502-fold factor after calibration.

Interestingly, PFOS reveals kinetics like PFHxS (model III), which are both sulfonic acids. No or low saturation can be evidenced after hatching (saturation constant of 1.10 µM for a high dose level of 0.76 µM), whilst, before hatching the saturation constant decreases to 73.3 nM suggesting that, in the range of the tested dose levels, low uptake may occur. To an even greater extent than for PFHxS, the predicted organ/medium exposure partition coefficients are strongly under-predicted by the QSAR VIVD model and increase by 10400-fold after the calibration (Table 2).

The impact of the hatching dynamics within a zfe population over development is exemplified using the PFOS TKs: Figure 7 represents the TK at the individual level (one zfe) and at the population level (using zfe pool of 30 individuals). Individual TK profiles shift from a low level before hatching to a high concentration level after hatching, whereas the population TK profile is smoother.

Interestingly, it can be noticed that the calibrated value of ϕ suggests a chorion permeability increase 24 hours earlier than the average times of hatching (µ1, µ2, and µ3) for PFOS, PFHxS, and PFOA. The first hatching

batch seems negligible in the hatching dynamics, thus suggesting that the permeabilization of the chorion is mainly explained by 2 batches occurring at approximately 40 hpf and 65 hpf (Figure 7). In contrast, the chorion permeability in the case of PFBA occurs mainly at approximately 68 hpf (*ie* the beginning of the third day post-fertilization) and 94 hpf (the beginning of the fourth day), with a very small first batch at approximately 50 hpf.

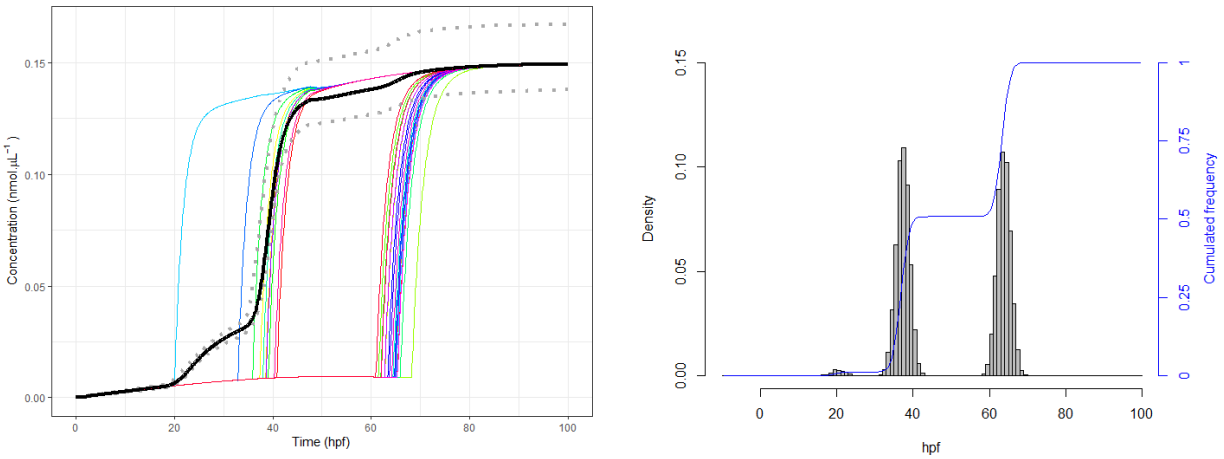

Figure 7. PFOS individual and population toxicokinetic profiles in zfe (left panel) and prediction of the frequency of permeabilized chorions using the calibrated value of ϕ (right panel).

Colored lines represent 30 individual TK profiles with random times of chorion loss. Black and grey lines represent the resultant average TK profile at the population level. Exposure to PFOS was simulated in zfe using the highest PFOS dose level (0.76µM) and experimental conditions as performed by Vogs et al. (2019) (28°C, 0:24 light:dark exposure conditions).

3.5. External validation

Data have been handled as described in paragraph 2.2.2. More particularly, quantities have been preferred to concentrations, when available, to ensure consistency throughout the different studies' conversions.

Simulations have been performed using the posterior distribution of the calibrated parameters. To this end, the exposure conditions have been adapted for each study to be similar to the conditions described in the publications. The predictions for each study have been thus compared to the observed values (Figures 8, S22). 18 values are within 3-fold error (49%), 15 between 3 and 10-fold error (40%), and 4 out of the 10-fold error (11%). PFBA seems predicted with less accuracy, but few data are available for this compound, and observed concentrations reveal a huge variability.

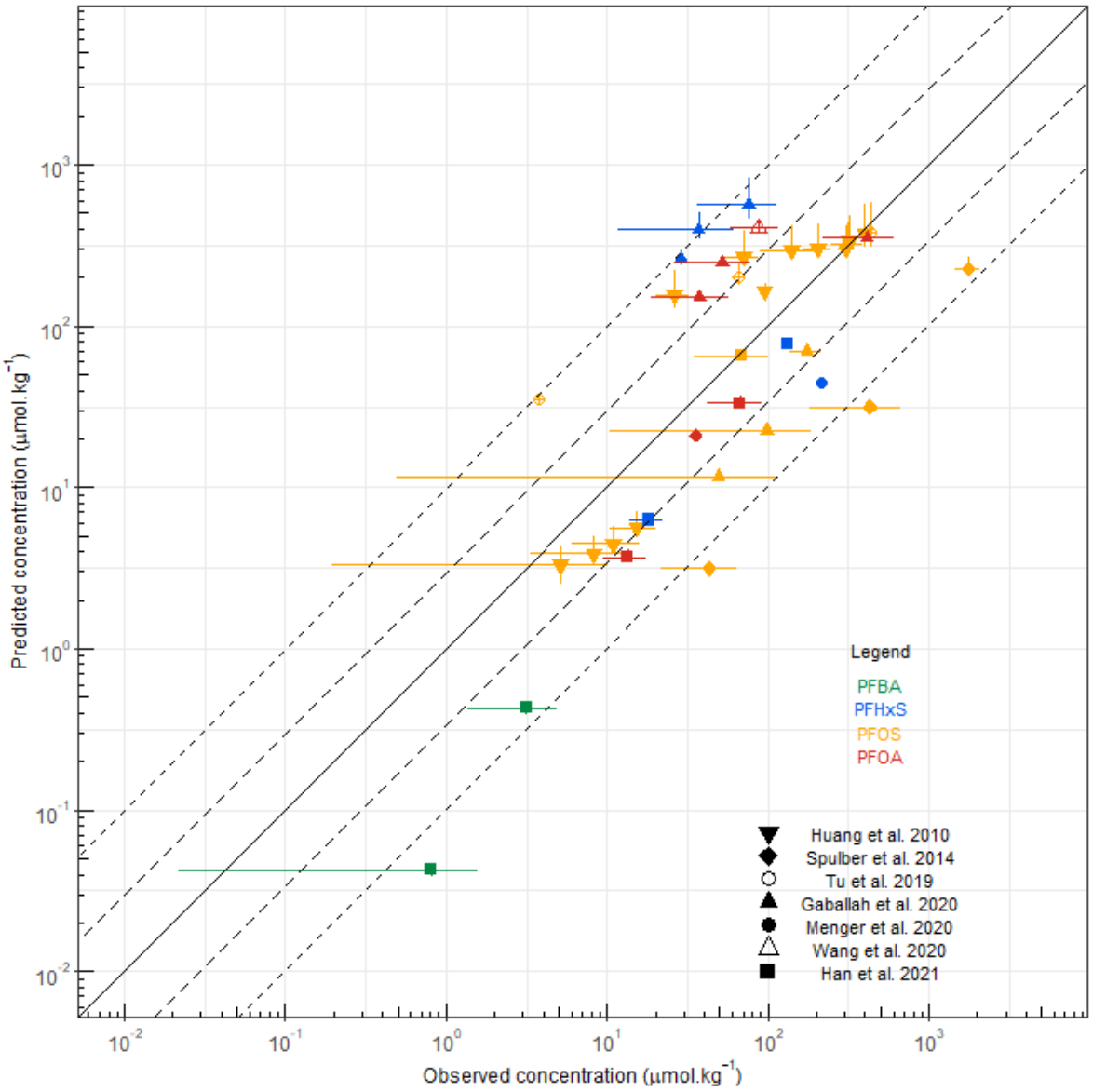

Figure 8. Evaluation of the model predictive capacities: observed vs. predicted internal concentrations for PFBA, PFHxS, PFOS, and PFOA on the external dataset.

3.6. Intra tissue concentrations

The current model relies on an aggregate of several tissues. Therefore, the kinetics of each compound in four organs of interest (brain, liver, eyes, and yolk) can be easily pictured (Figure 9). The shape of the kinetics in each organ roughly follows the compound kinetics at the whole-body scale with slight tissue differences.

The steady-state concentrations seem to be reached rapidly in tissues while no steady state could be observed in the global zfe. The zfe concentration is depending on the compound amount in each organ but also on the size of these organs (yolk is decreasing in size for instance whilst other tissues' volumes are

increasing). Each compounds TK profile in the brain, liver, and eyes are similar accordingly to their similar corrected partition coefficients (9-56% variation).

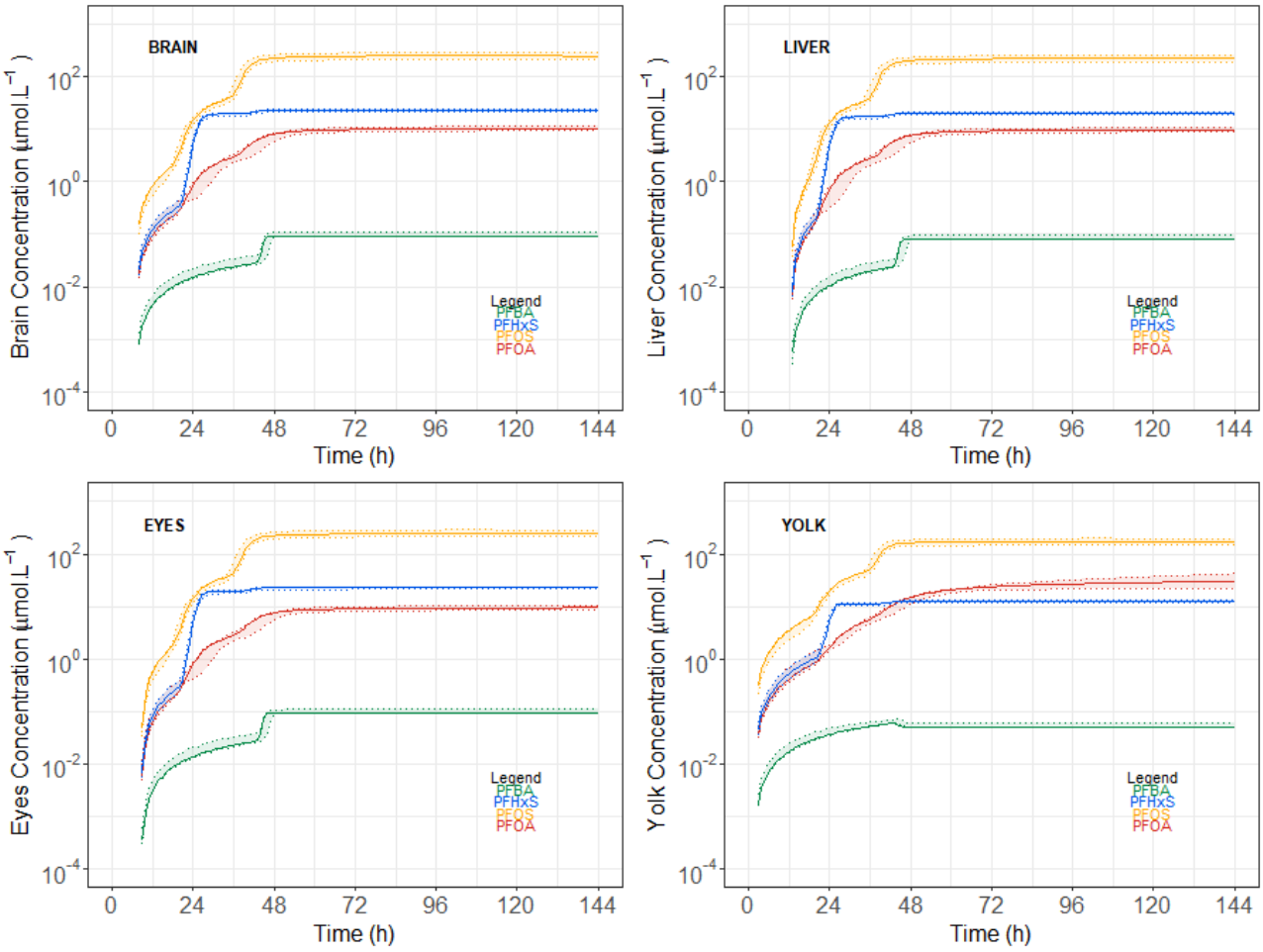

Figure 9. Predicted brain, liver, eyes, and yolk sac concentrations of PFBA, PFHxS, PFOA, and PFOS in the whole embryo exposed to 1 µM under the same experimental conditions as described in Vogs et al. (2019), for the selected versions of the model. The colored trajectories are the internal predicted concentrations at the joint a posteriori mode. The area between the dotted lines corresponds to the 95% credibility interval.

4. Discussion

The existing zfe PBTK model has been successfully updated using PFBA, PFHxS, PFOA, and PFOS, and all of their measured concentrations from Vogs et al. (2019). By considering the critical impact of experimental temperature and light cycle settings on zfe development and hatching, as well as possible saturation processes and the hatching dynamics within a zfe population over development, the predictions and robustness of the model under the different experimental designs have been improved compared to the previous version of the PBTK model (Billat et al., 2022) (data not shown).

In the previous version of the PBTK model, the hatching was set to occur at 48 hpf and the hatching dynamics within a zfe population was not considered. In the improved model presented here, different hatching scenarios have been considered depending on light exposure and temperature. The sub-model developed for this purpose successfully predicts the data described in (Villamizar et al., 2012). This work highlights the necessity to consider the hatching dynamics within a zfe population over development and suggests that internal concentrations could follow a bimodal distribution within a zfe sample depending on the hatching status of the individuals (exemplified on Figure 7 for the PFOS at 50 hpf with two subpopulations). Consequently, a bimodal distribution of the physiological response can be observed under similar exposure conditions and confound the response investigated. This drawback may be overcome by pooling enough zfe per sample to have an insight into the average internal concentration when performing the effect assay.

The hatching process may be a critical step in chemical uptake as it removes the chorion which may act as a chemical barrier (Hagedorn et al., 1997; Pelka et al., 2017; Schwartz et al., 2021). Also, hatching is not a linear process over developmental time and requires an enzymatic and ionic process, thereby increasing the permeability of chemicals before the actual hatching (Kim et al., 2006; Muraina et al., 2020; Trikić et al., 2011). In the zfe, the hatching glands are differentiated and mature at 48 hpf but their stimulation is depending on hormonal signals (De la Paz et al., 2017), suggesting that permeabilization can start as early as 48 hpf. In agreement with this observation, the calibrated values of ϕ for PFOS, PFHxS, and PFOA suggest that the permeabilization of the chorion mainly occurs in two batches at approximately 40 hpf and 65 hpf, a few hours before hatching (Figure 7). In agreement with our model, Hagenaars et al. (2011) and Vogs et al.

(2019)reported that under control conditions almost all of the zfe hatched between 48 and 60 hpf. On the contrary, the dynamics of the chorion permeability to PFBA (2.1 hours after the theoretical time of hatching), suggests that the permeabilization and/or the hatching may be delayed for this substance compared to the hatching dynamics reported by Villamizar et al. (2012). No adverse effects of the four PFAS have been evidenced at the tested dose levels of Vogs et al. (2019). Consequently, it sounds reasonable to assume that the tested compounds at the current dose levels have not interfered with normal biological processes such as ontogenesis and hatching (Hagenaars et al., 2011; Tu et al., 2019; Ulhaq et al., 2013). Therefore, inter-laboratory and/or zfe family/lineage variabilities on hatching dynamics can be responsible for our observation and underline the need to monitor this variable in control conditions regardless of the TK and/or toxicodynamics (TD) endpoints monitored.

With regards to kinetics, the chorion is not a passive structure as it seems to store chemicals. For example, it has been suggested that PFAS may bind weakly to N-glycoproteins in the chorion (Bonsignorio et al., 1996). This binding could influence the TK of chemicals, specifically when the chorion:water partition coefficients are higher than the tissue:water partition coefficients. In the case of PFBA, the chorion:water partition coefficient is estimated to be 0.881, meaning approximately 10-16 fold higher than the tissue:water partition coefficients, while the chorion-partition coefficient is lower for the other PFAS (3-4 fold lower for PFHxS, 4-9 fold lower for PFOA, and 10-15 fold lower for PFOS). Altogether, this indicates that PFBA binding to the chorion may partially explain the decrease in the observed internal concentration around the hatching time through the loss of the chorion and its bound PFBA, as predicted well by the PBTK model. However, PFAS concentrations in the chorion need to be determined to prove this model-generated hypothesis.

The PBTK model also includes an uptake flux for the chorion binding ($\varphi_{water:chorion}$). This flow is found to be a high value, suggesting that binding to the chorion is very rapid or even immediate. The same is true for the water:zfe flows which gave high values for all the tested compounds. Thus, two hypotheses can be envisaged; either that the equilibrium between water and perivitelline space has been previously reached during the prehatching period or, that the water:zfe flow after permeabilization start is very rapid as previously suggested (Brox et al., 2014a). Interestingly, the water:chorion:zfe flow rates increase with the LogP value of

the compound, as PFOS>PFHxS≈PFOA>PFBA, and are inversely correlated with their water solubility, suggesting that the more lipophilic the molecule, the faster the uptake.

Saturation uptake processes are included in the two models (one or two saturation independent parameters) that most accurately simulate the calibration data. The model for the two sulfonic acids, PFHxS and PFOS, includes saturation processes on both pre- and post-hatching uptake flows modelled by two independent EC_{50}, whilst the model for the two carboxylic acids, PFOA and PFBA, includes a common EC_{50} for the two uptake flows. Therefore, the question arises whether active transport depends on the functional end group, and in turn, if and how this influence PFAS uptake in zfe. Both active and passive transport mechanisms for uptake and efflux exist for PFAAs (Ebert et al., 2020; Keiter et al., 2016). The SLC transporters superfamily is involved in active uptake and notably the saturable Oatp transporters (Kimura et al., 2017; Popovic et al., 2014; Zhao et al., 2016). In addition, PFAS/PFAS interaction has been reported at the level of transporters (Keiter et al., 2016; Popovic et al., 2014; Yang et al., 2009), therefore the kinetics of PFAS mixtures could be different from the kinetics of single congeners (as observed in (Menger et al., 2020)).

For all four compounds, calibration results suggest an underestimation of the partition coefficients predicted by the QSAR approach by 2.22-10400 orders of magnitude. Since the calibrated tissue:water partition coefficients are in the range of published BCFs (wet weight/volume) (Vogs et al., 2019), these results suggest that the QSAR VIVD model performs poorly for the selected PFAS. This may be related to the unique physicochemical properties of PFAS (acidic and lipophilic with a long-fluorinated carbon chain), whilst the VIVD model has been initially developed and validated using small neutral or acidic molecules. In addition, the VIVD model is a generic QSAR model relying on Henderson-Hasselbalch relationships but does not consider active transports, while nonlinear active transport with saturation is suggested by the PBTK model to influence the uptake of the studied PFAS.

The validation dataset predictions exhibit variable accuracy for a given PFAS. This variability can be partially explained by the uncertainty of the experimental protocols. Indeed, Kimura et al. (2017) have demonstrated in *in vitro* experiments that PFAS uptake is dependent on medium pH (the lower the pH, the higher the uptake). The tested compounds are acidic thus decreasing the pH of the water and favoring a higher uptake. Therefore,

variability in the water pH can lead to an underprediction of the uptake and thus of the internal concentrations but also to different toxicological findings as previously reported (Wasel et al., 2021). In the calibration dataset, the exposure media with PFOA and PFBA have been adjusted to pH 7.4. In the validation dataset, however, only 2 out of 7 studies have mentioned using a buffer during the exposure course (Gaballah et al., 2020; Wang et al., 2020). Considering the role of pH on PFAS TK profiles and toxicity, this stresses the importance for authors to include such details to ensure good quality data.

Recently, Warner et al. (2022) published a three-compartmental model for the zfe including chorion, yolk, and zfe using the same dataset from Vogs et al. (2019) to describe PFOA and PFOS kinetics. In their model, the authors have also added a possible saturation of the influx transporters for both PFOA and PFOS at the level of the chorion and the zfe. Regarding the saturation of the zfe uptake post-hatching, the values determined by Warner et al. (2022) and the present study are similar for PFOA (58.5 µM and 86.1 µM respectively). For PFOS, the present model suggests that saturation occurs before hatching ($EC_{sat,c}$: 73.3 nM) and is lower than described in Warner et al. (2022) (chorion: 1.30 µM, zfe:1.17 µM). After hatching however, the saturation constant increased in our model up to 1.09µM, which is closer to the values of Warner et al. (2022). The prediction discrepancies between Warner et al. (2022) and the present work may be, at least partially, explained by the structural differences in the model. In the three-compartmental model, the chorion is considered as a compartment exchanging with the water and the zfe, *i.e.* before hatching, the chemical should enter the chorion compartment before entering the zfe itself (Warner et al., 2022). On the contrary, in the present model, the chorion is considered as a barrier with sorption capacities, *i.e.* there are no direct exchanges between the chemical bound to the chorion and the zfe. The predictive performances of the two models in the calibration dataset are balanced. For PFOA, the PBTK model outperforms the compartmental model: 12.5% and 57% of the predictions fall within the 2-fold error interval for the three-compartmental and PBTK models, respectively. Inversely, for PFOS, the three-compartmental model performs better: 71.4% and 30% of the predictions fall within the 2-fold error interval for the compartmental and PBTK models, respectively. However, the present model has been developed using all the concentrations from the dataset, while only 6 out of 9 time points were considered for the second concentration of PFOS and PFOA by the

model of Warner et al. (2022). In addition, Warner et al. (2022) did not include PFHxS and PFBA, as done here.

5. Conclusion

In this study, a zfe PBTK model has been further improved considering temperature- and light-dependent hatching process within a zfe population, as well as potential uptake saturation processes of a chemical at the chorion, the zfe, or both. The PBTK model has successfully fitted measured internal concentrations in the whole zfe for the four PFAS: PFBA, PFHxS, PFOA, and PFOS. The model exhibits different TK profiles for sulfonic and carboxylic acids suggesting different active transport mechanisms for these two PFAS sub-groups. Thereby, the presented PBTK model offers an improved method for testing new TK hypotheses. In addition, it provides a practical tool for designing new experimental assays by predicting the nominal exposure concentration to achieve a targeted internal dose. Finally, it has the potential to estimate concentrations in organs, enabling future research requiring this type of measurement, necessary for a complete understanding of TK and its integration in the evaluation of adverse health risks.

SUPPORTING INFORMATION

Details of parameterization and simulation methods, properties of the test compounds, additional modeling results, and model code.

AUTHOR CONTRIBUTIONS

Bibliographic analysis, data collection, model development, and simulation were done by PB, CV, CBl and RB. PB, CV, CB, EW, FB, CBl, CBr, and RB contributed to the paper drafting.

The manuscript was written through the contributions of all authors. All authors have given approval to the final version of the manuscript.

FUNDING

This study has received funding from the European Union's H2020 research, the innovation program under grant agreement N° 825712 (project OBERON), the French national grant ANR-19-CE34-0005, and by a grant from the Swedish Research Council FORMAS (2014-1454).

DATA AVAILABILITY

The datasets of the current research can be available from the corresponding author after a reasonable request.

STATEMENTS AND DECLARATIONS

Ethics approval

Not applicable.

Consent to participate

Not applicable.

Consent for publication

Not applicable.

Competing Interests

The authors have no relevant financial or non-financial interests to disclose.

REFERENCES

Billat, P.A., Brochot, C., Brion, F., Beaudouin, R., 2022. A PBPK model to evaluate zebrafish eleutheroembryos' actual exposure: bisphenol A and analogs' (AF, F, and S) case studies. Environ Sci Pollut Res Int.

Blake, B.E., Pinney, S.M., Hines, E.P., Fenton, S.E., Ferguson, K.K., 2018. Associations between longitudinal serum perfluoroalkyl substance (PFAS) levels and measures of thyroid hormone, kidney function, and body mass index in the Fernald Community Cohort. Environmental Pollution 242, 894-904.

Böhme, S., Baccaro, M., Schmidt, M., Potthoff, A., Stark, H.J., Reemtsma, T., Kuhnel, D., 2017. Metal uptake and distribution in the zebrafish (Danio rerio) embryo: differences between nanoparticles and metal ions. Environmental Science-Nano 4, 1005-1015.

Bois, F.Y., 2009. GNU MCSim: Bayesian statistical inference for SBML-coded systems biology models. Bioinformatics 25, 1453-1454.

Bonsignorio, D., Perego, L., DelGiacco, L., Cotelli, F., 1996. Structure and macromolecular composition of the zebrafish egg chorion. Zygote 4, 101-108.

Brox, S., Ritter, A.P., Küster, E., Reemtsma, T., 2014a. Influence of the perivitelline space on the quantification of internal concentrations of chemicals in eggs of zebrafish embryos (Danio rerio). Aquat Toxicol 157, 134-140.

Brox, S., Ritter, A.P., Küster, E., Reemtsma, T., 2014b. A quantitative HPLC–MS/MS method for studying internal concentrations and toxicokinetics of 34 polar analytes in zebrafish (Danio rerio) embryos. Anal Bioanal Chem 406, 4831-4840.

Canedo, A., Rocha, T.L., 2021. Zebrafish (Danio rerio) using as model for genotoxicity and DNA repair assessments: Historical review, current status and trends. Sci Total Environ 762, 144084.

De la Paz, J.F., Beiza, N., Paredes-Zúñiga, S., Hoare, M.S., Allende, M.L., 2017. Triazole Fungicides Inhibit Zebrafish Hatching by Blocking the Secretory Function of Hatching Gland Cells. Int J Mol Sci 18.

DeWitt, J.C., 2015. Toxicological effects of perfluoroalkyl and polyfluoroalkyl substances. Springer.

Ebert, A., Allendorf, F., Berger, U., Goss, K.U., Ulrich, N., 2020. Membrane/Water Partitioning and Permeabilities of Perfluoroalkyl Acids and Four of their Alternatives and the Effects on Toxicokinetic Behavior. Environ Sci Technol 54, 5051-5061.

EFSA CONTAM Panel, Schrenk, D., Bignami, M., Bodin, L., Chipman, J.K., del Mazo, J., Grasl-Kraupp, B., Hogstrand, C., Hoogenboom, L., Leblanc, J.-C., Nebbia, C.S., Nielsen, E., Ntzani, E., Petersen, A., Sand, S., Vleminckx, C., Wallace, H., Barregård, L., Ceccatelli, S., Cravedi, J.-P., Halldorsson, T.I., Haug, L.S., Johansson, N., Knutsen, H.K., Rose, M., Roudot, A.-C., Van Loveren, H., Vollmer, G., Mackay, K., Riolo, F., Schwerdtle, T., 2020. Risk to human health related to the presence of perfluoroalkyl substances in food. EFSA Journal 18, e06223.

Fenton, S.E., Ducatman, A., Boobis, A., DeWitt, J.C., Lau, C., Ng, C., Smith, J.S., Roberts, S.M., 2021. Per- and Polyfluoroalkyl Substance Toxicity and Human Health Review: Current State of Knowledge and Strategies for Informing Future Research. Environmental Toxicology and Chemistry 40, 606-630.

Fisher, C., Simeon, S., Jamei, M., Gardner, I., Bois, Y.F., 2019. VIVD: Virtual in vitro distribution model for the mechanistic prediction of intracellular concentrations of chemicals in in vitro toxicity assays. Toxicol In Vitro 58, 42-50.

Fitzgerald, J.A., Könemann, S., Krümpelmann, L., Županič, A., Vom Berg, C., 2021. Approaches to Test the Neurotoxicity of Environmental Contaminants in the Zebrafish Model: From Behavior to Molecular Mechanisms. Environmental Toxicology and Chemistry 40, 989-1006.

Gaballah, S., Swank, A., Sobus, J.R., Howey, X.M., Schmid, J., Catron, T., McCord, J., Hines, E., Strynar, M., Tal, T., 2020. Evaluation of Developmental Toxicity, Developmental Neurotoxicity, and Tissue Dose in Zebrafish Exposed to GenX and Other PFAS. Environ Health Perspect 128, 47005.

Garcia, G.R., Noyes, P.D., Tanguay, R.L., 2016. Advancements in zebrafish applications for 21st century toxicology. Pharmacol Ther 161, 11-21.

Gelman, A., Rubin, D.B., 1996. Markov chain Monte Carlo methods in biostatistics. Stat Methods Med Res 5, 339-355.

Glüge, J., Scheringer, M., Cousins, I.T., DeWitt, J.C., Goldenman, G., Herzke, D., Lohmann, R., Ng, C.A., Trier, X., Wang, Z., 2020. An overview of the uses of per- and polyfluoroalkyl substances (PFAS). Environ Sci Process Impacts 22, 2345-2373.

Grech, A., Brochot, C., Dorne, J.L., Quignot, N., Bois, F.Y., Beaudouin, R., 2017. Toxicokinetic models and related tools in environmental risk assessment of chemicals. Sci Total Environ 578, 1-15.
Hagedorn, M., Kleinhans, F.W., Freitas, R., Liu, J., Hsu, E.W., Wildt, D.E., Rall, W.F., 1997. Water distribution and permeability of zebrafish embryos, Brachydanio rerio. J Exp Zool 278, 356-371.
Hagenaars, A., Vergauwen, L., De Coen, W., Knapen, D., 2011. Structure–activity relationship assessment of four perfluorinated chemicals using a prolonged zebrafish early life stage test. Chemosphere 82, 764-772.
Han, J., Gu, W., Barrett, H., Yang, D., Tang, S., Sun, J., Liu, J., Krause, H.M., Houck, K.A., Peng, H., 2021. A Roadmap to the Structure-Related Metabolism Pathways of Per- and Polyfluoroalkyl Substances in the Early Life Stages of Zebrafish (Danio rerio). Environ Health Perspect 129, 77004.
Hart, N.H., Donovan, M., 1983. Fine structure of the chorion and site of sperm entry in the egg of Brachydanio. Journal of Experimental Zoology 227, 277-296.
Hill, A.J., Teraoka, H., Heideman, W., Peterson, R.E., 2005. Zebrafish as a model vertebrate for investigating chemical toxicity. Toxicological Sciences 86, 6-19.
Huang, H., Huang, C., Wang, L., Ye, X., Bai, C., Simonich, M.T., Tanguay, R.L., Dong, Q., 2010. Toxicity, uptake kinetics and behavior assessment in zebrafish embryos following exposure to perfluorooctanesulphonicacid (PFOS). Aquat Toxicol 98, 139-147.
Kahn, L.G., Philippat, C., Nakayama, S.F., Slama, R., Trasande, L., 2020. Endocrine-disrupting chemicals: implications for human health. The Lancet Diabetes & Endocrinology 8, 703-718.
Kang, J.-H., Kim, Y.-J., Yang, M.-S., Shin, D.H., Kim, D.-W., Park, I.Y., Park, C.-W., 2021. Co-Spray Dried Nafamostat Mesylate with Lecithin and Mannitol as Respirable Microparticles for Targeted Pulmonary Delivery: Pharmacokinetics and Lung Distribution in Rats. Pharmaceutics 13, 1519.
Kannan, K., Corsolini, S., Falandysz, J., Fillmann, G., Kumar, K.S., Loganathan, B.G., Mohd, M.A., Olivero, J., Wouwe, N.V., Yang, J.H., Aldous, K.M., 2004. Perfluorooctanesulfonate and Related Fluorochemicals in Human Blood from Several Countries. Environ Sci Technol 38, 4489-4495.
Keiter, S., Burkhardt-Medicke, K., Wellner, P., Kais, B., Färber, H., Skutlarek, D., Engwall, M., Braunbeck, T., Keiter, S.H., Luckenbach, T., 2016. Does perfluorooctane sulfonate (PFOS) act as chemosensitizer in zebrafish embryos? Science of The Total Environment 548-549, 317-324.
Kim, D.H., Hwang, C.N., Sun, Y., Lee, S.H., Kim, B., Nelson, B.J., 2006. Mechanical analysis of chorion softening in prehatching stages of zebrafish embryos. IEEE Trans Nanobioscience 5, 89-94.
Kimura, O., Fujii, Y., Haraguchi, K., Kato, Y., Ohta, C., Koga, N., Endo, T., 2017. Uptake of perfluorooctanoic acid by Caco-2 cells: Involvement of organic anion transporting polypeptides. Toxicol Lett 277, 18-23.
Kühnert, A., Vogs, C., Altenburger, R., Küster, E., 2013. The internal concentration of organic substances in fish embryos—A toxicokinetic approach. Environmental Toxicology and Chemistry 32, 1819-1827.
Menger, F., Pohl, J., Ahrens, L., Carlsson, G., Örn, S., 2020. Behavioural effects and bioconcentration of per- and polyfluoroalkyl substances (PFASs) in zebrafish (Danio rerio) embryos. Chemosphere 245, 125573.
Morris, J.B., 1990. First-pass metabolism of inspired ethyl acetate in the upper respiratory tracts of the F344 rat and Syrian hamster. Toxicology and Applied Pharmacology 102, 331-345.
Muraina, I.A., Maret, W., Bury, N.R., Hogstrand, C., 2020. Hatching gland development and hatching in zebrafish embryos: A role for zinc and its transporters Zip10 and Znt1a. Biochemical and Biophysical Research Communications 528, 698-705.
Nagel, R., 2002. DarT: The embryo test with the zebrafish Danio rerio - a general model in ecotoxicology and toxicology. Altex-Alternativen Zu Tierexperimenten 19, 38-48.
OCDE, 2021. Test No. 250: EASZY assay - Detection of Endocrine Active Substances, acting through estrogen receptors, using transgenic tg(cyp19a1b:GFP) Zebrafish embrYos.
OECD, 2013. Test No. 236: Fish Embryo Acute Toxicity (FET) Test.
Pelka, K.E., Henn, K., Keck, A., Sapel, B., Braunbeck, T., 2017. Size does matter – Determination of the critical molecular size for the uptake of chemicals across the chorion of zebrafish (Danio rerio) embryos. Aquatic Toxicology 185, 1-10.
Popovic, M., Zaja, R., Fent, K., Smital, T., 2014. Interaction of environmental contaminants with zebrafish organic anion transporting polypeptide, Oatp1d1 (Slco1d1). Toxicology and Applied Pharmacology 280, 149-158.
Saltelli, A., Annoni, P., Azzini, I., Campolongo, F., Ratto, M., Tarantola, S., 2010. Variance based sensitivity analysis of model output. Design and estimator for the total sensitivity index. Computer Physics Communications 181, 259-270.

Satoh, T., Hosokawa, M., 2010. Carboxylesterases: structure, function and polymorphism in mammals. Journal of Pesticide Science 35, 218-228.
Schwartz, A.V., Sant, K.E., Navarrete, J., George, U.Z., 2021. Mathematical modeling of the interaction between yolk utilization and fish growth in zebrafish, Danio rerio. Development 148.
Silva Brito, R., Canedo, A., Farias, D., Rocha, T.L., 2022. Transgenic zebrafish (Danio rerio) as an emerging model system in ecotoxicology and toxicology: Historical review, recent advances, and trends. Sci Total Environ 848, 157665.
Siméon, S., Brotzmann, K., Fisher, C., Gardner, I., Braunbeck, T., Maclennan, R., Bois, F., 2020. Development of a generic zebrafish embryo PBPK model and application to the developmental toxicity assessment of valproic acid analogs. . Reproductive Toxicology 93, 219-229.
Simeon, S., Brotzmann, K., Fisher, C., Gardner, I., Silvester, S., Maclennan, R., Walker, P., Braunbeck, T., Bois, F.Y., 2020. Development of a generic zebrafish embryo PBPK model and application to the developmental toxicity assessment of valproic acid analogs. Reproductive Toxicology 93, 219-229.
Sobol', I.M., Tarantola, S., Gatelli, D., Kucherenko, S.S., Mauntz, W., 2007. Estimating the approximation error when fixing unessential factors in global sensitivity analysis. Reliability Engineering & System Safety 92, 957-960.
Spulber, S., Kilian, P., Wan Ibrahim, W.N., Onishchenko, N., Ulhaq, M., Norrgren, L., Negri, S., Di Tuccio, M., Ceccatelli, S., 2014. PFOS induces behavioral alterations, including spontaneous hyperactivity that is corrected by dexamfetamine in zebrafish larvae. PLoS One 9, e94227.
Tal, T., Vogs, C., 2021. Invited Perspective: PFAS Bioconcentration and Biotransformation in Early Life Stage Zebrafish and Its Implications for Human Health Protection. Environmental Health Perspectives 129, 071304.
Trikić, M.Z., Monk, P., Roehl, H., Partridge, L.J., 2011. Regulation of Zebrafish Hatching by Tetraspanin cd63. PLoS One 6, e19683.
Truong, L., Rericha, Y., Thunga, P., Marvel, S., Wallis, D., Simonich, M.T., Field, J.A., Cao, D., Reif, D.M., Tanguay, R.L., 2022. Systematic developmental toxicity assessment of a structurally diverse library of PFAS in zebrafish. Journal of Hazardous Materials 431, 128615.
Tu, W., Martínez, R., Navarro-Martin, L., Kostyniuk, D.J., Hum, C., Huang, J., Deng, M., Jin, Y., Chan, H.M., Mennigen, J.A., 2019. Bioconcentration and Metabolic Effects of Emerging PFOS Alternatives in Developing Zebrafish. Environ Sci Technol 53, 13427-13439.
Ulhaq, M., Carlsson, G., Örn, S., Norrgren, L., 2013. Comparison of developmental toxicity of seven perfluoroalkyl acids to zebrafish embryos. Environmental Toxicology and Pharmacology 36, 423-426.
Villamizar, N., Ribas, L., Piferrer, F., Vera, L.M., Sánchez-Vázquez, F.J., 2012. Impact of Daily Thermocycles on Hatching Rhythms, Larval Performance and Sex Differentiation of Zebrafish. Plos One 7, e52153.
Vogs, C., Johanson, G., Näslund, M., Wulff, S., Sjödin, M., Hellstrandh, M., Lindberg, J., Wincent, E., 2019. Toxicokinetics of Perfluorinated Alkyl Acids Influences Their Toxic Potency in the Zebrafish Embryo (Danio rerio). Environ Sci Technol 53, 3898-3907.
Wang, J., Shi, G., Yao, J., Sheng, N., Cui, R., Su, Z., Guo, Y., Dai, J., 2020. Perfluoropolyether carboxylic acids (novel alternatives to PFOA) impair zebrafish posterior swim bladder development via thyroid hormone disruption. Environment International 134, 105317.
Warner, R.M., Sweeney, L.M., Hayhurst, B.A., Mayo, M.L., 2022. Toxicokinetic Modeling of Per- and Polyfluoroalkyl Substance Concentrations within Developing Zebrafish (Danio rerio) Populations. Environ Sci Technol.
Wasel, O., Thompson, K.M., Gao, Y., Godfrey, A.E., Gao, J., Mahapatra, C.T., Lee, L.S., Sepúlveda, M.S., Freeman, J.L., 2021. Comparison of zebrafish in vitro and in vivo developmental toxicity assessments of perfluoroalkyl acids (PFAAs). Journal of Toxicology and Environmental Health, Part A 84, 125-136.
Wiegand, C., Pflugmacher, S., Giese, M., Frank, H., Steinberg, C., 2000. Uptake, Toxicity, and Effects on Detoxication Enzymes of Atrazine and Trifluoroacetate in Embryos of Zebrafish. Ecotoxicology and Environmental Safety 45, 122-131.
Yang, C.-H., Glover, K.P., Han, X., 2009. Organic anion transporting polypeptide (Oatp) 1a1-mediated perfluorooctanoate transport and evidence for a renal reabsorption mechanism of Oatp1a1 in renal elimination of perfluorocarboxylates in rats. Toxicol Lett 190, 163-171.
Zhao, W., Zitzow, J.D., Weaver, Y., Ehresman, D.J., Chang, S.-C., Butenhoff, J.L., Hagenbuch, B., 2016. Organic Anion Transporting Polypeptides Contribute to the Disposition of Perfluoroalkyl Acids in Humans and Rats. Toxicological Sciences 156, 84-95.

Zheng, X.-M., Liu, H.-L., Shi, W., Wei, S., Giesy, J.P., Yu, H.-X., 2012. Effects of perfluorinated compounds on development of zebrafish embryos. Environmental Science and Pollution Research 19, 2498-2505.

Supplementary information

PBTK modeled perfluoroalkyl acid kinetics in zebrafish eleutheroembryos suggests impacts on bioconcentrations by chorion porosity dynamics

Pierre-André Billat[a], Carolina Vogs[b,c], Clément Blassiau[a], Céline Brochot[a], Emma Wincent[c], François Brion[d,e], Rémy Beaudouin[a,e*].

[a] INERIS, Experimental toxicology and modeling unit (TEAM), Parc ALATA BP2, Verneuil en Halatte, France
[b] Department of Biomedical Science and Veterinary Public Health, Swedish University of Agricultural Science (SLU), Uppsala, Sweden.
[c] Institute of Environmental Medicine, Karolinska Institutet (KI), Stockholm, Sweden
[d] INERIS, Ecotoxicology of substances and environments unit (ESMI), Parc ALATA BP2, Verneuil en Halatte, France
[e] UMR-I 02 SEBIO, Parc ALATA BP2, Verneuil en Halatte, France INERIS
* Phone: +33 3 44 55 82 38; fax: +33 3 44 55 67 67; e-mail: Remy.Beaudouin@ineris.fr

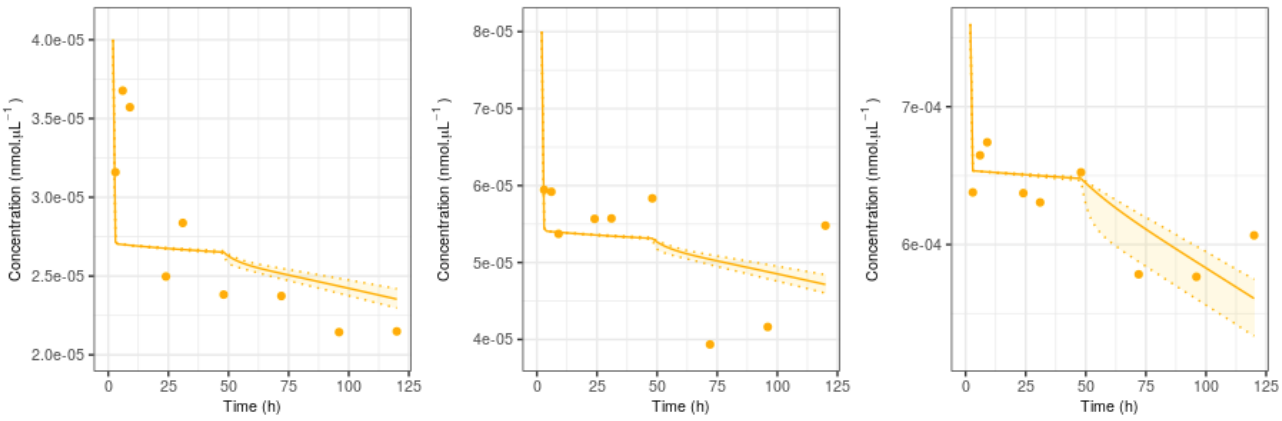

$4x10^{-5}$ nmol.µL^{-1} (C1) < $8x10^{-5}$ nmol.µL^{-1} (C2) < $7.6x10^{-4}$ nmol.µL^{-1} (C3)

Figure S1. Observed and predicted PFOS concentrations in the culture medium with zfe over time.
C1, C2 and C3 are the nominal concentrations of PFOS. The coloured dots are the geometric means of measured medium concentrations over time (n = 6). The coloured trajectories are the predicted concentrations in the culture medium at the level of the *a posteriori* joint distribution of the calibrated parameters. Finally, the area between the dotted lines is the credible interval at 95%.

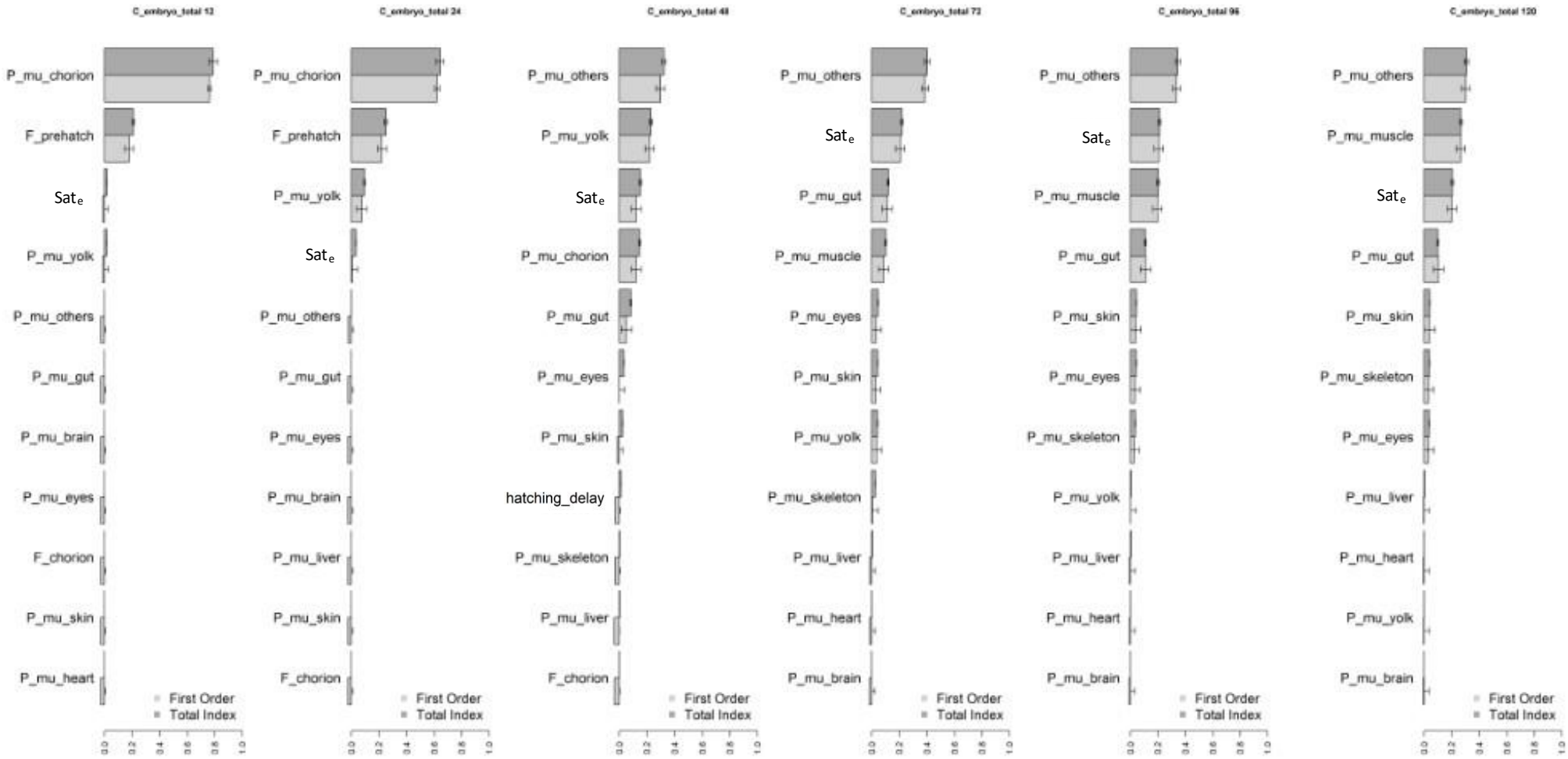

Figure S2. Sensitivity analysis of model II, including corrected partition coefficients, saturation (Sat_e), flows and permeability delay (hatching_delay), on total PFBA concentrations in ZFE (chorion, embryo and yolk), at 12,24, 48, 72, 96 and 120 hpf (from left to right, respectively). The 11 most influential parameters are represented.

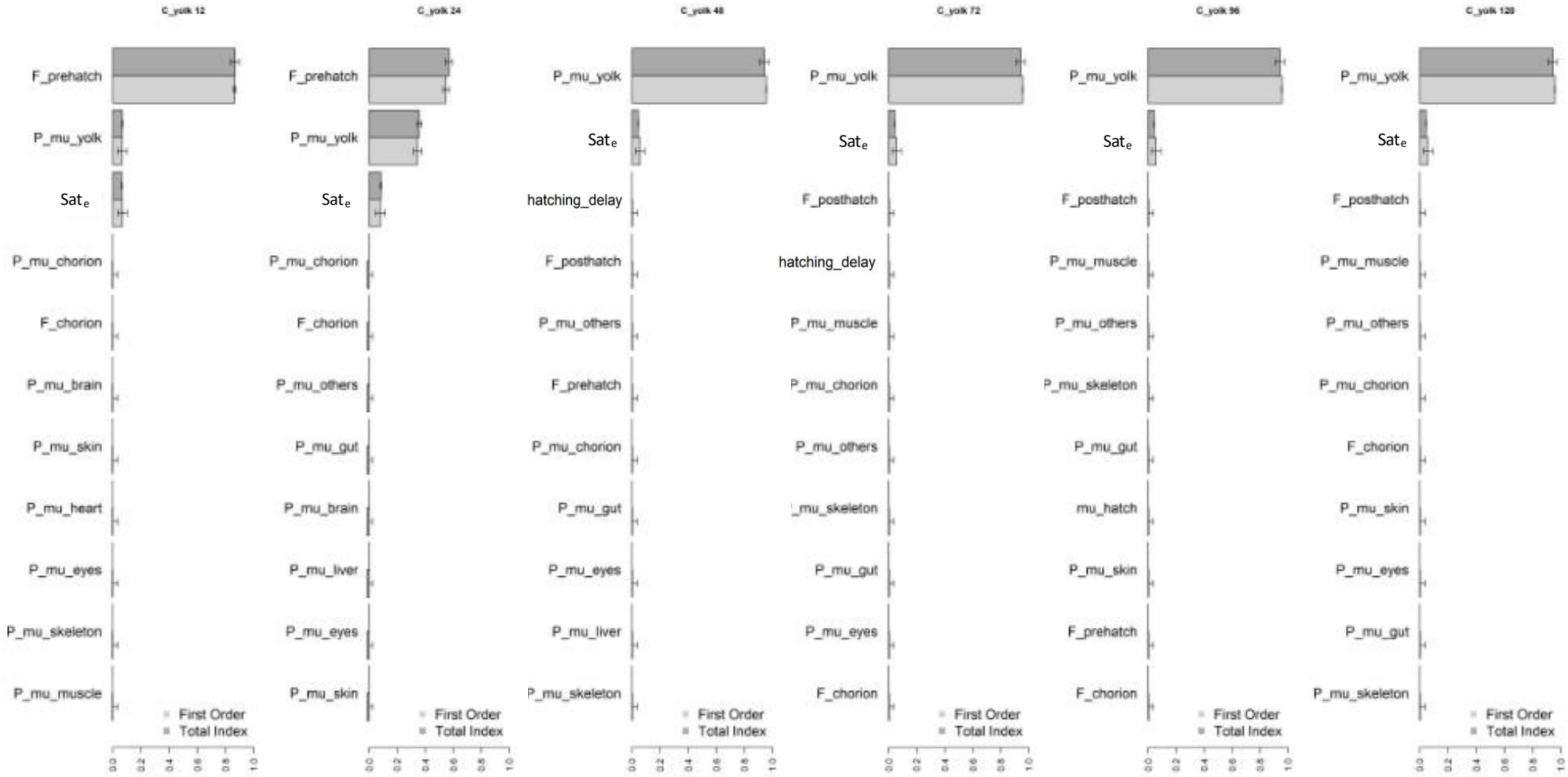

Figure S3. Sensitivity analysis of model II, including corrected partition coefficients, saturation (Sat_e), flows and permeability delay (hatching_delay), on yolk PFBA concentrations, at 12,24, 48, 72, 96 and 120 hpf (from left to right, respectively). The 11 most influential parameters are represented.

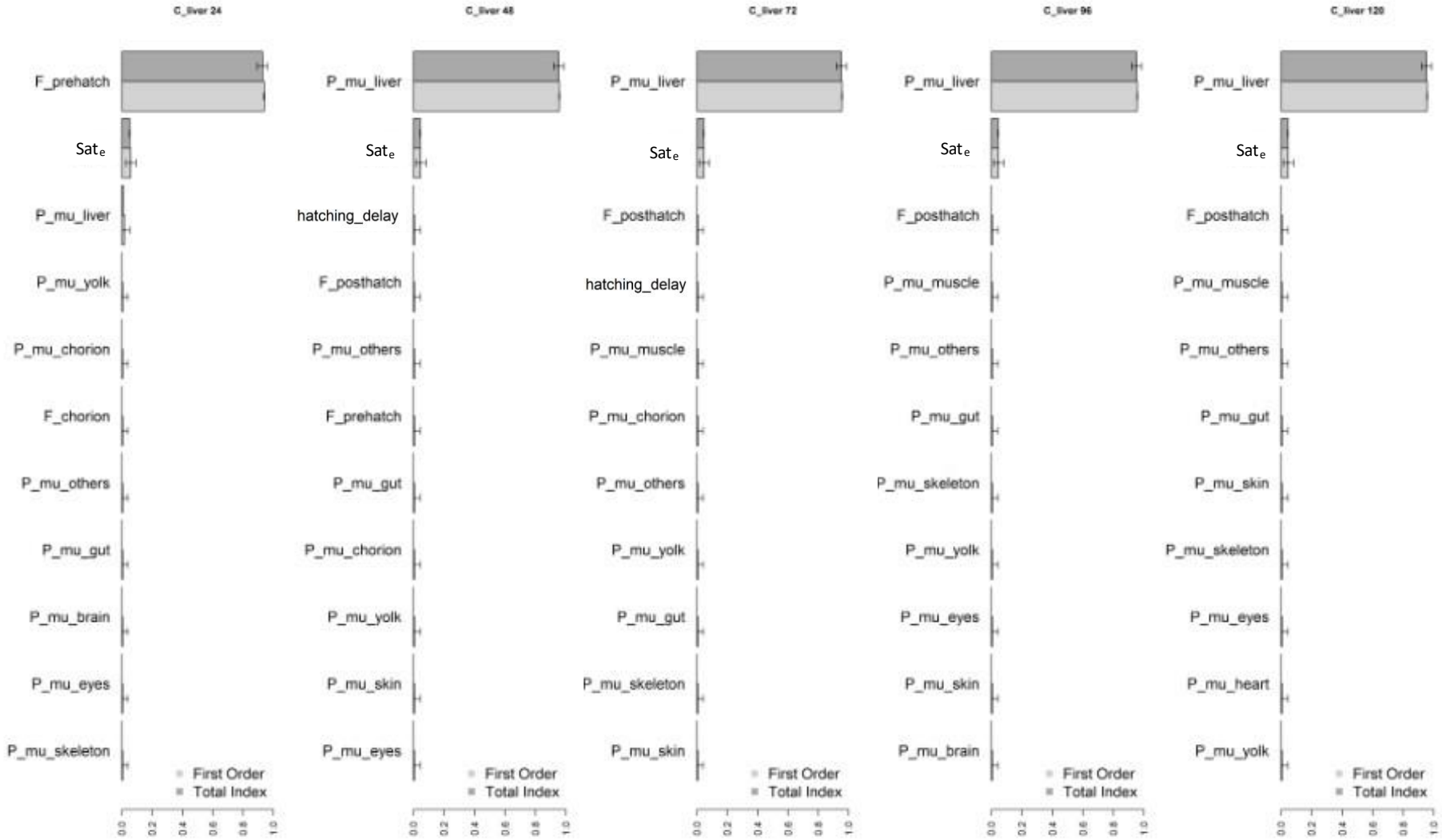

Figure S4. Sensitivity analysis of model II, including corrected partition coefficients, saturation (Sat_e), flows and permeability delay (hatching_delay), on liver PFBA concentrations in ZFE, at 24, 48, 72, 96 and 120 hpf (from left to right, respectively). The 11 most influential parameters are represented.

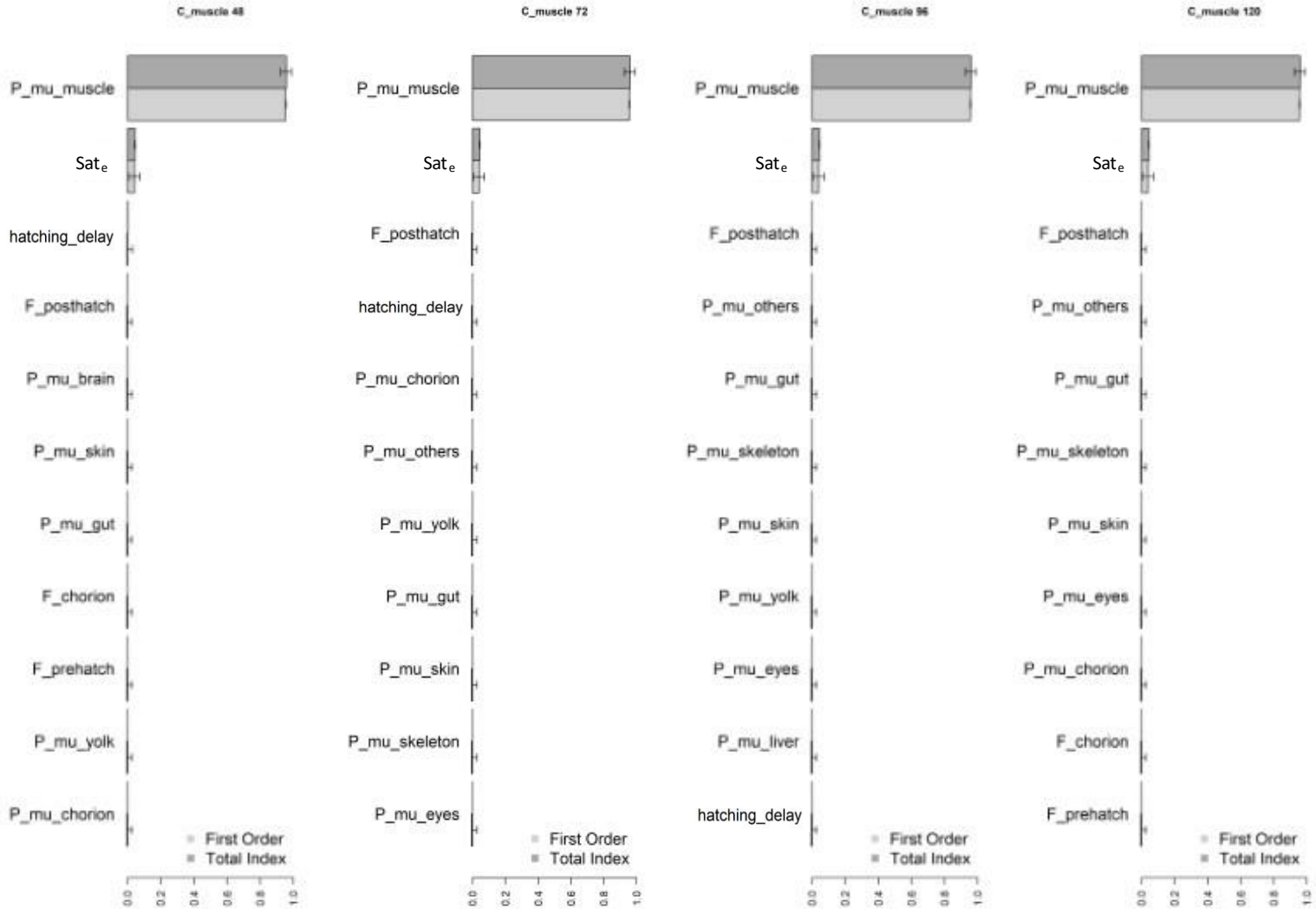

Figure S5. Sensitivity analysis of model II, including corrected partition coefficients, saturation (Sat_e), flows and permeability delay (hatching_delay), on muscle PFBA concentrations in ZFE, at 48, 72, 96 and 120 hpf (from left to right, respectively). The 11 most influential parameters are represented.

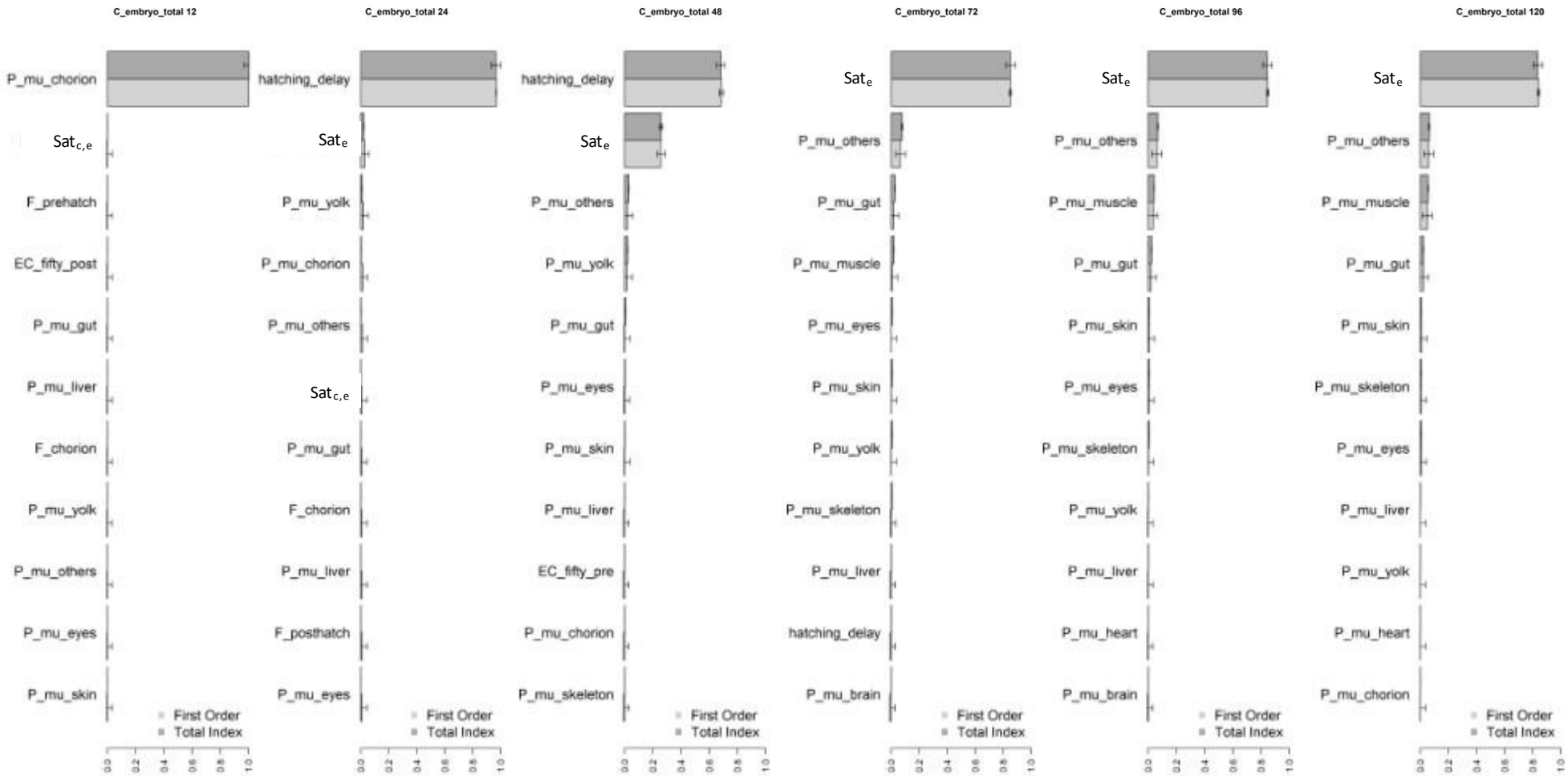

Figure S6. Sensitivity analysis of model III, including corrected partition coefficients, saturations ($Sat_{c,e}$, Sat_e), flows and permeability delay (hatching_delay), on total PFHxS concentrations in ZFE (chorion, embryo and yolk), at 12, 24, 48, 72, 96 and 120 hpf (from left to right, respectively). The 11 most influential parameters are represented.

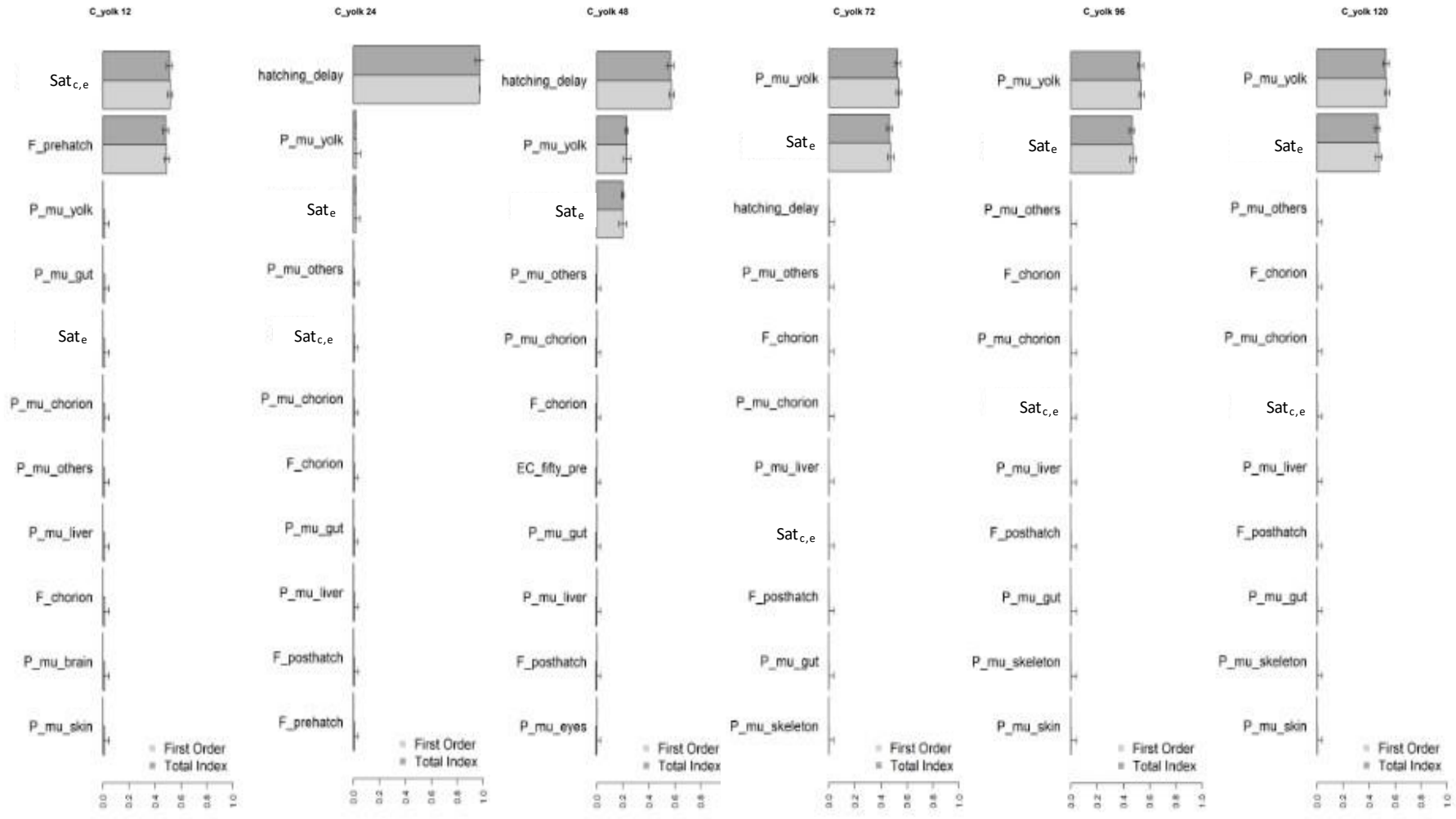

Figure S7. Sensitivity analysis of model III, including corrected partition coefficients, saturations ($Sat_{c,e}$, Sat_e), flows and permeability delay (hatching_delay), on yolk PFHxS concentrations, at 12,24, 48, 72, 96 and 120 hpf (from left to right, respectively). The 11 most influential parameters are represented.

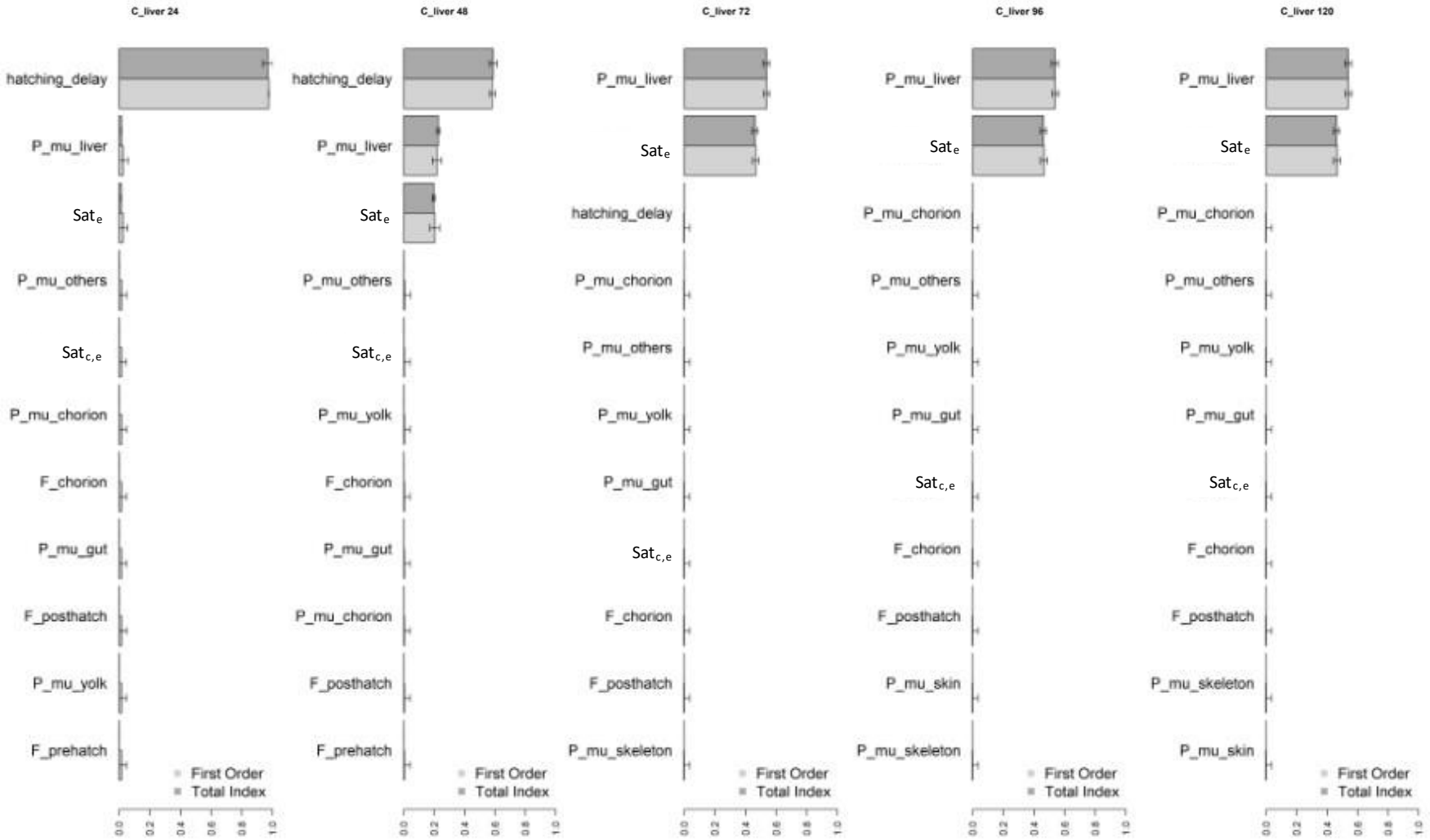

Figure S8. Sensitivity analysis of model III, including corrected partition coefficients, saturations ($Sat_{c,e}$, Sat_e), flows and permeability delay (hatching_delay), on liver PFHxS concentrations in ZFE, at 24, 48, 72, 96 and 120 hpf (from left to right, respectively). The 11 most influential parameters are represented.

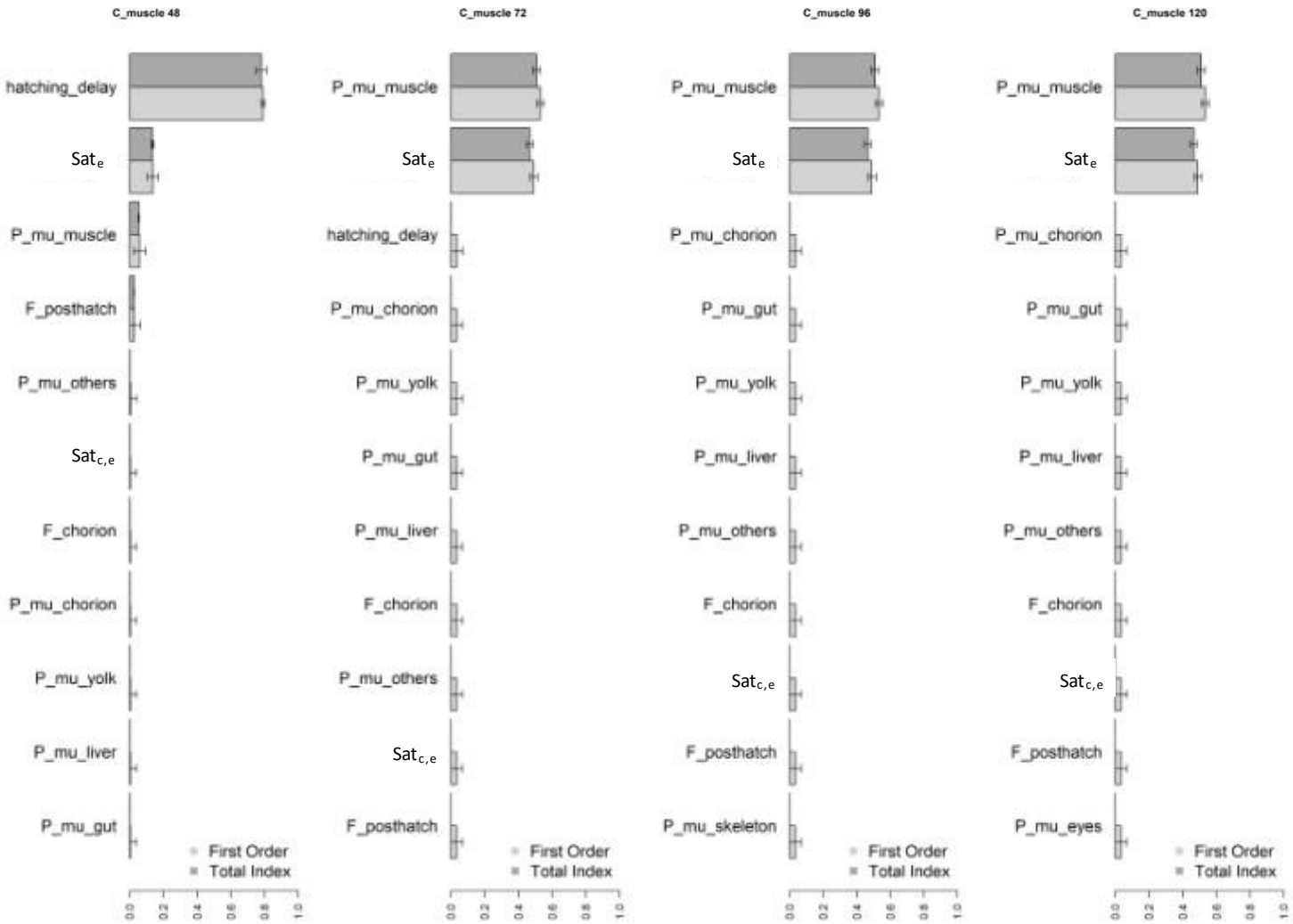

Figure S9. Sensitivity analysis of model III, including corrected partition coefficients, saturations ($Sat_{c,e}$, Sat_e), flows and permeability delay (hatching_delay), on muscle PFHxS concentrations in ZFE, at 48, 72, 96 and 120 hpf (from left to right, respectively). The 11 most influential parameters are represented.

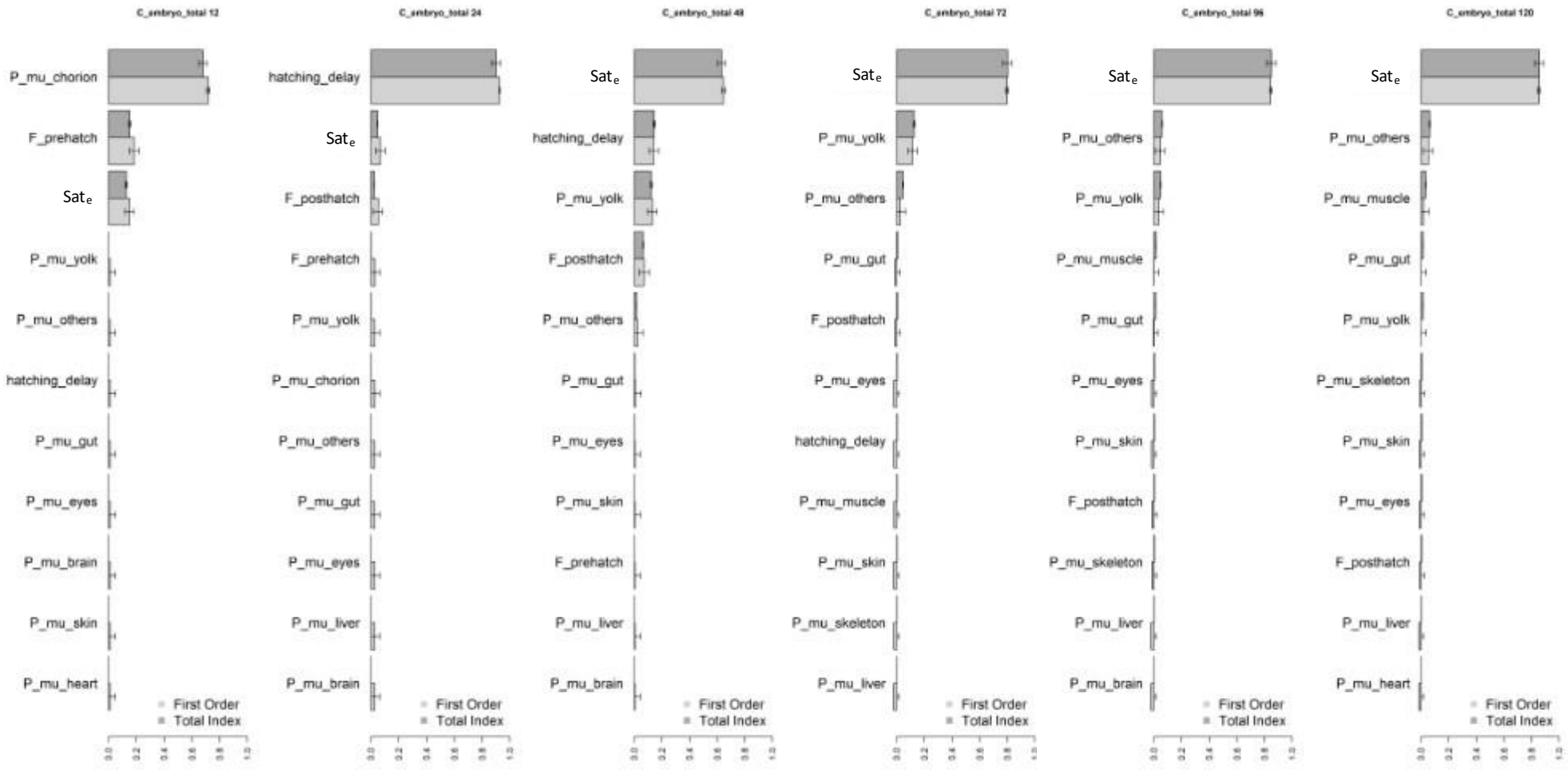

Figure S10. Sensitivity analysis of model II, including corrected partition coefficients, saturation (Sat_e), flows and permeability delay (hatching_delay), on total PFOA concentrations in ZFE (chorion, embryo and yolk), at 12, 24, 48, 72, 96 and 120 hpf (from left to right, respectively). The 11 most influential parameters are represented.

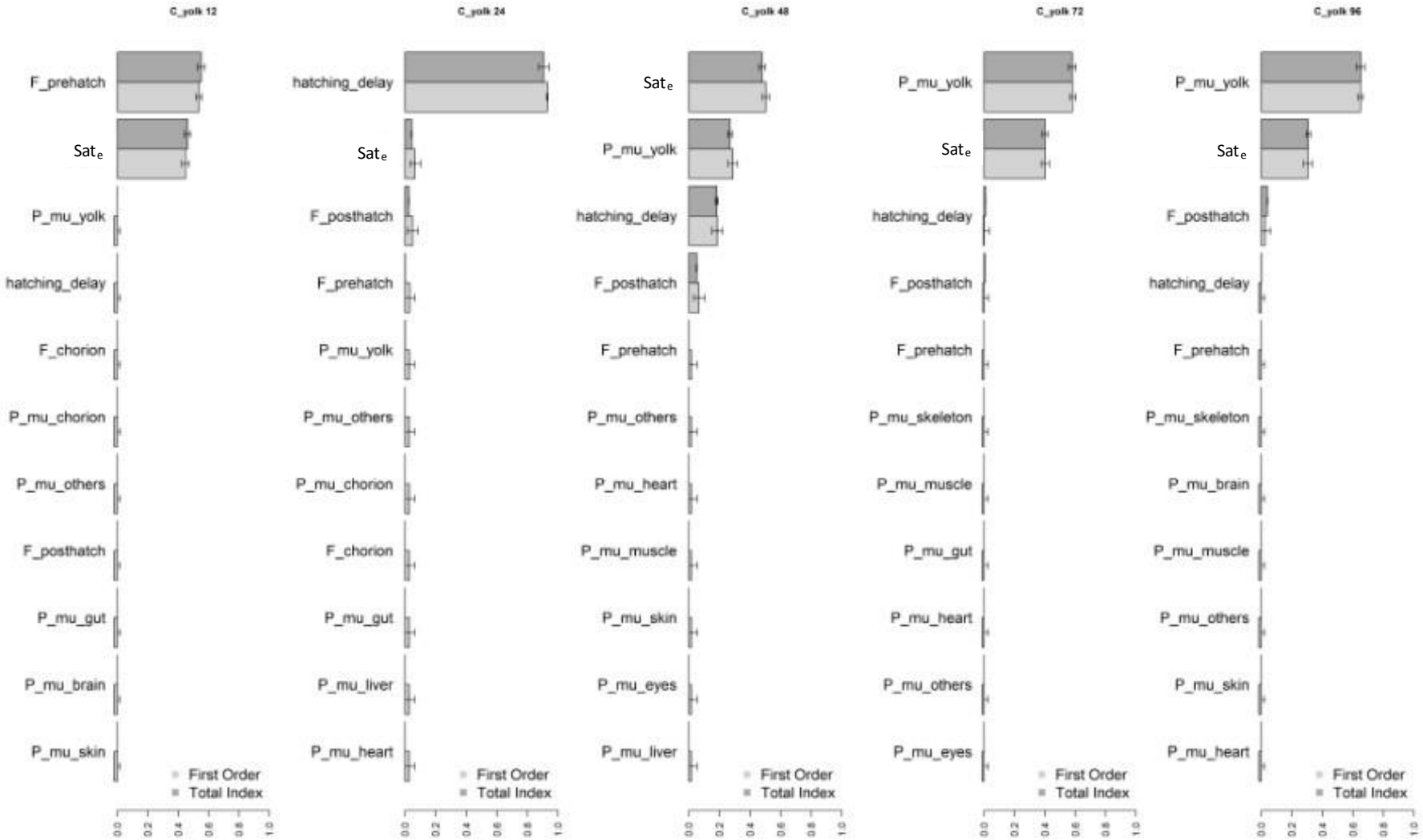

Figure S11. Sensitivity analysis of model II, including corrected partition coefficients, saturation (Sat_e), flows and permeability delay (hatching_delay), on yolk PFOA concentrations, at 12, 24, 48, 72 and 96 hpf (from left to right, respectively). The 11 most influential parameters are represented.

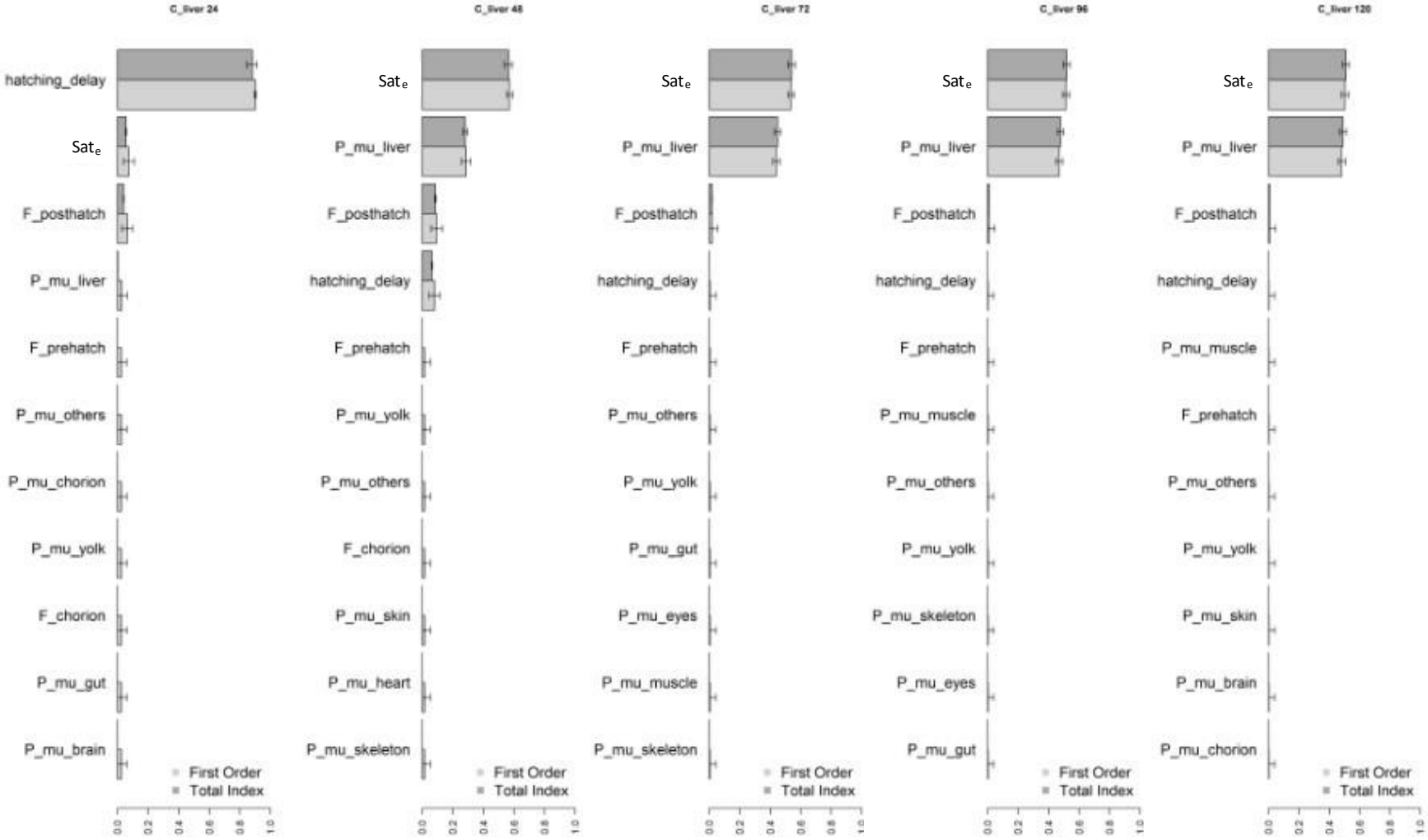

Figure S12. Sensitivity analysis of model II, including corrected partition coefficients, saturation (Sat_e), flows and permeability delay (hatching_delay), on liver PFOA concentrations in ZFE, at 24, 48, 72, 96 and 120 hpf (from left to right, respectively). The 11 most influential parameters are represented.

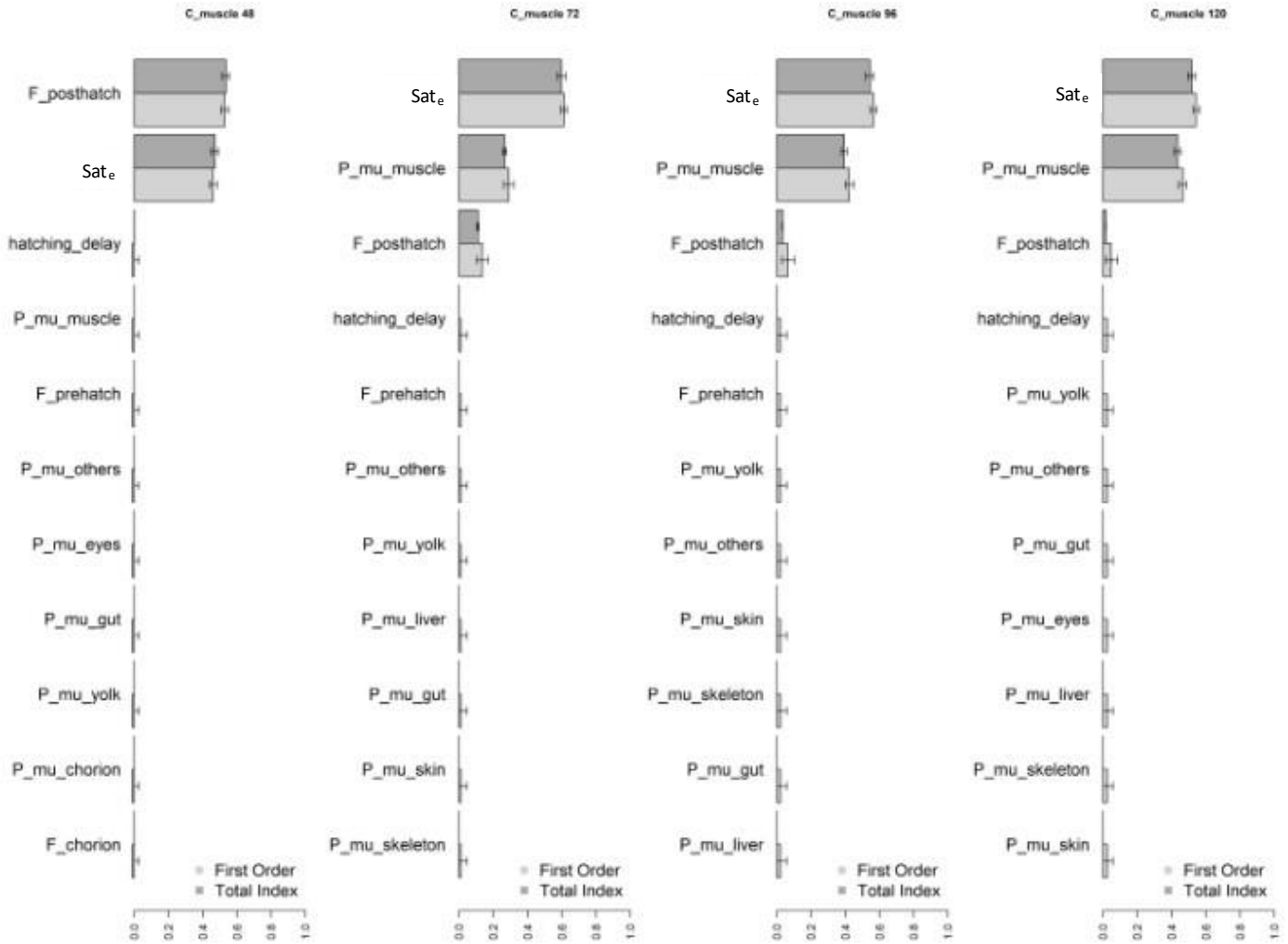

Figure S13. Sensitivity analysis of model II, including corrected partition coefficients, saturation (Sat_e), flows and permeability delay (hatching_delay), on muscle PFOA concentrations in ZFE, at 48, 72, 96 and 120 hpf (from left to right, respectively). The 11 most influential parameters are represented.

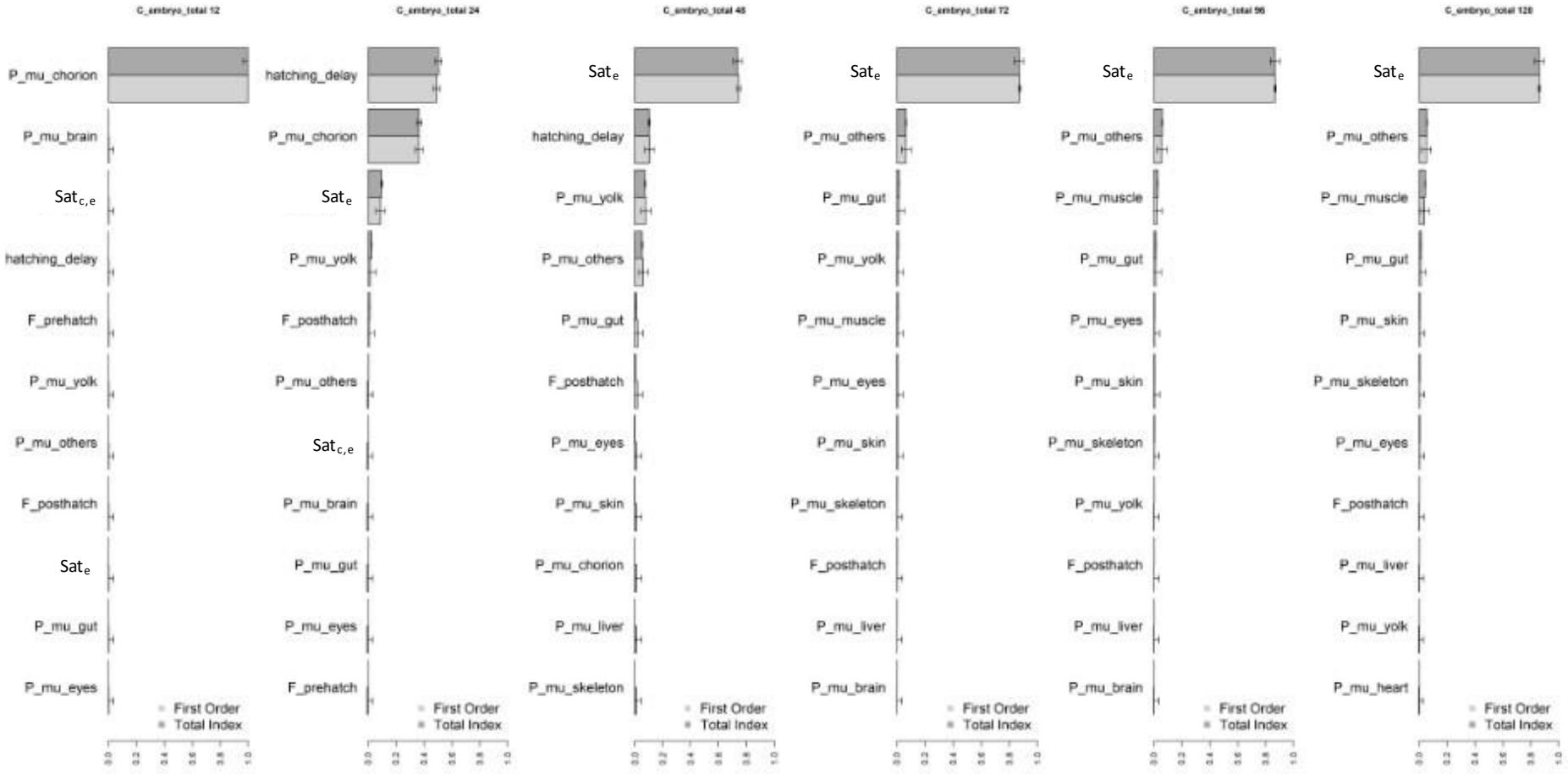

Figure S14. Sensitivity analysis of model III, including corrected partition coefficients, saturations ($Sat_{c,e}$, Sat_e), flows and permeability delay (hatching_delay), on total PFOS concentrations in ZFE (chorion, embryo and yolk), at 12, 24, 48, 72, 96 and 120 hpf (from left to right, respectively). The 11 most influential parameters are represented.

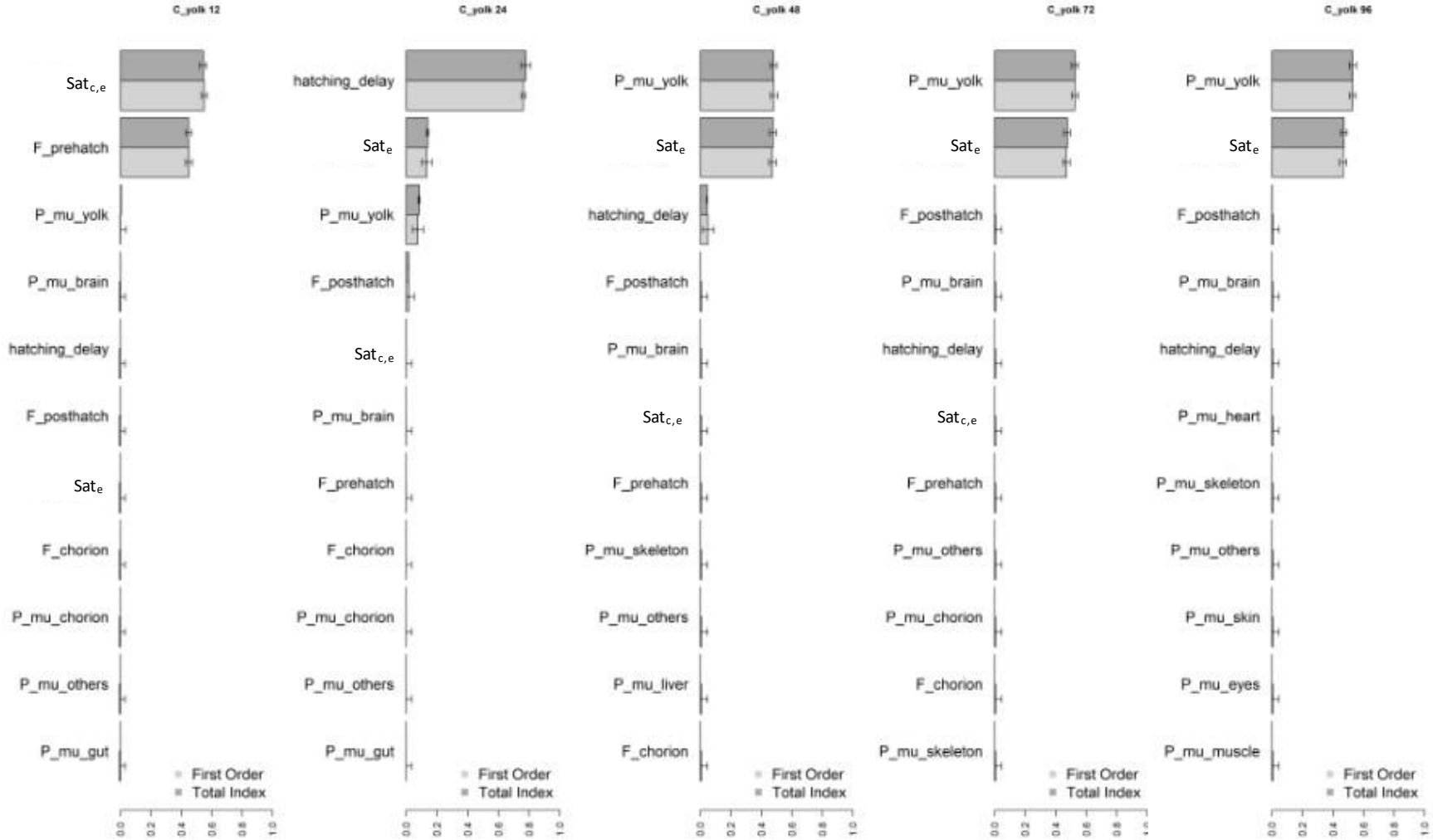

Figure S15. Sensitivity analysis of model III, including corrected partition coefficients, saturations ($Sat_{c,e}$, Sat_e), flows and permeability delay (hatching_delay), on yolk PFOS concentrations, at 12, 24, 48, 72, and 96 hpf (from left to right, respectively). The 11 most influential parameters are represented.

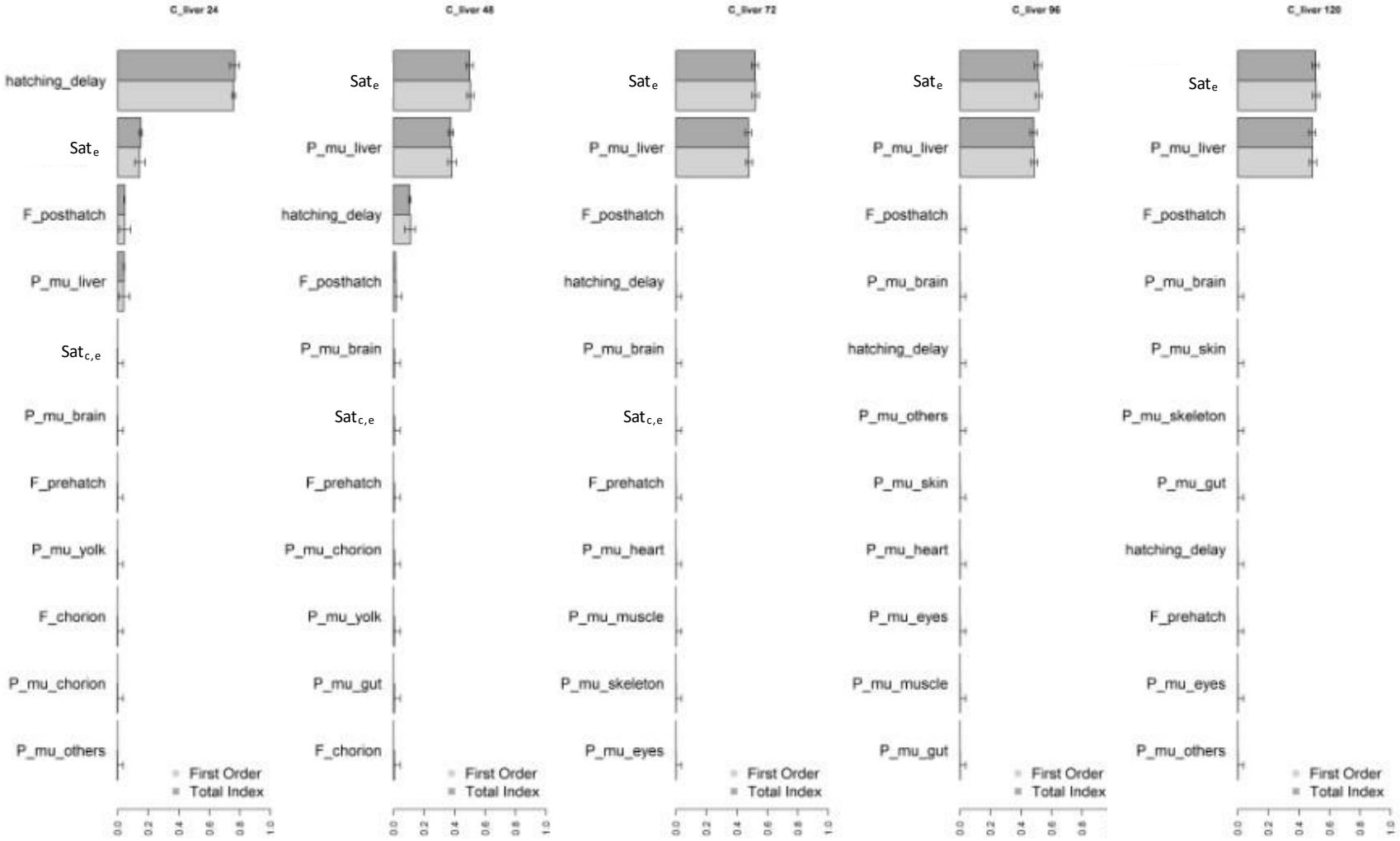

Figure S16.p Sensitivity analysis of model III, including corrected partition coefficients, saturations ($Sat_{c,e}$, Sat_e), flows and permeability delay (hatching_delay), on liver PFOS concentrations in ZFE, at 24, 48, 72, 96 and 120 hpf (from left to right, respectively). The 11 most influential parameters are represented.

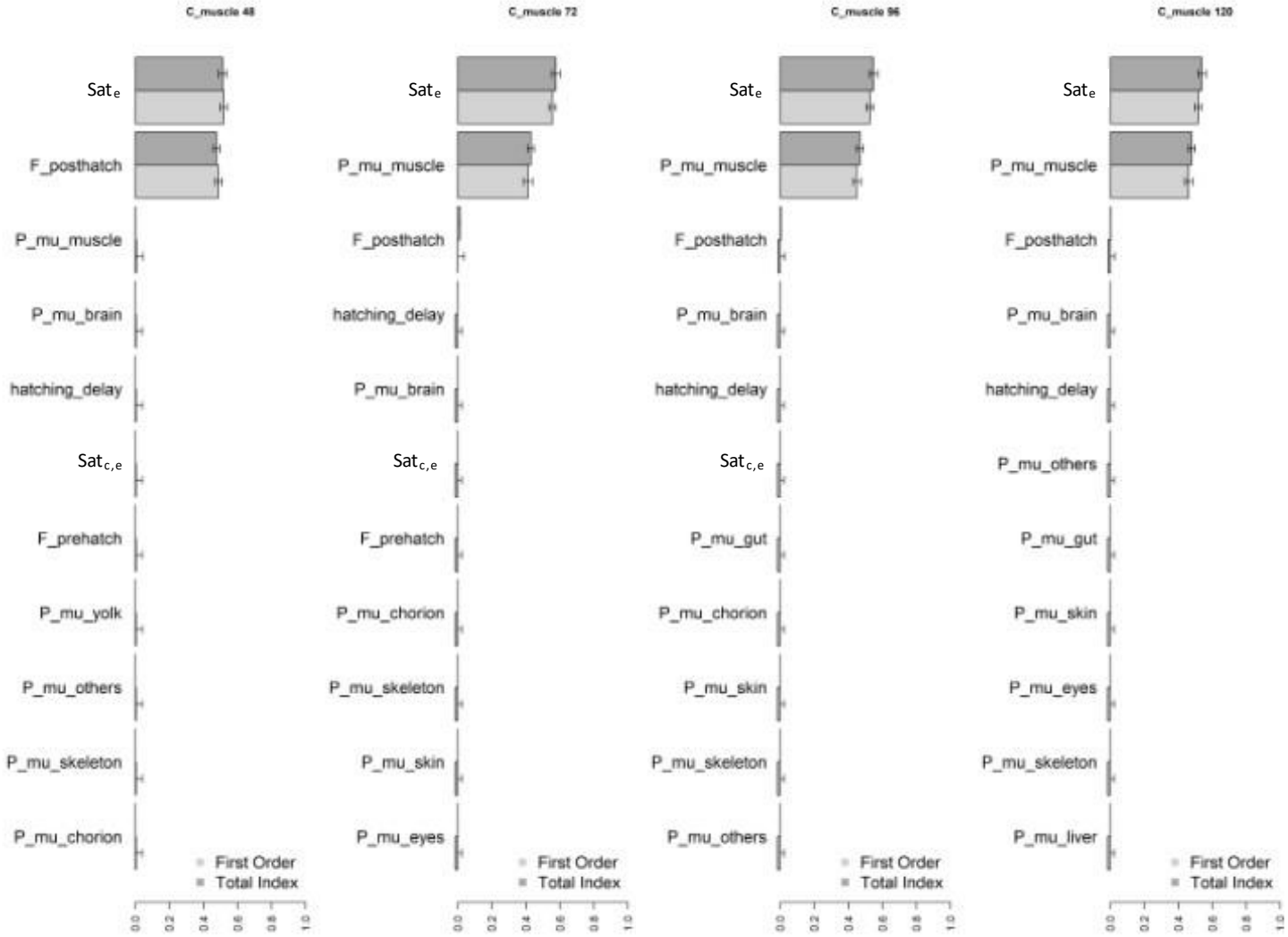

Figure S17. Sensitivity analysis of model III, including corrected partition coefficients, saturations ($Sat_{c,e}$, Sat_e), flows and permeability delay (hatching_delay), on muscle PFOS concentrations in ZFE, at 24, 48, 72, 96 and 120 hpf (from left to right, respectively). The 11 most influential parameters are represented.

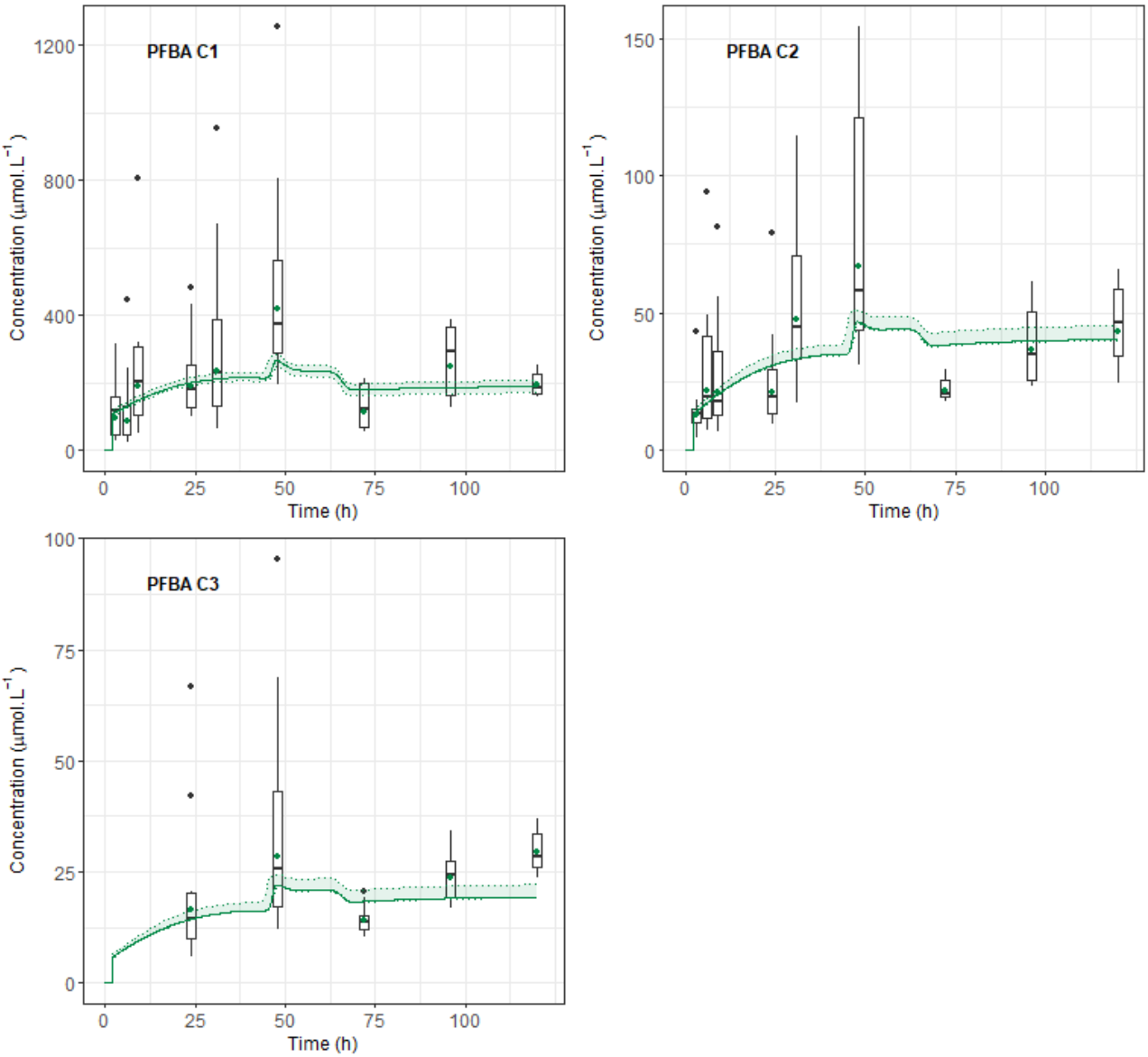

Figure S18. Predicted and observed internal concentrations of PFBA in the whole embryo exposed to 4800 µM (C1), 550 µM (C2) and 240 µM (C3) in function of time, using Model II. The coloured points are geometric means of the experimental data. Boxplots have been superimposed on the experimental points. The coloured trajectories are the internal predicted concentrations at the joint a posteriori mode. The area between the dotted lines corresponds to the 95% credibility interval

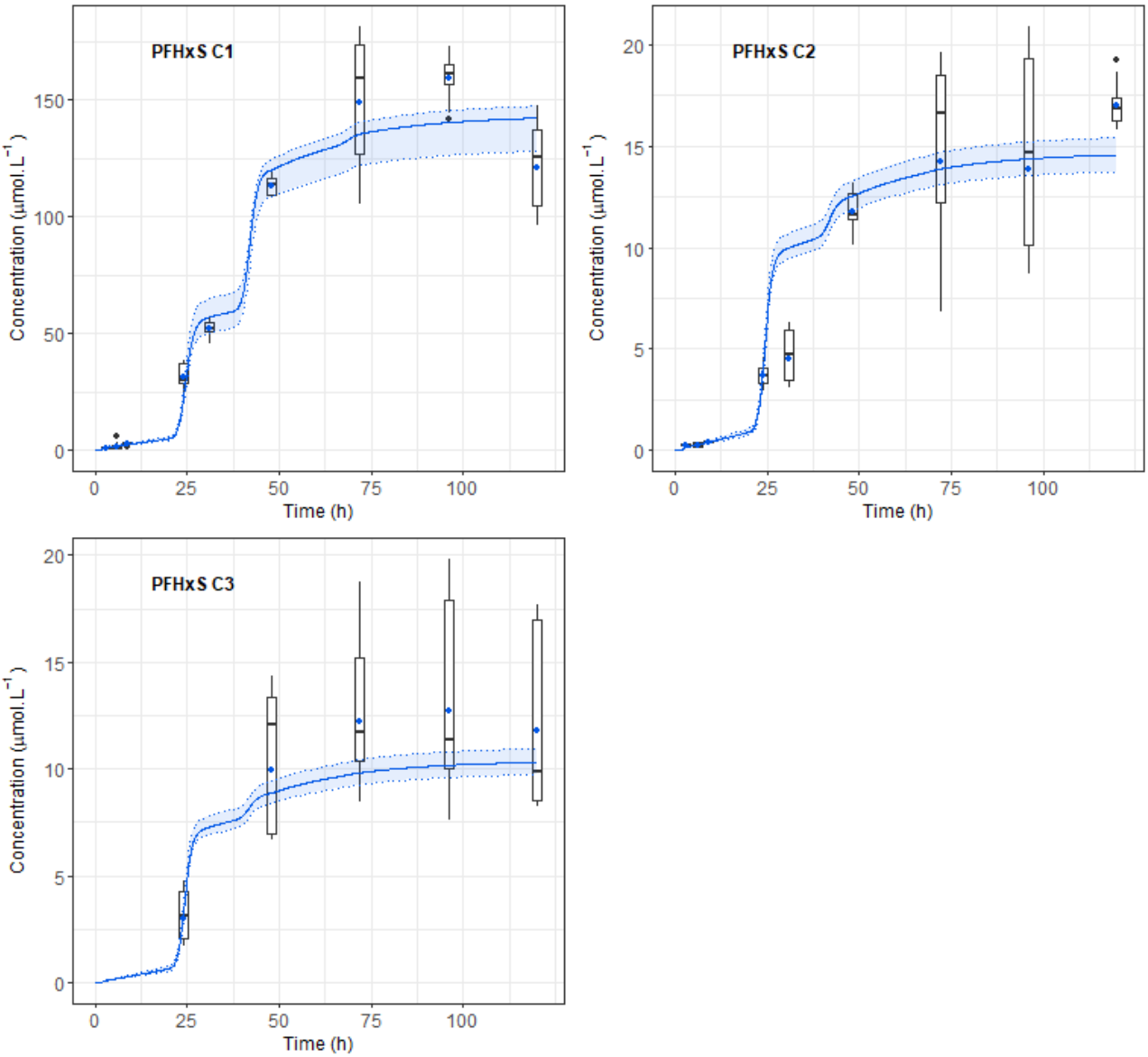

Figure S19. Predicted and observed internal concentrations of PFHxS in the whole embryo exposed to 7.8 µM (C1), 8.0E^{-1} µM (C2) and 6.0E^{-1}µM (C3) in function of time, using Model III. The coloured points are geometric means of the experimental data. Boxplots have been superimposed on the experimental points. The coloured trajectories are the internal predicted concentrations at the joint a posteriori mode. The area between the dotted lines corresponds to the 95% credibility interval

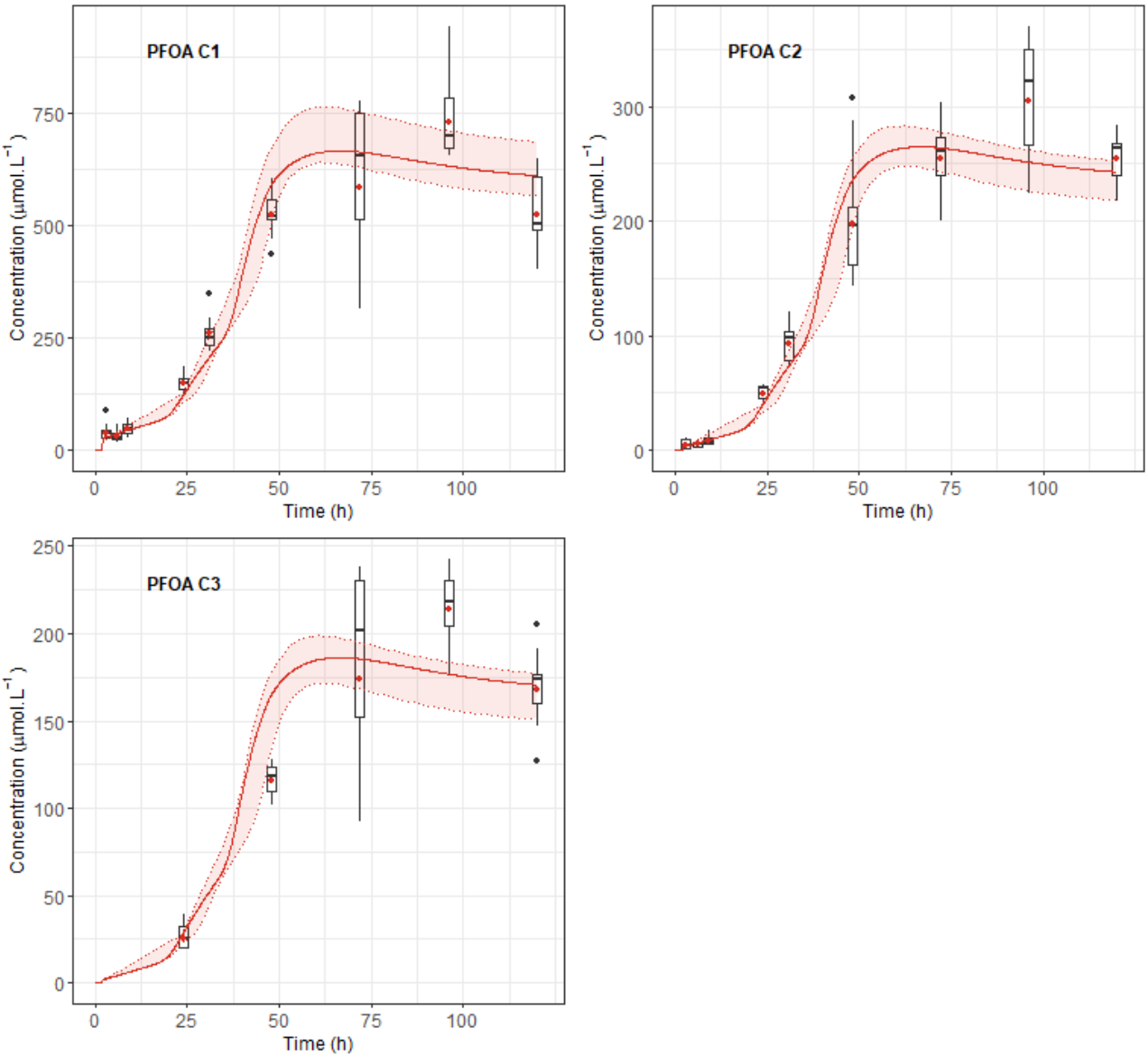

Figure S20. Predicted and observed internal concentrations of PFOA in the whole embryo exposed to 340 µM (C1), 41 µM (C2) and 21 µM (C3) in function of time, using Model II.

The coloured points are geometric means of the experimental data. Boxplots have been superimposed on the experimental points. The coloured trajectories are the internal predicted concentrations at the joint a posteriori mode. The area between the dotted lines corresponds to the 95% credibility interval

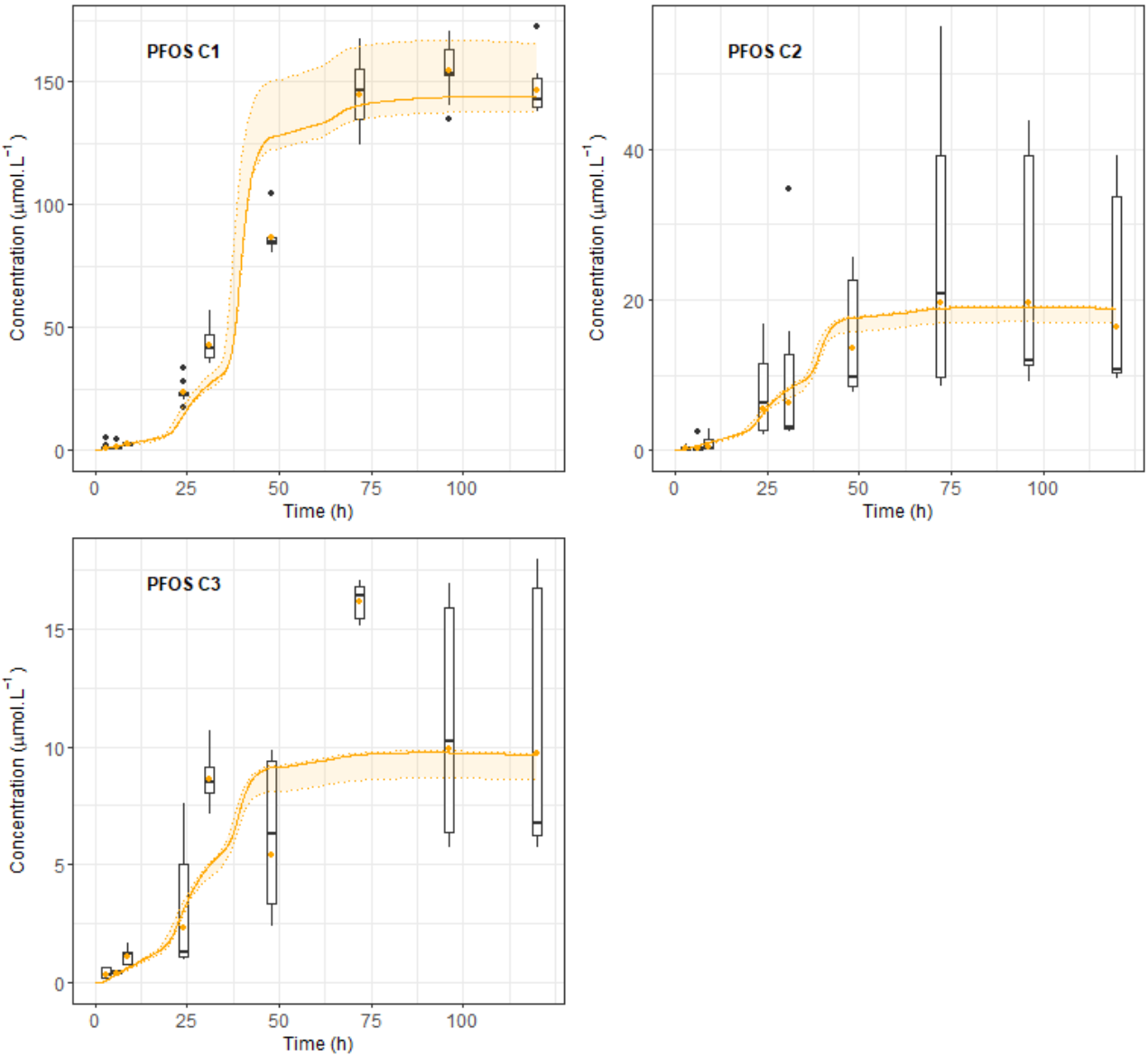

Figure S21. Predicted and observed internal concentrations of PFOS in the whole embryo exposed to 7.6E^{-1} µM (C1), 8.0E^{-2} µM (C2) and 4.0E^{-2} µM (C3) in function of time, using Model III.

The coloured points are geometric means of the experimental data. Boxplots have been superimposed on the experimental points. The coloured trajectories are the internal predicted concentrations at the joint a posteriori mode. The area between the dotted lines corresponds to the 95% credibility interval

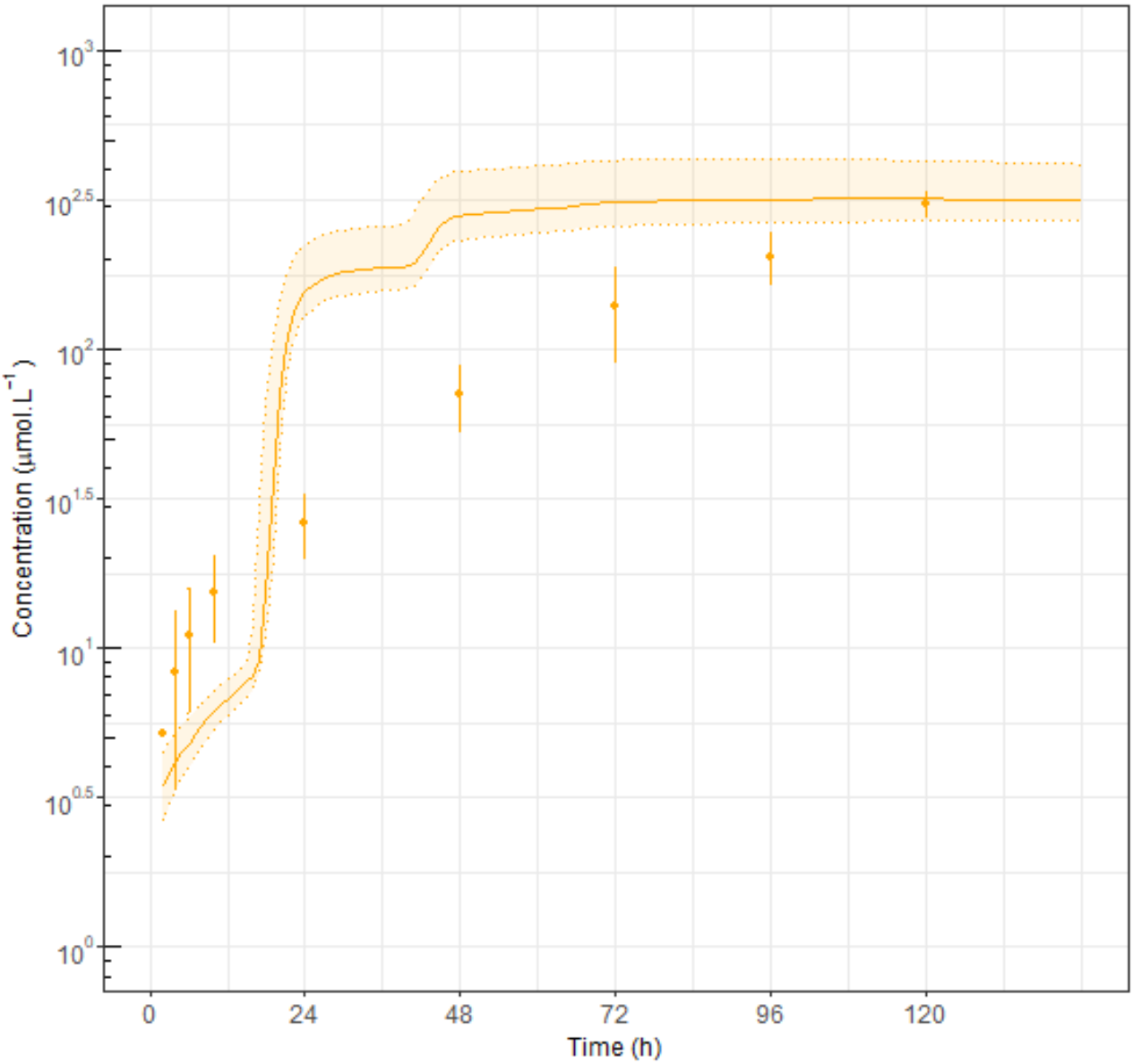

Figure S22. Predicted and observed internal concentrations of PFOS in the whole embryo dosed with PFOS at 8.0 µM using model III.
The coloured points are experimental concentrations derived from quantitative data of Huang et al. (2010). The coloured trajectories are the internal predicted concentrations at the joint *a posteriori* mode. The area between the dotted lines corresponds to the 95% credibility interval

Table S1. Compounds (PFBA, PFHxS, PFOA and PFOS) partition coefficients estimated based on VIVD model (Fisher et al., 2019) used in the Bayesian-PBPK model

Parameter	PFBA	PFHxS	PFOA	PFOS	Comment
Tissues partition coefficients					
yolk / water	0. 0255	0.0256	0.102	0. 0294	VIVD QSAR model
liver / water	0. 0407	0.0409	0.0571	0.0415	
gut / water	0. 0379	0.0381	0.0466	0.0384	
muscle / water	0.0419	0.0421	0.0550	0.0426	
skeleton / water	0.0419	0. 0421	0.0550	0.0426	
eyes / water	0.0464	0.0467	0.0557	0.0470	
brain / water	0.0458	0.0461	0.0608	0.0466	
heart / water	0.0419	0.0421	0.0550	0.0425	
skin / water	0.0464	0.0467	0.0557	0.0470	
other tissues / water	0.0321	0.0323	0.0457	0.0328	
Other partition coefficients					
polymer / water	$1.00E^{-12}$	$1.00E^{-12}$	$1.00E^{-12}$	1.58	Fixed: no loss of product detected in the blank experiment
air / water unbound	Nonvolatile				VIVD QSAR model

Table S2. Prior distributions of the fixed and calibrated parameters used in the Bayesian-PBPK model

Scaling factor	Distribution law	Values	Comment
f_{pc}	LogNormal	(1, 3)	-
Flow rates			
$F_{polymer}$ (µL/h/mm²)	Fixed	1.00E^{-12}	5.70 for PFOS
F_{air} (µL/h/mm^3)	Fixed	1.00E^{-12}	No exchange
$\varphi_{e:w}$ (µL/h/mm²)	Uniform	[1.00E^{-8} ; 100]	-
$\varphi_{e:chorion:w}$ (µL/h)	Uniform	[1.00E^{-8} ; 100]	-
Metabolism (µmol/h)	Fixed	0	No observed metabolism
$EC_{sat,e}$ (nmol/µL)	LogNormal	(1.00E^{-2}, 3.00)	(1.00E^{-8}, 3.00) for PFBA
$EC_{sat,c,e}$ (nmol/µL)	LogNormal	(1.00E^{-2}, 3.00)	(1.00E^{-8}, 3.00) for PFBA
ϕ *(h)*	Normal	(0, 2)	Truncated from -24h to +24h for PFBA
Chorion water partition coefficient	LogNormal	(1,3)	-

Table S3. Prior and posterior (MPV) values of partition coefficients

Parameter	PFBA		PFHxS		PFOA		PFOS	
Tissues partition coefficients	Priors	MPV	Priors	MPV	Priors	MPV	Priors	MPV
yolk / water	0.0255	0.0566	0.0256	12.8	0.102	18.7	0.0294	305
liver / water	0.0407	0.0903	0.0409	20.5	0.0571	10.5	0.0415	430
gut / water	0.0379	0.0841	0.0381	19.1	0.0466	8.56	0.0384	398
muscle / water	0.0419	0.0930	0.0421	21.1	0.055	10.1	0.0426	442
skeleton / water	0.0419	0.0930	0.0421	21.1	0.055	10.1	0.0426	442
eyes / water	0.0464	0.1029	0.0467	23.4	0.0557	10.2	0.047	487
brain / water	0.0458	0.1016	0.0461	23.1	0.0608	11.2	0.0466	483
heart / water	0.0419	0.0930	0.0421	21.1	0.055	10.1	0.0425	441
skin / water	0.0464	0.1029	0.0467	23.4	0.0557	10.2	0.047	487
other tissues / water	0.0321	0.0712	0.0323	16.2	0.0457	8.39	0.0328	340
chorion / water	LogNormal(1,3)	0.881	LogNormal(1,3)	5.38	LogNormal(1,3)	2.68	LogNormal(1,3)	31.7

Table S4. Mean parameter values used in the sensitivity analysis

Parameters	Unit	PFBA	PFHxS	PFOA	PFOS	Distribution	Code names
Flow Post-hatch water /Embryo	(µL/h/mm²)	82.7	99.4	0.801	99.9	Uniform +/- 10%	F_posthatch
Flow Pre-hatch water /Chorion/Embryo	(µL/h)	4.04^{E-4}	1.17^{E-2}	7.09^{E-3}	0.793	Uniform +/- 10%	F_prehatch
Flow water /Chorion	(µL/h)	1.71^{E-2}	81.4	19.0	98.6	Uniform +/- 10%	F_chorion
Corrected partition coefficients							
chorion / water		0.881	5.38	2.68	31.7	Uniform +/- 10%	P_mu_chorion
yolk / water		5.66^{E-2}	12.9	18.7	305	Uniform +/- 10%	P_mu_yolk
liver / water		9.03^{E-2}	20.5	10.5	431	Uniform +/- 10%	P_mu_liver
gut / water		8.41^{E-2}	19.1	8.56	398	Uniform +/- 10%	P_mu_gut
muscle / water		9.29^{E-2}	21.1	10.1	442	Uniform +/- 10%	P_mu_muscle
skeleton / water		9.29^{E-2}	21.1	10.1	442	Uniform +/- 10%	P_mu_skeleton
eyes / water		0.103	23.4	10.2	487	Uniform +/- 10%	P_mu_eyes
brain / water		4.58^{E-2}	23.1	11.2	484	Uniform +/- 10%	P_mu_brain
heart / water		9.29^{E-2}	21.1	10.1	442	Uniform +/- 10%	P_mu_heart
skin / water		0.103	23.4	10.2	487	Uniform +/- 10%	P_mu_skin
other tissues / water		7.13^{E-2}	16.2	8.39	341	Uniform +/- 10%	P_mu_others
Permeability delay	(hours)	2.11	-23.8	-27.4	-28.7	Uniform +/- 10%	hatching_delay
Chorion/Embryo absorption saturation constant (MIII)	(nmol/µL)	-	5.32^{E-3}	-	7.33^{E-5}	Uniform +/- 10%	EC_fifty_pre
Embryo absorption saturation constant (MII & MIII)	(nmol/µL)	3.76	5.84^{E-2}	8.61^{E-2}	1.09^{E-3}	Uniform +/- 10%	EC_fifty_post

Table S5. Model structures performance among the different tested PFAAs (green= retained structure)

Model Structure	PFBA	PFHxS	PFOA	PFOS
Model 0 (Without Saturation)	AIC= 173 BIC= 161 RMSE= 0.0474 NRMSE= 1.08	AIC= 155 BIC= 167 RMSE= 0.00889 NRMSE= 0.504	AIC= 886 BIC= 898 RMSE= 0.402 NRMSE= 2.97	AIC= 777 BIC= 789 RMSE= 0.0640 NRMSE= 1.98
Model I ($EC_{sat,e}$ after hatching only)	AIC= 304 BIC= 318 RMSE= 0.0585 NRMSE= 1.30	AIC= 169 BIC= 182 RMSE= 0.00781 NRMSE= 0.446	AIC= 274 BIC= 288 RMSE= 0. 0.0923 NRMSE= 0.769	AIC= 209 BIC= 223 RMSE= 0.0562 NRMSE= 1.45
Model II ($EC_{sat,e}$before and after hatching)	AIC= 91.2 BIC= 105 RMSE= 0.0398 NRMSE= 0.879	AIC= 262 BIC= 278 RMSE= 0.0102 NRMSE= 0.526	AIC= 93.1 BIC= 107 RMSE= 0.0457 NRMSE= 0.564	AIC= 256 BIC= 270 RMSE= 0.0171 NRMSE= 1.32
Model III ($EC_{sat,e}$ & $EC_{sat,c,e}$)	AIC= 110 BIC= 126 RMSE= 0.0345 NRMSE= 0.814	AIC= 110 BIC= 126 RMSE= 0.00784 NRMSE= 0.629	AIC= 159 BIC= 175 RMSE= 0.0393 NRMSE= 0.523	AIC= 46.4 BIC= -62.4 RMSE= 0.0102 NRMSE= 1.12

Model Code
Code of structural model (MCSim)

```
# Zebra fish embryo PK model
# Dynamic version, with linear metabolism
# Frederic Bois, April 2017. Reproductive Toxicology 2020
# Rémy Beaudouin, Janvier 2020.
# P-A Billat, 2021-2022.

# Units:
# quantities:    nmol
# volumes:       mm3
# concentrations: nmol/mm3
# time:          hours
# ============================================================================

####################
# 26/10 : saturation and hatching
# 9/11 : chorion compartements, saturation plastic, and minor name changes
# 09/05 : effect of light and temperature on hatching
# 21/05 : population model
# 27/07 : correction of A_FC


#####################################################################
####################          Variables                ##############
#####################################################################

States  = {         Q_water,                    # Quantity in water (nmol)
                            Q_water_add,
                            Q_air,                      # ~       in air
                            Q_plastic,                  # ~       bound on plastic
                            Q_met,                      # Q of metabolites in system(nmoles)
                            Q_yolk,                     # Quantity per embryo in yolk (nmol)
                            Q_liver,                    # ~               in liver
                            Q_gut,                      # ~               in digestive tract
                            Q_muscle,                   # ~               in muscles
                            Q_skeleton,                 # ~               in skeleton
                            Q_eyes,                     # ~               in eyes
                            Q_brain,                    # ~               in brain
                            Q_heart,                    # ~               in heart
                            Q_skin,                     # ~               in skin pigmented cells
                            Q_others,                   # ~               in other tissues
                            Q_chorion                   # ~               in chorion
                            };

Inputs  = {Event_labile,
                    N_embryo,
                    Light}                      # Number of embryos per well;

Outputs = { # Concentration in embryo (nmol/mm3)
                            C_yolk,     # Concentration  in yolk
                            C_liver,    # ~           in liver (metabolizes)
                            C_gut,      # ~           in digestive tract
```

```
C_muscle,       # ~       in muscles
C_skeleton,     # ~       in skeleton
C_eyes,         # ~       in eyes
C_brain,        # ~       in brain
C_heart,        # ~       in heart
C_skin,         # ~       in skin pigmented cells
C_others,       # ~       in other tissues
C_chorion,      # ~       in chorion
Q_water_e,
C_embryo,       # ~       in embryo, not including yolk
C_embryo_total, # ~        in embryo, including yolk

# Quantity in embryo
Q_embryo,               # Quantity in embryo, not including yolk
Q_embryo_total,         # Quantity in N embryo, including yolk

# Embryo biometric variables
V_embryo,       # volume per embryo (mm3)
V_yolk,         # volume of yolk (mm3)
V_embryo_total, # Sum of embryo and yolk volumes (mm3)
V_water_embryo,

V_liver,        # ~         liver
V_gut,          # ~         gut
V_muscle,       # ~         muscles
V_skeleton,     # ~         skeleton
V_eyes,         # ~         eyes
V_brain,        # ~         brain
V_heart,        # ~         heart
V_skin,         # ~         skin
V_others,       # ~         others embryonic tissues

# System related variables
V_air,                  # Volum of air in the system
S_p_w,                  # surface area of water in contact with wall (mm2)
C_water,                # Concentration of parent in water (nmol/mm3)
C_air,                  # Concentration of parent in air
V_content,
F_yolk,
F_liver ,
F_gut,
F_skeleton,
F_eyes,
F_brain,
F_heart,
F_skin,
F_others ,
F_muscle ,
F_embryo_dyn ,
F_x,
F_hatch,

# Coumpound related variables
Q_check,        # Quantity mass balance check, per embryo
```

```
                    Q_water_supp,
                    Saturation,
                    };

#####################################################################
###################          Parameters          ###################
#####################################################################

        Pi = 3.14159265358979323846; # Number Pi

#########################  System physics parameters  #########################

        V_well;                     # Volume of a culture well (mm3)
        D_well;                     # Diameter of a well (mm)
        V_water;                    # volume of culture medium at time 0 (mm3)
        S_a_w;                      # surface area of water in contact with air (mm2)

        Temperature = 301.15;       # experimental temperature (degrees K) = 28°C + 273.15
        TR   = 298.15 ;             # Reference temperatures in °K (25°C)
        TA   = 6930 ;               # Arrhenius temperature in Kelvin
        A_FC;                       # Arrhenius temperatures fonction
        T_fec = 0;                  # time of egg fecundation (can be > t0 experiement)

#########################  Exposure design parameters  #########################

        Dose;                       # Total dose of parent (nmol) in total water at start
        Light;                      # Daily light exposure duration (h)

#########################  Substance specific parameters  #########################

        fui;                    # Fraction unionized in water
        F_plastic ;             # (in uL/h/mm2)  adsorption rates for non-specific binding on plastic;
        F_air ;                 # flow (in uL/h/mm2)  evaporation and absorption rates water/air;
        F_posthatch;            # flow (in uL/h/mm2 BSA)  exchanges rates water/embryo;
        F_chorion;              # flow (in uL/h)  exchanges rates water/embryo;
        F_prehatch ;            # flow (in uL/h) from water to embryo through the chorion

        Michaelis = 0;          # Flag for Michaelis-Menten vs linear metabolism (0 = linear)
        K_met;                  # Metabolic clearance per liver cell, if linear metabolism, uL/h
        Vmax;                   # Maximum formation rate of metabolite, if saturable metabolism, nmol/h
        Km;                     # Michaelis-Menten constant, if satutable metabolism, nmol/uL
        EC_fifty;               # Saturation EC50 (nmol/uL)
        EC_fifty_pre;           # Saturation EC50 (nmol/uL)
        EC_fifty_post;
        Q_plastic_max =1E10;    # Plastic binding saturation

        # Parameters recomputed in initialize section: must be specified in the input file
        P_pw;                   # Plastic / water partition coefficient
        P_aw;                   # Air / water partition coefficient

        #P_mu_x = partition coefficients ORGAN/MEDIUM.
        P_mu_yolk;              # yolk partition coefficient / Medium unbound
        P_mu_liver;             # liver partition coefficient / Medium unbound
        P_mu_gut;               # ~ partition coefficient / Medium unbound
```

```
P_mu_muscle;        # ~ partition coefficient / Medium unbound
P_mu_skeleton;      # ~ partition coefficient / Medium unbound
P_mu_eyes;          # ~ partition coefficient / Medium unbound
P_mu_brain;         # ~ partition coefficient / Medium unbound
P_mu_heart;         # ~ partition coefficient / Medium unbound
P_mu_skin;          # ~ partition coefficient / Medium unbound
P_mu_others;        # ~ partition coefficient / Medium unbound
P_mu_chorion;       # ~ partition coefficient / Medium unbound


#########################  Embryo growth parameters  #########################

# Volume of the embryo without yolk at 0 and 120 hpf (uL)
    V_embryo_0   = 0.005;
    V_embryo_120 = 0.370597 ;
    V_cell_liver = 3.4e-6;          # volume of a liver cell (uL)


# Starting times for organ growth (hours) (from K. Brotzmann)
    tau_liver    =  16 ;
    tau_gut      =  10 ;
    tau_skeleton =  48 ;
    tau_eyes     =  11 ;
    tau_brain    =   9 ;
    tau_heart    =  30 ;
    tau_skin     =  24 ;
    tau_muscle   =  60 ;
    tau_others   =   0 ;

# Chorion parameter
    V_chorion    = 0.005334128;     #Volume of the chorion (uL)
    S_chorion    = 1.54;            #Surface of the chorion (mm²)

    sigma_hatch  ;                  # variabilty of the daily hatching time
    hatching_delay  ;               # Start of permeability change
    mu_hatch_1      ;               # Correction of the hatching time on Day 1
    mu_hatch_2      ;               # Correction of the hatching time on Day 2
    mu_hatch_3      ;               # Correction of the hatching time on Day 3

    Wnorm_1_ref ;                   # relative weight of 48h dpf hatching at 25°C
    Wnorm_3_ref ;                   # relative weight of 96h dpf hatching at 25°C

    Wnorm_1 ;                       # relative weight of 48h dpf hatching at Temperature
    Wnorm_3 ;                       # relative weight of 96h dpf hatching at Temperature

    TA_W = 75688.3 ;

# Yolk parameters
    K_d_yolk ;
    V_yolk_0 = 0.207 ;

# Organ growth rates (1/h), FB adjustment from rescaled organ volumes as fractions of total embryo
(without yolk) at 120 hpf
    K_g_liver    = (60* 5.29509e-06);
```

```
        K_g_gut     = (60* 2.2779e-05);
        K_g_skeleton = (60* 1.82294e-05);
        K_g_eyes    = (60* 1.20414e-05);
        K_g_brain   = (60* 2.22253e-06);
        K_g_heart   = (60* 3.01003e-06);
        K_g_skin    = (60* 1.3672e-05);
        K_g_others  = (60* 3.92738e-05);
        K_g_muscle  = (60* 5.07074e-05);

########################## Other parameters ##########################

        sigma;              # Statistical parameter
        ffpc;               # Fudge factor for partition coefficients


######################################################################
###################          Initialization          ###################
######################################################################

# ----------------------------------------
Initialize { # assumes that start time is zero, should be revised if not

# Arrhenius temperatures function
        A_FC = exp ( (TA / TR) - (TA / Temperature) ) ;

        K_d_yolk = (0.000313*60) * A_FC;        # Yolk consumption rate constant (1/h)

# Adjusted starting times for organ growth (hours)
        tau_liver   =  tau_liver   / A_FC;
        tau_gut     =  tau_gut     / A_FC;
        tau_skeleton =  tau_skeleton / A_FC;
        tau_eyes    =  tau_eyes    / A_FC;
        tau_brain   =  tau_brain   / A_FC;
        tau_heart   =  tau_heart   / A_FC;
        tau_skin    =  tau_skin    / A_FC;
        tau_muscle  =  tau_muscle  / A_FC;
        tau_others  =  tau_others  / A_FC;

# Adjusted partition coefficients
        P_mu_yolk     = P_mu_yolk    * ffpc;
        P_mu_liver    = P_mu_liver   * ffpc;
        P_mu_gut      = P_mu_gut     * ffpc;
        P_mu_muscle   = P_mu_muscle  * ffpc;
        P_mu_skeleton = P_mu_skeleton * ffpc;
        P_mu_eyes     = P_mu_eyes    * ffpc;
        P_mu_brain    = P_mu_brain   * ffpc;
        P_mu_heart    = P_mu_heart   * ffpc;
        P_mu_skin     = P_mu_skin    * ffpc;
        P_mu_others   = P_mu_others  * ffpc;
        P_aw          = P_aw         * ffpc;

# Concentration in water without embryo in the well (nmol/uL)
        Q_water  = 0;
        Q_plastic = 0;
```

```
        Q_air    = 0;

        S_a_w   =  Pi * 0.25 * D_well * D_well; # Surface area of water in contact with recipient area(nm2)
        S_p_w = 4 * V_water / D_well + Pi * 0.25 * D_well * D_well;

# Total volume of 1 embryo at start (uL)
        V_embryo_total = (V_yolk_0 + V_embryo_0);


# Total volume of water + embryo (uL)
        V_content = V_water + ( N_embryo * V_embryo_total );

# Volume of air (uL) in the (sealed) well head-space, per embryo
        V_air = V_well - V_content;


# Effect of Light on hatching process

        mu_hatch_1 =   (Light < 6?    49.0158:
                        (Light < 18?        46.9:  49.1));          # mean hatching time on Day 2 at ref T°C
        mu_hatch_2 =   (Light < 6?   66.0025 :
                        (Light < 18?        70.4: 65.6 ));          # mean hatching time at Day 3 at ref T°C
        mu_hatch_3 =   (Light < 6?    92.5042 :
                        (Light < 18?        92.7 : 89.0 ));         # mean hatching time at Day 4 at ref T°C
        sigma_hatch =  (Light < 6?    1.75728:
                        (Light < 18?        1.16: 1.48625 ));       # SD hatching time at ref T°C

        Wnorm_1_ref =           (Light < 6?   0.01345:
                (Light < 18?        0.0510142: 0.0932336)); # relative weight of 48hpf hatching at ref T°C
        Wnorm_3_ref =           (Light < 6?   0.495197:
                (Light < 18?       0.322533: 0.309805));   # relative weight of 96hpf hatching at exp T°C
        TA_hatch      =   (Light < 6?   25098.8:
                (Light < 18?       81598.5: 27691.9));       # relative weight of 96hpf hatching at exp T°C


# Effect of Temperature on hatching process

        W1_tmp = Wnorm_1_ref * exp ( ( TA_W / TR) - (TA_W / Temperature) ) ;
        W3_tmp = Wnorm_3_ref  / exp ( ( TA_W / TR) - (TA_W / Temperature) ) ;

        Wnorm_1 = ( W1_tmp > 1 ?  1  : W1_tmp  );
        Wnorm_3 = ( W3_tmp < 0 ?  0  : W3_tmp  );
}


#####################################################################
###################             Dynamics                ###################
#####################################################################

Dynamics {

# Scaling coefficients of organ volumes (change with time)
        sc_liver    = (t < (tau_liver           + T_fec) ?  0.0  : ((exp(K_g_liver            * A_FC * (t - tau_liver      -
T_fec )) - 1) ));
```

```
        sc_gut      = (t < (tau_gut           + T_fec) ?  0.0  : ((exp(K_g_gut           * A_FC * (t - tau_gut       -
T_fec )) - 1) ));
        sc_skeleton = (t < (tau_skeleton + T_fec) ?  0.0  : ((exp(K_g_skeleton      * A_FC * (t - tau_skeleton -
T_fec )) - 1) ));
        sc_eyes     = (t < (tau_eyes          + T_fec) ?  0.0  : ((exp(K_g_eyes          * A_FC * (t - tau_eyes      -
T_fec )) - 1) ));
        sc_brain    = (t < (tau_brain         + T_fec) ?  0.0  : ((exp(K_g_brain         * A_FC * (t - tau_brain     -
T_fec )) - 1) ));
        sc_heart    = (t < (tau_heart         + T_fec) ?  0.0  : ((exp(K_g_heart         * A_FC * (t - tau_heart     -
T_fec )) - 1) ));
        sc_skin     = (t < (tau_skin          + T_fec) ?  0.0  : ((exp(K_g_skin          * A_FC * (t - tau_skin      -
T_fec )) - 1) ));
        sc_muscle   = (t < (tau_muscle    + T_fec) ?  0.0  : ((exp(K_g_muscle        * A_FC * (t - tau_muscle   -
T_fec )) - 1) ));
        sc_others   = (t < (tau_others   + T_fec) ?  0.0  : ((exp(K_g_others          * A_FC * (t - tau_others   -
T_fec )) - 1) ));

# Organ volumes (uL):
        V_liver           = V_embryo_120 * sc_liver;
        V_gut             = V_embryo_120 * sc_gut;
        V_skeleton        = V_embryo_120 * sc_skeleton;
        V_eyes            = V_embryo_120 * sc_eyes;
        V_brain           = V_embryo_120 * sc_brain;
        V_heart           = V_embryo_120 * sc_heart;
        V_skin            = V_embryo_120 * sc_skin;
        V_muscle          = V_embryo_120 * sc_muscle;
        V_others   = (t < T_fec ? 0.0  : V_embryo_120 * sc_others + V_embryo_0 );


# Yolk volume dynamics (uL)
        V_yolk        = (t < T_fec ? 0.0  : V_yolk_0 * exp(- K_d_yolk * (t- T_fec) ) );
        # Volume of yolk (uL), decreases approximately exponentially with time

# Embryo biometrics dynamics (uL)
        V_embryo      = V_liver + V_gut + V_skeleton + V_eyes + V_brain + V_heart + V_skin + V_others +
V_muscle ;                                              # Volume of the embryo without yolk (uL)
        V_embryo_total  = V_yolk + V_embryo;            # Volume of the embryo (L)

        ################### Water quantity dynamics ###################

        V_content = V_water + ( V_embryo_total* N_embryo );          # Total volume of water +
embryo(uL) only V_embryo_total is assumed to change with time
        S_p_w    = 4 * V_content / D_well + Pi * 0.25 * D_well * D_well; # Surface area of water in contact
with plastic, with the embryo in the well (mm2)
        C_water           = Q_water / V_water;          # Concentration unbound in water (nmol/uL)

# Compute dimension PER EMBRYO
        V_water_embryo = ( N_embryo   > 0.1 ? V_water / N_embryo : 1E-12);
        Q_water_e         = ( N_embryo   > 0.1 ? Q_water / N_embryo : 1E-12);   # Quantity available per
embryo in water (nmol/uL)
        C_water_e         = ( N_embryo   > 0.1 ? Q_water_e /V_water_embryo : 1E-12 ); # concentration
per embryo in water (nmol/uL). If Q is not limiting, C_water = C_water_e
        V_air  = V_well - V_content;                                  # Volume of air (uL) in head-space
        C_air  = Q_air / V_air;                                       # concentration (nmol/uL)
```

```
# Flow changes with time (proportion of embryo without chorion :
https://journals.plos.org/plosone/article?id=10.1371/journal.pone.0052153)
        F_x = CDFNormal((t - T_fec - (hatching_delay+ mu_hatch_1) )/sigma_hatch) * Wnorm_1
+ CDFNormal((t - T_fec - (hatching_delay+ mu_hatch_2) )/sigma_hatch) * (1.0 -Wnorm_1 -Wnorm_3)
+ CDFNormal((t - T_fec - (hatching_delay+ mu_hatch_3) )/sigma_hatch) * Wnorm_3  ;

F_hatch = CDFNormal((t - T_fec - ( mu_hatch_1) )/sigma_hatch) * Wnorm_1
                + CDFNormal((t - T_fec - ( mu_hatch_2) )/sigma_hatch) * (1.0 -Wnorm_1 -Wnorm_3)
                + CDFNormal((t - T_fec - (mu_hatch_3) )/sigma_hatch) * Wnorm_3  ;

F_embryo_dyn = ( F_prehatch * N_embryo * (1-F_x) ) + ( F_posthatch * N_embryo *  pow(V_embryo_total,
0.667) * F_x ) ;

# Saturation = 1 ; # Hatching =  0 if t < T_hacth and then Hatching = 1
# Saturation = (1-F_x) * 1 + ( 1 / ( 1 + C_water_e / EC_fifty) ) * F_x ;# Saturation Femb
# Saturation = (  1 / ( 1 +  C_water_e / EC_fifty) ); # Saturation Femb et Fchorion
Saturation = (1-F_x)* (  1 / ( 1 +  C_water_e / EC_fifty_pre)) + F_x * (1 / ( 1 +  C_water_e / EC_fifty_post) );


# Organ flow  (V_i / V_embryo_total ~ S_i / S_embryo_total)
        F_yolk   =  (V_yolk    > 1E-12 ? (F_embryo_dyn * V_yolk    / V_embryo_total) : 1E-12 );
        F_liver  =  (V_liver   > 1E-12 ? (F_embryo_dyn * V_liver   / V_embryo_total) : 1E-12 );
        F_gut    =  (V_gut     > 1E-12 ? (F_embryo_dyn * V_gut     / V_embryo_total) : 1E-12 );
        F_skeleton =  (V_skeleton > 1E-12 ? (F_embryo_dyn * V_skeleton/ V_embryo_total) : 1E-12 );
        F_eyes   =  (V_eyes    > 1E-12 ? (F_embryo_dyn * V_eyes    / V_embryo_total) : 1E-12 );
        F_brain  =  (V_brain   > 1E-12 ? (F_embryo_dyn * V_brain   / V_embryo_total) : 1E-12 );
        F_heart  =  (V_heart   > 1E-12 ? (F_embryo_dyn * V_heart   / V_embryo_total) : 1E-12 );
        F_skin   =  (V_skin    > 1E-12 ? (F_embryo_dyn * V_skin    / V_embryo_total) : 1E-12 );
        F_others =  (V_others  > 1E-12 ? (F_embryo_dyn * V_others  / V_embryo_total) : 1E-12 );
        F_muscle =  (V_muscle  > 1E-12 ? (F_embryo_dyn * V_muscle  / V_embryo_total) : 1E-12 );
        F_yolk   =  (V_yolk    > 1E-12 ? (F_embryo_dyn * V_yolk    / V_embryo_total) : 1E-12 );


# Organ concentrations (V can be null)

        C_yolk      =  ( V_yolk      > 1E-12 ? Q_yolk    / (N_embryo * V_yolk)       : 1E-12 ) ;
        C_liver     =  ( V_liver     > 1E-12 ? Q_liver   / (N_embryo * V_liver)      : 1E-12 ) ;
        C_gut       =  ( V_gut       > 1E-12 ? Q_gut     / (N_embryo * V_gut)        : 1E-12 ) ;
        C_muscle    =  ( V_muscle    > 1E-12 ? Q_muscle  / (N_embryo * V_muscle)     : 1E-12 ) ;
        C_skeleton  =  ( V_skeleton  > 1E-12 ? Q_skeleton / (N_embryo * V_skeleton): 1E-12 ) ;
        C_eyes      =  ( V_eyes      > 1E-12 ? Q_eyes    / (N_embryo * V_eyes)       : 1E-12 ) ;
        C_brain     =  ( V_brain     > 1E-12 ? Q_brain   / (N_embryo * V_brain)      : 1E-12 ) ;
        C_heart     =  ( V_heart     > 1E-12 ? Q_heart   / (N_embryo * V_heart)      : 1E-12 ) ;
        C_skin      =  ( V_skin      > 1E-12 ? Q_skin    / (N_embryo * V_skin)       : 1E-12 ) ;
        C_others    =  ( V_others    > 1E-12 ? Q_others  / (N_embryo * V_others)     : 1E-12 ) ;
        C_chorion   =  ( V_chorion   > 1E-12 ? Q_chorion / (N_embryo *  V_chorion)   : 1E-12 ) ;

# Possible saturation of plastic binding
        Sat_g = (1 - Q_plastic/Q_plastic_max);
```

```
        dt(Q_water) =  F_air * S_a_w * C_air / P_aw  - F_air * S_a_w * C_water * fui      # air exchanges
                + Sat_g * F_plastic * ( Q_plastic/P_pw - S_p_w * C_water)                 # plastic exchanges
                + F_yolk *    (C_yolk    / P_mu_yolk    - C_water*  Saturation  )         # yolk
                + F_liver *   (C_liver   / P_mu_liver   - C_water*  Saturation  )         # liver
                + F_gut   *   (C_gut     / P_mu_gut     - C_water*  Saturation  )         # gut
                + F_muscle *  (C_muscle  / P_mu_muscle  - C_water*  Saturation  )         # muscle
                + F_skeleton * (C_skeleton / P_mu_skeleton - C_water*  Saturation  )      # skeleton
                + F_eyes *    (C_eyes    / P_mu_eyes    - C_water*  Saturation  )         # eyes
                + F_brain *   (C_brain   / P_mu_brain   - C_water*  Saturation  )         # brain
                + F_heart *   (C_heart   / P_mu_heart   - C_water*  Saturation  )         # heart
                + F_skin *    (C_skin    / P_mu_skin    - C_water*  Saturation  )         # skin
                + F_others *  (C_others  / P_mu_others  - C_water*  Saturation  )         # others
                + N_embryo * F_chorion  * (C_chorion  / P_mu_chorion  - (1-F_hatch)* C_water);
        # chorion, Q chorion back to water after hatching

        ################### Air quantity dynamics ###################

dt(Q_air)  = F_air * S_a_w * (C_water * fui  -  C_air / P_aw);                # quantity (nmol)

        ################### Plastic quantity dynamics ###################

dt(Q_plastic) = Sat_g * F_plastic * (S_p_w * C_water - Q_plastic/P_pw);  # Quantity on plastic (nmol)

################ Quantity and concentration in organs (M), null before organogenesis  ################

# Quantity in chorion (nmol/uL)
        dt(Q_chorion)= N_embryo * F_chorion *( (1-F_hatch) * C_water - C_chorion / P_mu_chorion) ;   #
Q chorion back to water after hatching

# Quantity and concentration in yolk (nmol/uL)
        dt(Q_yolk) = F_yolk * (  C_water *  Saturation - C_yolk / P_mu_yolk );

# Linear metabolism in embryo, per embryo
        N_cells   = V_liver / V_cell_liver;                                   # null before liver organogenesis
        dt(Q_met) = (Michaelis > 0.5 ?
          N_embryo * N_cells * C_liver * Vmax / (Km + C_liver) :              # MM
          N_embryo * N_cells * C_liver * K_met);                              # linear

# Quantity and concentration in liver (nmol/mg), null before organogenesis
        dt(Q_liver) = F_liver * (  C_water *  Saturation - (C_liver/ P_mu_liver ) - dt(Q_met));

# Quantity and concentration in gut (nmol/mg), null before organogenesis
        dt(Q_gut) = F_gut * (  C_water *  Saturation- C_gut / P_mu_gut );

# Quantity and concentration in muscle (nmol/mg), null before organogenesis
        dt(Q_muscle) = F_muscle * (  C_water *  Saturation -  C_muscle / P_mu_muscle ) ;

# Quantity and concentration in skeleton (nmol/mg), null before organogenesis
        dt(Q_skeleton) = F_skeleton * (  C_water *  Saturation -   C_skeleton  / P_mu_skeleton ) ;

# Quantity and concentration in eyes (nmol/mg), null before organogenesis
        dt(Q_eyes) = F_eyes * (  C_water *  Saturation -  C_eyes   / P_mu_eyes) ;

# Quantity and concentration in brain (nmol/mg), null before organogenesis
```

```
        dt(Q_brain) = F_brain * ( C_water *  Saturation  - C_brain / P_mu_brain )  ;

# Quantity and concentration in heart (nmol/mg), null before organogenesis
        dt(Q_heart) = F_heart *( C_water *  Saturation- C_heart  / P_mu_heart ) ;

# Quantity and concentration in skin (nmol/mg), null before organogenesis
        dt(Q_skin) = F_skin  * (  C_water *  Saturation-   C_skin  / P_mu_skin );

# Quantity and concentration in gut (nmol/mg), null before organogenesis
        dt(Q_others) = F_others  * ( C_water *  Saturation  -   C_others  / P_mu_others );


        ############### Quantity and concentration in embryo (nmol/uL) ###############

        dt(Q_water_add) = 0;
        Q_embryo   = Q_liver + Q_gut   + Q_muscle  + Q_skeleton +
                              Q_eyes  + Q_brain + Q_heart   + Q_skin     + Q_others + Q_chorion * (1-F_x) ;
        C_embryo     = (t < T_fec ? 1E-10  : Q_embryo / (N_embryo * V_embryo) );
        Q_embryo_total =   (Q_embryo + Q_yolk );
        C_embryo_total =  (Q_embryo + Q_yolk) / ( N_embryo * (V_embryo_total + V_chorion * (1-F_x) ));
}

CalcOutputs {
  Q_water_supp =  Q_water + Q_embryo_total + Q_air + Q_plastic + Q_met - Q_water_add;

                    # Safeguards against negative of null values
 C_embryo      = (C_embryo       > 0 ? C_embryo    : 1E-12);
 C_embryo_total = (C_embryo_total      > 0 ? C_embryo_total    : 1E-12);
 C_water             = (C_water              > 0 ? C_water   : 1E-12);
 C_brain             = (C_brain              > 0 ? C_brain   : 1E-12);

 Q_check       = (Q_water_add + Q_water_supp) - ( Q_water  + Q_embryo_total + Q_air + Q_plastic +
Q_met);
}
End.
```

REFERENCES

Fisher, C., Simeon, S., Jamei, M., Gardner, I., Bois, Y.F., 2019. VIVD: Virtual in vitro distribution model for the mechanistic prediction of intracellular concentrations of chemicals in in vitro toxicity assays. Toxicol In Vitro 58, 42-50.

Huang, H., Huang, C., Wang, L., Ye, X., Bai, C., Simonich, M.T., Tanguay, R.L., Dong, Q., 2010. Toxicity, uptake kinetics and behavior assessment in zebrafish embryos following exposure to perfluorooctanesulphonicacid (PFOS). Aquat Toxicol 98, 139-147.